

**Mediterranean-type climate in the South Aegean
(Eastern Mediterranean) during the Late Miocene:
Evidence from isotope and element proxies**

Dissertation
zur Erlangung des Grades
“Doktor der Naturwissenschaften”
im Promotionsfach Geologie/Paläontologie

am Fachbereich Chemie, Pharmazie und Geowissenschaften
der Johannes Gutenberg-Universität Mainz

Regina Mertz
geboren in Nürtingen

Mainz 2009

Dekan: not displayed for reasons of data protection

1. Berichterstatter: not displayed for reasons of data protection

2. Berichterstatter: not displayed for reasons of data protection

Tag der mündlichen Prüfung: 20.3.2009

Erklärung

Ich versichere hiermit, die vorliegende Arbeit selbständig und nur unter Verwendung der angegebenen Quellen und Hilfsmittel verfasst zu haben.

Mainz, Januar 2009

"Die Natur versteht keinen Spass, sie ist immer wahr, sie hat immer recht, und die Fehler und Irrtümer sind immer die der Menschen."

Johann Wolfgang von Goethe

Preface

This thesis was developed within a three-year period from 2006 until 2008 as part of the research project “Seasonality and interannual climate variability during the Late Miocene: Testing and tuning climate models using oxygen isotope stratigraphy, growth increment analysis and new ground data” initiated by Prof. Dr. Thomas C. Brachert. The project was funded by the German Research Foundation (DFG) via grants BR 1153/9-1, 9-2 and 9-3, and was affiliated to the Johannes Gutenberg-Universität Mainz and Universität Leipzig, respectively. In addition, radiogenic isotope and trace element data were measured at the Max-Planck-Institut für Chemie at Mainz. This thesis consists of three manuscripts including R. Mertz-Kraus as first author and are published or in press with international journals applying peer review systems:

- (1) **Mertz-Kraus, R.**, Brachert, T.C., Reuter, M., 2008. *Tarbellastraea* (Scleractinia): A new stable isotope archive for Late Miocene paleoenvironments in the Mediterranean. *Palaeogeography, Palaeoclimatology, Palaeoecology*, 257(3): 294-307.
- (2) **Mertz-Kraus, R.**, Brachert, T.C., Reuter, M., Galer, S.J.G., Fassoulas, C., Iliopoulos, G., 2009. Late Miocene sea surface salinity variability and paleoclimate conditions in the Eastern Mediterranean inferred from coral aragonite $\delta^{18}\text{O}$. *Chemical Geology*, doi:10.1016/j.chemgeo.2009.01.010.
- (3) **Mertz-Kraus, R.**, Brachert, T.C., Jochum, K.P., Reuter, M., Stoll, B., 2009. LA-ICP-MS analyses on coral growth increments reveal heavy winter rain in the Eastern Mediterranean at 9 Ma. *Palaeogeography, Palaeoclimatology, Palaeoecology*, doi:10.1016/j.palaeo.2008.11.015.

In all cases, sample preparation, isotope (except of oxygen and carbon), trace element and further analytical work, data evaluation and interpretation as well as writing of the manuscripts were done by the first author. The complete analytical data set relevant for the thesis is provided as supplementary material on a data CD (Appendix A to C). Besides publication in peer-reviewed journals, results of the thesis were presented by 16 talks and poster presentations at several international conferences and workshops (Appendix D).

Content

Erklärung.....	V
Preface	I
Content.....	III
Summary	V
Kurzfassung.....	VII
1. Introduction	1
1.1. Mediterranean climate: Present and past.....	2
1.2. Late Miocene paleogeography of the Mediterranean region.....	4
1.3. Investigating past environments	5
1.3.1. Proxies and archives.....	5
1.3.2. Non-chemical proxies.....	6
1.3.3. Traditional stable isotope ratios	7
1.3.4. Non-traditional stable isotope ratios	8
1.3.5. Element concentrations and ratios	9
1.4. Environmental reconstructions for the Late Miocene Mediterranean	11
1.5. References	12
2. <i>Tarbellastraea</i> (Scleractinia): A new stable isotope archive for Late Miocene paleoenvironments in the Mediterranean.....	21
2.1. Abstract	22
2.2. Introduction	23
2.2.1. General.....	23
2.2.2. Geologic setting	26
2.2.3. Sampling sites	27
2.3. Material and methods.....	28
2.3.1. Sampling techniques.....	28
2.3.2. Stable isotopes and data analysis	31
2.4. Results	33
2.4.1. Preservation	33
2.4.2. Isotope records.....	33
2.4.3. Tortonian stable isotope records	34
2.4.4. Early Messinian stable isotope records	36
2.5. Discussion.....	36
2.6. Conclusion.....	40
2.7. References	40
3. Late Miocene sea surface salinity variability and paleoclimate conditions in the Eastern Mediterranean inferred from coral aragonite $\delta^{18}\text{O}$	47
3.1. Abstract	48
3.2. Introduction	49
3.3. Geological context	52
3.4. Sampling sites.....	53
3.5. Material and methods.....	56
3.5.1. Sample preparation.....	56
3.5.2. Radiogenic strontium isotope analyses	58
3.5.3. Stable isotope analyses and data processing.....	58

3.6. Results	60
3.6.1. Radiogenic strontium isotope ratios.....	60
3.6.2. Stable oxygen isotope ratios.....	62
3.7. Discussion	65
3.7.1 Radiogenic strontium isotope ratios.....	65
3.7.2. Mean annual $\delta^{18}\text{O}$ compositions.....	66
3.7.3. Mean seasonal $\delta^{18}\text{O}$ amplitudes.....	71
3.7.4. Spectral analysis.....	73
3.8. Conclusions	74
3.9. References	75
4. LA-ICP-MS analyses on coral growth increments reveal heavy winter rain in the Eastern Mediterranean at 9 Ma.....	81
4.1. Abstract	82
4.2. Introduction	83
4.3. Geological setting and sampling site	86
4.4. Material and methods.....	88
4.4.1. Sample description.....	88
4.4.2. Scanning electron microscope (SEM), X-ray diffraction (XRD), and X-ray fluorescence (XRF) analyses.....	88
4.4.3. Laser ablation ICP mass spectrometry	90
4.5. Results.....	96
4.5.1. Coral preservation.....	96
4.5.2. Mineralogical and chemical compositions of the insoluble residue	96
4.5.3. Coral trace element concentrations	98
4.6. Discussion	100
4.6.1. Sr/Ca and U/Ca	100
4.6.2. Non-lattice bound elements and insoluble residue	103
4.6.3. Sources of the insoluble residue	104
4.6.4. Relation between geochemical pattern and climate.....	109
4.7. Conclusions	110
4.8. References	111
Acknowledgements	121
Appendix.....	123
Appendix A: Stable oxygen and carbon isotope data.....	124
Appendix B: Radiogenic strontium isotope data.....	125
Appendix C: LA-ICP-MS data.....	126
Appendix D: Conference and workshop contributions	127

Summary

The present-day climate in the Mediterranean region is characterized by mild, wet winters and hot, dry summers. There is contradictory evidence as to whether the present-day conditions (“Mediterranean climate”) already existed in the Late Miocene. This thesis presents seasonally-resolved isotope and element proxy data obtained from Late Miocene reef corals from Crete (Southern Aegean, Eastern Mediterranean) in order to illustrate climate conditions in the Mediterranean region during this time. There was a transition from greenhouse to icehouse conditions without a Greenland ice sheet during the Late Miocene. Since the Greenland ice sheet is predicted to melt fully within the next millennia, Late Miocene climate mechanisms can be considered as useful analogues in evaluating models of Northern Hemispheric climate conditions in the future.

So far, high resolution chemical proxy data on Late Miocene environments are limited. In order to enlarge the proxy database for this time span, coral genus *Tarbellastraea* was evaluated as a new proxy archive, and proved reliable based on consistent oxygen isotope records of *Tarbellastraea* and the established paleoenvironmental archive of coral genus *Porites*. In combination with lithostratigraphic data, global $^{87}\text{Sr}/^{86}\text{Sr}$ seawater chronostratigraphy was used to constrain the numerical age of the coral sites, assuming the Mediterranean Sea to be equilibrated with global open ocean water. $^{87}\text{Sr}/^{86}\text{Sr}$ ratios of *Tarbellastraea* and *Porites* from eight stratigraphically different sampling sites were measured by thermal ionization mass spectrometry. The ratios range from 0.708900 to 0.708958 corresponding to ages of 10 to 7 Ma (Tortonian to Early Messinian).

Spectral analyses of multi-decadal time-series yield interannual $\delta^{18}\text{O}$ variability with periods of ~ 2 and ~ 5 years, similar to that of modern records, indicating that pressure field systems comparable to those controlling the seasonality of present-day Mediterranean climate existed, at least intermittently, already during the Late Miocene. In addition to sea surface temperature (SST), $\delta^{18}\text{O}$ composition of coral aragonite is controlled by other parameters such as local seawater composition which as a result of precipitation and evaporation, influences sea surface salinity (SSS). The Sr/Ca ratio is considered to be independent of salinity, and was used, therefore, as an additional proxy to estimate seasonality in SST. Major and trace element concentrations in coral aragonite determined by laser ablation inductively coupled plasma mass spectrometry yield significant variations along a transect perpendicular to coral growth increments, and record varying environmental conditions. The comparison between the average SST seasonality of 7°C and 9°C , derived from average annual $\delta^{18}\text{O}$ (1.1‰) and Sr/Ca (0.579 mmol/mol) amplitudes,

respectively, indicates that the $\delta^{18}\text{O}$ -derived SST seasonality is biased by seawater composition, reducing the $\delta^{18}\text{O}$ amplitude by 0.3‰. This value is equivalent to a seasonal SSS variation of 1‰, as observed under present-day Aegean Sea conditions.

Concentration patterns of non-lattice bound major and trace elements, related to trapped particles within the coral skeleton, reflect seasonal input of suspended load into the reef environment. $\delta^{18}\text{O}$, Sr/Ca and non-lattice bound element proxy records, as well as geochemical compositions of the trapped particles, provide evidence for intense precipitation in the Eastern Mediterranean during winters. Winter rain caused freshwater discharge and transport of weathering products from the hinterland into the reef environment.

There is a trend in coral $\delta^{18}\text{O}$ data to more positive mean $\delta^{18}\text{O}$ values (−2.7‰ to −1.7‰) coupled with decreased seasonal $\delta^{18}\text{O}$ amplitudes (1.1‰ to 0.7‰) from 10 to 7 Ma. This relationship is most easily explained in terms of more positive summer $\delta^{18}\text{O}$. Since coral diversity and annual growth rates indicate more or less constant average SST for the Mediterranean from the Tortonian to the Early Messinian, more positive mean and summer $\delta^{18}\text{O}$ indicate increasing aridity during the Late Miocene, and more pronounced during summers.

The analytical results implicate that winter rainfall and summer drought, the main characteristics of the present-day Mediterranean climate, were already present in the Mediterranean region during the Late Miocene. Some models have argued that the Mediterranean climate did not exist in this region prior to the Pliocene. However, the data presented here show that conditions comparable to those of the present-day existed either intermittently or permanently since at least about 10 Ma.

Kurzfassung

Milde, feuchte Winter und heiße, trockene Sommer sind kennzeichnend für das heutige Klima im Mittelmeerraum. Die Frage, ob dieses „Mittelmeerklima“ bereits im späten Miozän (Torton und frühes Messin) vorherrschend war, wird konträr diskutiert. In der vorliegenden Arbeit werden an spätmiozänen Riffkorallen Kretas (südliche Ägäis, östliches Mittelmeer) gemessene, saisonal aufgelöste Isotopen- und Elementdaten vorgestellt, die Rückschlüsse auf die klimatischen Bedingungen im Mittelmeerraum während dieser Zeit erlauben. Diese Fragestellung ist für Modellierungen zukünftiger Klimaentwicklungen relevant, weil während des späten Miozäns ein Übergang von „Treibhaus“- zu „Eishaus“-Bedingungen stattfand, wobei die Eisbedeckung Grönlands noch nicht ausgebildet war. Da für den heutigen Grönländischen Eisschild ein Abschmelzen innerhalb der nächsten Jahrtausende vorhergesagt wird, kann das Verständnis spätmiozäner Klimamechanismen dazu dienen, Simulationen des zukünftigen Klimas der Nordhemisphäre zu überprüfen.

Hochaufgelöste chemische Proxydaten, die Aussagen über Umweltbedingungen im späten Miozän erlauben, standen bisher nur in geringem Maße zur Verfügung. Um diese Datenbasis zu erweitern, wurde mit der Korallengattung *Tarbellastraea* ein neues Proxyarchiv erschlossen. Die geologische Signifikanz der Proxydaten des neuen Archivs wurde unter anderem durch konsistente Sauerstoffisotopen-Datensätze von *Tarbellastraea* und der Korallengattung *Porites* nachgewiesen, die ein etabliertes spätmiozänes Umweltarchiv darstellt. Lithostratigraphische Daten und globale $^{87}\text{Sr}/^{86}\text{Sr}$ -Meerwasserchronostratigraphie erlauben eine numerische Kalibrierung der stratigraphischen Position der Beprobungslokationen der Korallen. Die $^{87}\text{Sr}/^{86}\text{Sr}$ -Verhältnisse der Gattungen *Tarbellastraea* und *Porites* aus acht stratigraphisch unterschiedlichen Fundstellen wurden mittels Thermionen-Massenspektrometrie gemessen und variieren zwischen 0,708900 und 0,708958. Dies entspricht einem Altersbereich zwischen 10 und 7 Ma (Torton bis frühes Messin).

Spektralanalysen von multidekadischen $\delta^{18}\text{O}$ -Zeitreihen liefern interannuelle Variabilitäten mit Perioden von ~ 2 und ~ 5 Jahren. Die Vergleichbarkeit mit rezenten spektralen Mustern interannueller $\delta^{18}\text{O}$ -Variabilität deutet darauf hin, dass während des späten Miozäns zumindest zeitweise Luftdruckkonfigurationen bestanden, die denen entsprechen, die die Saisonalität des heutigen Mittelmeerklimas kontrollieren. Da die $\delta^{18}\text{O}$ -Zusammensetzung des Korallenaragonits nicht ausschließlich von der

Meeresoberflächentemperatur (SST), sondern auch von anderen Faktoren mit Auswirkungen auf die Salinität des Oberflächenwassers (SSS) gesteuert wird, wurde zusätzlich das Sr/Ca-Verhältnis als SSS-unabhängiger Parameter zur Bestimmung der SST-Saisonalität gemessen. Analysen mittels Laserablation-Massenspektrometrie mit induktiv gekoppeltem Plasma als Ionenquelle zeigen signifikante Konzentrationsvariationen in Haupt- und Spurenelementen entlang der Wachstumsrichtung der aragonitischen Korallenskelette, verursacht durch variierende Umweltbedingungen. Der Vergleich der SST-Saisonalitäten von 7°C und 9°C, ermittelt jeweils anhand der durchschnittlichen jährlichen $\delta^{18}\text{O}$ - und Sr/Ca-Amplituden von 1,1‰ beziehungsweise 0,579 mmol/mol, weist daraufhin, dass die $\delta^{18}\text{O}$ -basierte SST-Saisonalität durch Variationen der Meerwasserzusammensetzung beeinflusst ist. Die daraus resultierende Verringerung der jährlichen $\delta^{18}\text{O}$ -Amplituden des Korallenaragonits um 0,3‰ entspricht einer saisonalen SSS-Variation von 1‰, die mit heutigen Verhältnissen in der Ägäis vergleichbar ist.

Konzentrationsmuster von nicht im Aragonitgitter gebundenen Haupt- und Spurenelementen, die durch eingeschlossene mineralische Partikel verursacht sind, weisen auf saisonalen Partikeltransport in den Riffbereich hin. $\delta^{18}\text{O}$, Sr/Ca und Elementkonzentrationsmuster, sowie die chemische Zusammensetzung der sedimentären Partikel zeigen, dass im spätmiozänen östlichen Mittelmeer Starkregenereignisse während der Wintermonate auftraten, die Verwitterungsprodukte aus dem Hinterland in den Riffbereich verfrachtet haben.

Zwischen 10 und 7 Ma ändert sich die $\delta^{18}\text{O}$ -Zusammensetzung der kretischen Korallen, wobei die Mittelwerte von $-2,7\text{‰}$ auf $-1,7\text{‰}$, bei einer gleichzeitigen Abnahme der jährlichen Amplitude von 1,1‰ auf 0,7‰, ansteigen. Dieser Trend lässt sich im Wesentlichen durch zunehmend positivere Sommer-Werte erklären. Da Korallendiversität und jährliche Wachstumsraten darauf hinweisen, dass im Mittelmeer die SST im Verlauf des späten Miozäns weitestgehend konstant war, impliziert die $\delta^{18}\text{O}$ -Änderung zunehmend aride Bedingungen vor allem während des Sommers.

Die experimentellen Ergebnisse zeigen, dass Winterregen und Sommertrockenheit, Merkmale wie sie für das heutige Mittelmeerklima charakteristisch sind, bereits im späten Miozän im Mittelmeerraum auftraten. Im Gegensatz zum Modell einer pliozänen Entwicklung des heutigen Mittelmeerklimas, ist von mit heutigen Verhältnissen vergleichbaren Bedingungen auszugehen, die entweder kontinuierlich oder episodisch seit mindestens etwa 10 Ma existieren.

1. Introduction

1.1. Mediterranean climate: Present and past

A strong seasonality of precipitation determines the present-day climate of the Mediterranean region. This is reflected in hot and dry summers and wet winters, known as a typical “Csa climate” according to the classification of Köppen (1931). Such Csa climates are characterized by less than 40 mm precipitation in the driest month and more than three times as much precipitation in the wettest month compared to the driest month. Usually, this type of climate in the mid-latitudes both north and south of the subtropical climate zone is termed Mediterranean climate (e.g., Lionello et al., 2006). Beside the Mediterranean region, this climate type also predominates coastal areas of California, South Africa and southern parts of Australia. For all regions with Mediterranean climate there is alternating influence of the large subtropical semi-permanent centers of high atmospheric pressure at the Horse latitudes (subtropical high) between 30 and 35° both north and south, in summer and the semi-permanent centers of low atmospheric pressure (subpolar low) during winter causes the seasonality of precipitation. In the special case of the Mediterranean region, during summer, the subtropical Azores High shifts polarward, resulting in higher temperature and little rainfall. In winter, it moves back towards the equator contemporaneously scaling down its dimension. As a consequence, the climate in the Mediterranean becomes more influenced by the subpolar Icelandic Low and the associated Westerlies, representing the prevailing winds in the mid-latitudes. The Westerlies transport humid air eastward by passing over the water surface of the North Atlantic. Related to the Westerlies are mid-latitude cyclones with periodic storms reaching the Mediterranean region bringing the majority of the annual precipitation to the Mediterranean region during the winter months. These winter cyclones are the dominant source of, e.g., Middle Eastern rainfall and river runoff. At present-day, precipitation data of Crete and Greece provided by the National Data Bank of Hydrological & Meteorological Information of Greece (NDBHMI, <http://ndbhmi.chi.civil.ntua.gr>) indicate annual precipitation ranging from about 300 to 900 mm and 300 to 1300 mm, respectively, with the majority of precipitation during the period from October until March.

The North Atlantic Oscillation (NAO) which describes the fluctuation of sea level pressure difference between the Icelandic Low and the Azores High is known to be one of the major sources of interannual variability of weather and climate around the world (e.g., Hurrell and Van Loon, 1997). The present-day winter climate of the Mediterranean region is subject to certain interannual alternations caused by the NAO (Hurrell, 1995). The strength of the NAO is reflected by the NAO-index which is defined as the difference of the normalized mean winter sea level pressure anomalies in the center of the Icelandic Low

(Stykkisholmur, Iceland) and the Azores High (Lisbon, Portugal), respectively (Hurrell, 1995). In years with a positive NAO-index, when the difference between Icelandic Low and the Azores High is greater than average (Hurrell and Van Loon, 1997), the Westerlies are stronger and shifted northward. This causes more humid and warmer winters in Central Europe, but cooler and drier winters in the Mediterranean region (Hurrell, 1995). For instance, it has been observed that during positive NAO years, Turkey becomes significantly cooler and drier (Cullen and deMenocal, 2000). In contrast, during a negative NAO-index phase, the Westerlies and humid air masses reach the Mediterranean region until Turkey and the Middle East, resulting in winters with humid conditions in these areas (Cullen and deMenocal, 2000). Additionally, the very dry conditions during the summer months in the Eastern Mediterranean region are likely to be related to the Asian monsoon regime (Rodwell and Hoskins, 1996).

The climate of the Mediterranean region during the Late Miocene is generally assumed to have been subtropical and warm. Consistently, Miocene climate model simulations indicate warmer and but also drier conditions than today for the Mediterranean region (Micheels et al., 2007). However, based on estimates from herpetofaunal assemblages, Böhme et al. (2008) used the term “washhouse climate” for the Late Miocene climate of large parts of Europe including the western part of the Mediterranean Basin at around 9 and 10 Ma. This washhouse climate was suggested to be associated with global warm conditions and several times more precipitation than present-day. In contrast, terrestrial Tortonian paleoflora of Crete indicate annual precipitation rates of approximately 700 to 1000 mm (Bruch et al., 2006) comparable to present-day conditions in Greece. However, little is known on the annual distribution of the precipitation for the Late Miocene. On the basis of palynological data, the modern climate in the Mediterranean region with strong seasonality of precipitation causing hot and dry summers and mild and wet winters is assumed to have not been established prior to ca. 3.6 Ma (Suc, 1984; Suc and Popescu, 2005). In contrast to this assumption, there is evidence compiled by Tzedakis (2007) that the modern Mediterranean climate has been developed pre-Pliocene: (1) The evergreen sclerophylls dominating modern Mediterranean-type climates already appeared during the Oligocene and Miocene (Mai, 1989; Palamarev, 1989); (2) Over the past 11 Myr, $\delta^{13}\text{C}$ of soil carbonates and mammalian tooth enamel refer to a domination of C3 over C4 plants in the Eastern Mediterranean region (Quade et al., 1994) including woodland settings in a winter rainfall regime with mean annual rainfall of 300 to 1000 mm; (3) Similarity to the modern pressure field systems of the Northern Hemisphere is indicated by pressure field

modeling tested with a multidecadal $\delta^{18}\text{O}$ time series from a Tortonian coral (Brachert et al., 2006b); (4) In response to uplift of the Himalayan-Tibetan plateau, the onset of the Indian monsoon contributing to the intensification of seasonal contrasts in precipitation in the Mediterranean, occurred ~ 9 Myr ago (Prell and Kutzbach, 1992; Zhisheng et al., 2001). Also, based on evidence from vegetational changes, Akgün et al. (2007) supported the assumption of a pre-Pliocene development of the Mediterranean-type climate by postulating a warm temperate climate with dry seasons in the Late Miocene in Anatolia (Turkey). The increase of xeromorphic taxa within a Tortonian plant assemblage from northwestern Crete indicates the beginning development of summer drought (Zidianakis et al., 2007?), likewise. For some regions in Spain, Casanovas-Vilara and Agustí (2007) concluded that pollen data, macromammal faunas and the interpretations based on rodent assemblages indicate the presence of open environments with a certain seasonality in humidity in those areas during the Late Miocene. Furthermore, it appears that present-day situation started to develop by the Late Vallesian (11.1 to 8.7 Ma, Late Miocene), although some regional climatic differentiation existed much earlier (Casanovas-Vilar and Agustí, 2007). This is in agreement with results of van Dam (2006) that the establishment of a dry summer season started in the Western Mediterranean at 10 to 8 Ma.

1.2. Late Miocene paleogeography of the Mediterranean region

During the Miocene, the Mediterranean region underwent substantial geodynamic changes (e.g., Harzhauser and Piller, 2007). While the Tethys connected the water masses of the Atlantic and the Pacific Oceans during the Oligocene and the Early Miocene, the collision between the Arabian Microplate and Eurasia, around 18 Myr ago, led to the closure of the Tethyan Seaway. This closure caused the separation between the Mediterranean Basin and the Indian Ocean (e.g., Rögl, 1998). However, short-lived connections existed intermittently until the around 14 Ma (Harzhauser et al., 2007). Essentially subduction-related melt formation processes during the Miocene in the eastern part of the Mediterranean basin were associated with volcanic activity occurring from about 10 to 7 Ma (Fytikas et al., 1984 and references therein).

Since Mesozoic to Tertiary times, convergence between Africa and Iberia led to an increasing isolation and the development of two marine gateways, the Betic and Rifan corridors, towards the Atlantic. As a result, the situation of the Mediterranean in the Late Miocene (Fig. 1) was very similar to the present-day configuration forming a semi-enclosed basin connected to the Atlantic in the west only through the Betic and Rifan corridors



Fig. 1: Outline map illustrating the Late Miocene paleogeography of the Mediterranean Basin and adjacent regions during the Tortonian at around 10 Ma (modified from Harzhauser and Piller, 2007).

(Kouwenhoven and van der Zwaan, 2006). During Late Miocene times, the closure of the Betic and Rifan corridors by interplay of tectonic and glacio-eustatic processes caused an increasing isolation of the Mediterranean basin. This triggered the "Messinian Salinity Crisis" (MSC), starting at 5.96 Ma (Krijgsman et al., 1999) when evaporites accumulated in the whole Mediterranean area during the Messinian between 5.96 and 5.33 Ma.

1.3. Investigating past environments

1.3.1. Proxies and archives

A proxy (short for proxy variable) is an analytically measurable variable used to infer the value of a parameter of interest. In climate research, prominent examples are element concentration ratios or traditional and non-traditional stable isotope ratios for deriving past ocean temperatures. Such proxies preserved in incremental growing biota (e.g., corals) as well as organic biomarkers (e.g., alkenones) are used to monitor changes of a variety of environmental parameters in the ocean waters over time (Wefer et al., 1999 and

references therein). Reef-building corals composed of aragonitic CaCO_3 are excellent climate archives providing continuous incremental records, often of multidecadal length, over their whole lifetime. They are highly sensitive not only to changes in sea surface temperature (SST), but also to sea surface salinity (SSS) and further oceanographic parameters (e.g., Druffel, 1997). Despite the advantage of covering larger time intervals, alternative environmental archives, e.g., cores from sea sediments, include problematic aspects: Their time resolution is low and they can be affected by bioturbation, which distorts the original sedimentary record. Therefore, proxy data from sclerochronological multidecadal records (e.g., corals, bivalves) appear to be more effective in reconstructing past environmental variability on subannual as well as interannual time scales (Swart, 1983; Gagan et al., 2000; Schöne et al., 2003).

Essential for the estimation of past oceanographic conditions is the quality of the preservation of the selected archive. One limiting factor for paleoenvironmental reconstructions from aragonitic archives such as coral skeletons is their susceptibility to chemical and microstructural alteration in most diagenetic environments (Land, 1967; Dullo, 1984; Constantz, 1986). Diagenetic modification disturbs the original geochemical proxy records reflecting environmental conditions (Tudhope et al., 2001; McGregor and Gagan, 2003). During diagenesis, selective removal of skeletal material or the formation of secondary calcium carbonate affects the quality of the proxy archive. For instance, secondary inorganic aragonite precipitated in skeletal pore spaces is enriched in ^{18}O , Sr and U relative to the original coral aragonite (e.g., Hendy et al., 2007). The related proxies measured on altered material would, therefore, indicate cooler SST than the original aragonite skeleton. Accordingly, reconstructions of seasonal to interannual climate variability from proxy records derived from fossil reef corals, in particular from the pre-Pleistocene, are still exceedingly rare.

1.3.2. Non-chemical proxies

There are factors influencing the growth of coral skeletons such as light, depth, sediment input, and water turbidity. However, the annual growth rates from corals growing in shallow waters (5 to 15 m depth) with normal ocean salinities are mainly dependent from SST (Druffel, 1997). Even in cases where the complete coral skeleton is transformed into calcite, so-called ghost structures of the annual growth increments are often preserved (e.g., Shinn, 1966; Insalaco, 1996; Reuter et al., 2005). For that reason, the annual growth rates of coral skeletons provide a non-chemical proxy for the reconstruction of paleo-SST (Lough

and Barnes, 2000; Brachert et al., 2006a). This proxy is indicative for minimum, maximum as well as average annual SST independent from the preservation mode of the coral skeleton.

Based on the species–energy theory (Wright, 1983) which is in agreement with earlier evidence on variation in diversity (e.g., Brown, 1981), studies on modern reefs have shown that the number of coral genera composing a reef community (generic richness) is mainly related to the available energy represented by the mean annual SST but also minimum and maximum SST (Fraser and Currie, 1996). Consequently, Rosen (1999) applied the generic richness of coral reefs as a proxy for reconstructing absolute SST values for past time periods. Recently, this proxy has been successfully adapted to Oligocene and Miocene stages in the Mediterranean (Bosellini and Perrin, 2008). This approach allows temperature estimates between 15 and 28°C with a resolution of <1°C and goes well beyond the simple interpretation that environments with corals are associated to a warm climate.

1.3.3. Traditional stable isotope ratios

A variety of isotope and element proxies are applied to infer environmental parameters using aragonitic-preserved coral skeletons. Oxygen isotope ratios in biogenic and anorganic carbonates represent an established traditional stable isotope system used as paleotemperature indicator (e.g., O'Neil et al., 1969; Shackleton, 1974). The temperature dependence in O isotope variation is based on the thermodynamic fractionation between ^{16}O and ^{18}O occurring during precipitation (Urey, 1947; Epstein et al., 1953; Grossman and Ku, 1986). The resulting stable oxygen isotope ratio expressed as $\delta^{18}\text{O}$ (defined as $[(^{18}/^{16}\text{O}_{\text{sample}} / ^{18}/^{16}\text{O}_{\text{standard}}) - 1] \times 1000$ reported in per mill) is one of the most used proxies for reconstructing paleo-SST (e.g., Corrège, 2006; Grottoli and Eakin, 2007). Since corals precipitate the aragonite out of equilibrium with the surrounding seawater, their skeletons are depleted in $\delta^{18}\text{O}$ relative to abiotic aragonite precipitated from the same seawater due to the so-called “vital effect” (Urey et al., 1951; McConnaughey, 1989). For instance, during fast calcification, significant kinetic fractionation occurs resulting in a depletion of the fast growing portions of the skeleton in ^{18}O compared to the slower growing portions (Land et al., 1975; McConnaughey, 1989). Consistently, Felis et al. (2003) found a strong dependence of the mean coral $\delta^{18}\text{O}$ on the mean extension rate at rates of less than 6mm/year. Biological processes during precipitation cause different isotopic compositions in different skeletal structural components (Meibom et al., 2006). However, several studies have demonstrated that the most important factors causing variations in the $\delta^{18}\text{O}$

composition of the skeletal carbonate of corals are temperature and isotopic composition of ambient seawater (e.g., Weber and Woodhead, 1970; 1972; Druffel, 1997; Gagan et al., 2000). Empirical studies have shown, that at constant $\delta^{18}\text{O}$ composition of seawater, an increase of 1°C in SST is coupled to a decrease in coral $\delta^{18}\text{O}$ of 0.18‰ to 0.22‰ (Druffel, 1997; Corrège, 2006). However, the $\delta^{18}\text{O}$ of ambient seawater is dependent on the mean $\delta^{18}\text{O}$ of seawater related to the amount of continental ice which is enriched in ^{16}O varying on timescales of 10^4 to 10^5 years (Epstein and Mayeda, 1953; Schrag et al., 1996). Additionally, the balance between precipitation/river discharge and evaporation in a distinct basin affects the $\delta^{18}\text{O}$ of seawater. The interaction between seafloor-basalt and seawater on mid-ocean ridge spreading centers due to hydrothermal circulation changing the $\delta^{18}\text{O}$ of the upper portions of the oceanic crust appears to be of no relevance because of buffering processes (Gregory and Taylor, 1981). Summarizing, in regions with low variations in seawater composition coral $\delta^{18}\text{O}$ reflects mainly SST variations. In regions with enhanced seasonality in precipitation or evaporation, modifying SSS and seawater $\delta^{18}\text{O}$, respectively, seasonal $\delta^{18}\text{O}$ records of coral skeletons are affected or even dominated by such changes in evaporation and precipitation (Cole et al., 1993; Quinn and Sampson, 2002). There are various relationships between $\delta^{18}\text{O}$ and SSS in ocean waters depending on local isotopic composition of rainfall and river water input (e.g., Corrège, 2006). Accordingly, in some cases there may be an uncertainty by the use of $\delta^{18}\text{O}$ as proxy for absolute as well as relative estimates of paleo-SST and paleo-SSS (Lea et al., 2003).

1.3.4. Non-traditional stable isotope ratios

Recently, the application of non-traditional stable isotope systems like $^{44}\text{Ca}/^{40}\text{Ca}$ (e.g., Nägler et al., 2000) or $^{88}\text{Sr}/^{86}\text{Sr}$ (e.g., Fietzke and Eisenhauer, 2006) as paleotemperature proxy was introduced and brought forward by the development of new mass spectrometry analytical techniques (multi collector inductively coupled plasma mass spectrometry and thermal ionization mass spectrometry using double or triple spike technique). These analytical techniques enable high-precision isotope ratio measurements resolving very subtle differences in isotope abundances. While a temperature dependence of Ca and Sr isotope fractionation during precipitation of calcite or aragonite has been demonstrated (Gussone et al., 2003; Marriott, 2004; Fietzke and Eisenhauer, 2006), Griffith et al. (2008) showed that these results cannot be generalized. Although they found consistent Ca temperature dependent fractionation of 0.013‰ per $^\circ\text{C}$ on seven species of planktonic foraminifera, other species did not show significant correlations between

temperature and $\delta^{44}\text{Ca}$ ($\delta^{44}\text{Ca} = [({}^{44/40}\text{Ca}_{\text{sample}} / {}^{44/40}\text{Ca}_{\text{standard}}) - 1] \times 1000$). As a cause for the temperature dependence of Ca isotope fractionation, temperature-dependent kinetic effects (Gussone et al., 2003), equilibrium fractionation (Marriott, 2004) or rate-controlled effects leading to the departure from hypothetical equilibrium $\text{Ca}^{2+} - \text{CaCO}_3$ isotope fractionation (Lemarchand, 2004) are suggested. Irrespective of the underlying mechanism causing apparent temperature-dependent isotope fractionation of non-traditional stable isotope systems, published results are promising and indicate a high potential as paleotemperature proxy.

1.3.5. Element concentrations and ratios

Element concentrations and ratios can provide information on paleoceanographic conditions. For instance, bivalent cations such as Mg^{2+} and Sr^{2+} are common in seawater and substitute Ca^{2+} on the basis of an ion-exchange reaction ($\text{CaCO}_3 + \text{X}^{2+} = \text{XCO}_3 + \text{Ca}^{2+}$) in biogenic carbonate precipitates. There is some controversy whether Sr^{2+} simply replaces Ca^{2+} in the aragonite lattice or resides in discrete strontianite (SrCO_3) domains (Greger et al., 1997). However, the substitution by these cations is not only dependent on the cation/Ca ratio in seawater. For instance, the Mg/Ca ratio in biogenic carbonate is a well-studied elemental proxy (e.g., Nürnberg, 1995; Rosenthal et al., 1997). The suitability for magnesium paleothermometry is based on the endothermic substitution of Mg in calcium carbonate, i.e., substitution is favored at higher temperatures. This applies to calcite as well as aragonite precipitated by foraminifera and corals (Rosenthal et al., 1997; Mitsuguchi 1996). For bivalve shells, however, only a weak dependence of Mg/Ca on temperature has been observed (Freitas et al., 2008). Beside Mg/Ca, also Sr/Ca and U/Ca are regarded to provide SST information independent from SSS in contrast to $\delta^{18}\text{O}$. The incorporation of Sr into the lattice appears to be mainly temperature dependent (Smith et al., 1979; Beck et al., 1992). However, Sr and U behave inversely compared to Mg, i.e., when SST increases Sr/Ca and U/Ca decrease. These proxies sometimes are used in combination with $\delta^{18}\text{O}$ to separate the coral $\delta^{18}\text{O}$ into the parts derived from SST and seawater compositional changes (McCulloch et al., 1994; Gagan et al., 1998). However, some studies have suggested that Sr/Ca in coral aragonite is not influenced by SST and the Sr/Ca composition of the ambient seawater alone (e.g., McCulloch et al., 1994; Alibert and McCulloch, 1997), but is also controlled by biological and kinetic effects (Allison et al., 2005). Additionally, growth and calcification rates (Goodkin et al., 2007) as well as symbiont activity (e.g., de Villiers et al., 1994; Cohen et al., 2001; 2002) affect the incorporation process. On glacial to interglacial

time scales the Sr/Ca composition of seawater has varied by 1 to 2 % caused by ice volume and sea level changes with higher values during glacial episodes (Stoll and Schrag, 1998) which is relevant in terms of long-term records of Sr/Ca for paleo-SST reconstructions. U also can replace Ca in the aragonite lattice (Amiel et al., 1973). However, dissolved U in seawater most frequently occurs as complexed uranyl carbonate ions (Djogic et al., 1986; Reeder et al., 2000). Their charge and ionic radius argue against a substitution of single Ca^{2+} cations in the aragonite lattice (Shen and Dunbar, 1995; Lazar et al., 2004) and substitution of complete CaCO_3 groups in the aragonite lattice by $\text{UO}_2(\text{CO}_3)_2^{2-}$ appears more plausible (Swart and Hubbard, 1982; Shen and Dunbar, 1995). For U/Ca, the incorporation process appears to be more complex than for Sr/Ca, therefore complicating the relationship between SST and U/Ca. Beside temperature (Min et al., 1995), additional parameter influencing the U incorporation into the coral skeleton are SSS, pH and the carbonate concentration of ocean water (Shen and Dunbar, 1995; Sinclair et al., 1998). For the aforementioned reasons, SST estimations for geological time periods based on chemical proxy records assuming conditions comparable with today could be biased. Combining diverse proxies appears to be the best approach in order to minimize bias.

Besides SST and SSS variations, modern corals provide subannual-scale information on, e.g., river runoff (McCulloch et al., 2003; Sinclair and McCulloch, 2004), soil erosion (Fleitmann et al., 2007), mining (Fallon et al., 2002) or pollution (Munksgaard et al., 2004). In these cases, information is based on variations of trace element concentrations within the coral aragonite. Aside from substituting for Ca within the aragonite lattice, chemical elements can also be incorporated as non-lattice bound components of the coral skeleton calcium carbonate in terms of constituents of detrital particles trapped in skeletal porosity. They are, e.g., taken up by feeding (Fallon et al., 2002) or passed through paracellular pathways between cells in the calicoblastic epithelium opening and closing due to polyp movement (Erez and Braun, 2007). Such particles in coral skeletons may indicate spatial and temporal variations in composition and amount of suspended material in surrounding water masses (Barnard et al., 1974; Naqvi, 1994; Neil et al., 1994). Besides riverine input, increasing the amount of suspended detrital particles in the reef environment, such non-lattice bound components can be related to subaerial explosive volcanic activity (Heikoop et al., 1996) or dust deposition into the ocean (LaVigne and Sherrell, 2006).

1.4. Environmental reconstructions for the Late Miocene Mediterranean

Since seasonality in precipitation is a major relevant characteristic of the present-day Mediterranean climate, seasonally resolved proxy records of the Miocene are of interest to derive environmental conditions of this time period. With regard to future environmental development relevant for mankind, the Late Miocene including a geographic configuration comparable to present-day is of importance because it represents a time of transition between greenhouse and icehouse conditions without a Greenland ice sheet (e.g., Zachos et al., 2001). The present-day Greenland ice sheet, predicted to deglaciate within the next millennia (e.g., Gregory et al., 2004), plays an important role in the Northern Hemisphere's climate system (e.g., Hurrell, 1995; Thompson and Wallace, 2001). Therefore, knowledge about environmental conditions such as seasonal variability in a world without Greenland ice sheet is of particular interest. Environmental dynamics during the Late Miocene, when the Greenland ice sheet had not yet formed, can serve as a past analogue relevant for climate modeling extrapolations to future times. However, seasonally resolved proxy data of the pre-3.6 Ma climate are rare because suitable geological archives are barely available. So far, mainly long-term records with a temporal resolution of several thousand years based on deep-sea sediments and foraminifera as proxy archives are provided (e.g., van der Zwaan and Gudjonsson, 1986). Exceptions are subannually-resolved $\delta^{18}\text{O}$ records of Late Miocene 10 Ma-old *Porites* skeletons from Crete in the Eastern Mediterranean (Brachert et al., 2006b). In the following, a combination of non-chemical, stable isotope as well as element proxies of seasonally resolved coral records and early marine carbonate cements both from shallow reef environments, is used to enlighten the climate conditions – annual seasonality as well as climatic extremes – and their development during the Late Miocene prior to the MSC in the Eastern Mediterranean.

In the following, a short introduction into the major paleoenvironmental aspects covered in this thesis is given:

Chapter 2: Coral reef communities of the Miocene Mediterranean were dominated by two genera: *Porites* and *Tarbellastrea*. The latter was widespread in the Mediterranean since the Oligocene, but became extinct during the Messinian. While *Porites* is an established proxy archive for paleoenvironmental studies, the potential of *Tarbellastraea* as a proxy archive, is unanswered. The aim of this chapter is to clarify whether proxy data from massive *Tarbellastraea* are geochemical and

paleoenvironmental meaningful. For that purpose stable oxygen isotope data of *Tarbellastraea* and *Porites* recovered from the same beds are compared and evaluated.

Chapter 3: Corals from eight sampling levels of Tortonian and Messinian age from Crete serve as basis to monitor pre-MSC environmental changes in the Eastern Mediterranean. The objectives are to determine the time-interval represented by the distinct levels applying $^{87}\text{Sr}/^{86}\text{Sr}$ seawater chronostratigraphy, and test whether the oxygen isotope composition of the analyzed *Porites* and *Tarbellastraea* reef corals document significant changes in mean annual $\delta^{18}\text{O}$ as well as in mean $\delta^{18}\text{O}$ seasonality during the course of the Late Miocene. Such variations provide information on the development of SST, seawater composition or SSS, respectively. Spectral analyses of multi-decadal time-series are used to reveal interannual $\delta^{18}\text{O}$ variability. Comparisons of the Miocene and modern interannual patterns allow to link the Miocene patterns to possible atmospheric pressure field configurations.

Chapter 4: Variations in trace element compositions measured using laser ablation inductively coupled plasma mass spectrometry (LA-ICP-MS) on coral material are supposed to complement the knowledge derived from stable isotope analyses on Late Miocene corals from Crete. The comparison of $\delta^{18}\text{O}$, Sr/Ca and U/Ca seasonality as well as SST seasonalities derived from these proxies clarifies if the annual $\delta^{18}\text{O}$ amplitudes only reflect SST seasonality or if they are biased by changes in seawater composition. Since the reef environment at the sampling location is assumed to be under the influence of a deltaic setting, variations in the element concentrations related to sediment input may provide information on variability of freshwater discharge into the reef environment.

1.5. References

- Akgün, F., Kayseri, M.S. and Akkiraz, M.S., 2007. Palaeoclimatic evolution and vegetational changes during the Late Oligocene-Miocene period in Western and Central Anatolia (Turkey). *Palaeogeography, Palaeoclimatology, Palaeoecology*, 253(1-2): 56-90.
- Alibert, C. and McCulloch, M.T., 1997. Strontium/calcium ratios in modern *Porites* corals from the Great Barrier Reef as a proxy for sea surface temperature: Calibration of the thermometer and monitoring of ENSO. *Paleoceanography*, 12(3): 345-363.

- Allison, N., Finch, A.A., Newville, M. and Sutton, S.R., 2005. Strontium in coral aragonite: 3. Sr coordination and geochemistry in relation to skeletal architecture. *Geochimica et Cosmochimica Acta*, 69(15): 3801-3811.
- Amiel, A.J., Miller, D.S. and Friedman, G.M., 1973. Incorporation of uranium in modern corals. *Sedimentology*, 20(4): 523-528.
- Barnard, L.A., Macintyre, I.G. and Pierce, J.W., 1974. Possible environmental index in tropical reef corals. *Nature*, 252(5480): 219-220.
- Beck, J.W., Edwards, R.L., Ito, E., Taylor, F.W., Récy, J., Rougerie, F., Joannot, P. and Henin, C., 1992. Sea-surface temperature from coral skeletal strontium/calcium ratios. *Science*, 257: 644-647.
- Böhme, M., Ilg, A. and Winklhofer, M., in press. Late Miocene "washhouse" climate in Europe. *Earth and Planetary Science Letters*.
- Bosellini, F.R. and Perrin, C., 2008. Estimating Mediterranean Oligocene-Miocene sea-surface temperatures: An approach based on coral taxonomic richness. *Palaeogeography Palaeoclimatology Palaeoecology*, 258(1-2): 71-88.
- Brachert, T.C., Reuter, M., Kroeger, K.F. and Lough, J., 2006a. Coral growth bands: A new and easy to use paleothermometer in paleoenvironment analysis and paleoceanography (late Miocene, Greece). *Paleoceanography* 21, PA4217.
- Brachert, T.C., Reuter, M., Felis, T., Kroeger, K.F., Lohmann, G., Micheels, A. and Fassoulas, C., 2006b. *Porites* corals from Crete (Greece) open a window into Late Miocene (10 Ma) seasonal and interannual climate variability. *Earth and Planetary Science Letters*, 245: 81-94.
- Brown, J.H., 1981. Two decades of Homage to Santa Rosalia: Towards a general theory of diversity. *American Zoologist*, 21(4): 877-888.
- Bruch, A.A., Utescher, T., Mosbrugger, V., Gabrielyan, I. and Ivanov, D.A., 2006. Late Miocene climate in the circum-Alpine realm - a quantitative analysis of terrestrial palaeofloras. *Palaeogeography, Palaeoclimatology, Palaeoecology*, 238: 270-280.
- Casnovas-Vilar, I. and Agustí, J., 2007. Ecogeographical stability and climate forcing in the Late Miocene (Vallesian) rodent record of Spain. *Palaeogeography, Palaeoclimatology, Palaeoecology*, 248(1-2): 169-189.
- Cohen, A.L., Layne, G.D., Hart, S.R. and Lobel, P.S., 2001. Kinetic control of skeletal Sr/Ca in a symbiotic coral: Implications for the paleotemperature proxy. *Paleoceanography*, 16(1): 20-26.
- Cohen, A.L., Owens, K.E., Layne, G.D. and Shimizu, N., 2002. The effect of algal symbionts on the accuracy of Sr/Ca paleotemperatures from coral. *Science*, 296: 331-333.
- Cole, J.E., Fairbanks, R.G. and Shen, G.T., 1993. Recent Variability in the Southern Oscillation: Isotopic Results from a Tarawa Atoll Coral. *Science*, 260(5115): 1790-1793.
- Constantz, B.R., 1986. The primary surface area of corals and variations in their susceptibility to diagenesis. In: Schroeder, J.H. and Purser, B.H. (Editors), *Reef Diagenesis*. Springer-Verlag, New York, pp. 53-76.
- Corrège, T., 2006. Sea surface temperature and salinity reconstruction from coral geochemical tracers. *Palaeogeography, Palaeoclimatology, Palaeoecology*, 232(2-4): 408-428.
- Cullen, H.M. and deMenocal, P.B., 2000. North Atlantic influence on Tigris-Euphrates streamflow. *International Journal of Climatology*, 20: 853-863.
- de Villiers, S., Shen, G.T. and Nelson, B.K., 1994. The Sr/Ca-temperature relationship in coralline aragonite: Influence of variability in $(\text{Sr}/\text{Ca})_{\text{seawater}}$ and skeletal growth parameters. *Geochimica et Cosmochimica Acta*, 58(1): 197-208.

- Djogic, R., Sipos, L. and Branica, M., 1986. Characterization of uranium(VI) in seawater. *Limnology and Oceanography*, 31(5): 1122-1131.
- Druffel, E.R.M., 1997. Geochemistry of corals: Proxies of past ocean chemistry, ocean circulation, and climate. *Proceedings National Academy of Sciences USA*, 94: 8354-8361.
- Dullo, W.-C., 1984. Progressive diagenetic sequence of aragonite structures: Pleistocene coral reefs and their modern counterparts on the eastern Red Sea coast, Saudi Arabia. *Palaeontographica Americana*, 54: 254-160.
- Epstein, S. and Mayeda, T., 1953. Variation of O¹⁸ content of waters from natural sources. *Geochimica et Cosmochimica Acta*, 4: 213-224.
- Epstein, S., Buchsbaum, R., Lowenstam, H.A. and Urey, H.C., 1953. Revised carbonate-water isotopic temperature scale. *Geological Society of America Bulletin*, 64: 1315-1326.
- Erez, J. and Braun, A., 2007. Calcification in hermatypic corals is based on direct seawater supply to the biomineralization site. *Geochimica et Cosmochimica Acta*, 71(15, Supplement 1): A260.
- Fallon, S.J., White, J.C. and McCulloch, M.T., 2002. *Porites* corals as a recorder of mining and environmental impacts: Misima Island, Papua New Guinea. *Geochimica et Cosmochimica Acta*, 66(1): 45-62.
- Felis, T., Pätzold, J. and Loya, Y., 2003. Mean oxygen-isotope signatures in *Porites* spp. corals: inter-colony variability and correction for extension-rate effects. *Coral Reefs*, 22: 328-336.
- Fietzke, J. and Eisenhauer, A., 2006. Determination of temperature-dependent stable strontium isotope (⁸⁸Sr/⁸⁶Sr) fractionation via bracketing standard MC-ICP-MS. *Geochemistry Geophysics Geosystems*, 7(8): Q08009.
- Fleitmann, D., Dunbar, R.B., McCulloch, M., Mudelsee, M., Vuille, M., McClanahan, T.R., Cole, J.E. and Eggins, S., 2007. East African soil erosion recorded in a 300 year old coral colony from Kenya. *Geophysical Research Letters*, 34: L04401.
- Fraser, R.H. and Currie, D.J., 1996. The Species Richness-Energy Hypothesis in a System Where Historical Factors Are Thought to Prevail: Coral Reefs. *The American Naturalist*, 148(1): 138.
- Freitas, P.S., Clarke, L.J., Kennedy, H.A. and Richardson, C.A., 2008. Inter- and intra-specimen variability masks reliable temperature control on shell Mg/Ca ratios in laboratory and field cultured *Mytilus edulis* and *Pecten maximus* (bivalvia). *Biogeosciences Discussions*, 5(1): 531-572.
- Fytikas, M., Innocenti, F., Manetti, P., Mazzuoli, R., Peccerillo, A. and Villari, L., 1984. Tertiary to Quaternary evolution of volcanism in the Aegean region. In: Dixon, J.E. and Robertson, A.H.F. (Editors), *The Geological Evolution of the Eastern Mediterranean*, Geological Society, London, Special Publications, 17 pp. 687-699.
- Gagan, M.K., Ayliffe, L.K., Beck, J.W., Cole, J.E., Druffel, E.R.M., Dunbar, R.B. and Schrag, D.P., 2000. New views of tropical paleoclimates from corals. *Quaternary Science Reviews*, 19: 45-64.
- Gagan, M.K., Ayliffe, L.K., Hopley, D., Cali, J.A., Mortimer, G.E., Chappell, J., McCulloch, M.T. and Head, M.J., 1998. Temperature and surface-ocean water balance of the mid-Holocene tropical eastern Pacific. *Science*, 279: 1014-1018.
- Goodkin, N.F., Hughen, K.A. and Cohen, A.L., 2007. A multicoral calibration method to approximate a universal equation relating Sr/Ca and growth rate to sea surface temperature. *Paleoceanography*, 22: PA1214.
- Gregor, R.B., Pingitore, N.E., Jr. and Lytle, F.W., 1997. Strontianite in Coral Skeletal Aragonite. *Science*, 275(5305): 1452-1454.

- Gregory, J.M., Huybrechts, P. and Raper, S.C.B., 2004. Threatened loss of the Greenland ice-sheet. *Nature*, 428: 616.
- Gregory, R.T. and Taylor, H.P., 1981. An oxygen isotope profile in a section of cretaceous oceanic crust, Samail ophiolite, Oman: evidence for $\delta^{18}\text{O}$ buffering of the oceans by deep (>5 km) seawater-hydrothermal circulation at mid-ocean ridges. *Journal of Geophysical Research*, 86(B4): 2737-2755.
- Griffith, E.M., Paytan, A., Kozdon, R., Eisenhauer, A., Ravelo, A.C., 2008. Influences on the fractionation of calcium isotopes in planktonic foraminifera. *Earth and Planetary Science Letters*.
- Grossman, E.L. and Ku, T.-L., 1986. Oxygen and carbon isotope fractionation in biogenic aragonite: temperature effects. *Chemical Geology (Isotope Geoscience Section)*, 59: 59-74.
- Grottoli, A.G. and Eakin, C.M., 2007. A review of modern coral $\delta^{18}\text{O}$ and $\Delta^{14}\text{C}$ proxy records. *Earth-Science Reviews*, 81(1-2): 67-91.
- Gussone, N., Eisenhauer, A., Heuser, A., Dietzel, M., Bock, B., Böhm, F., Spero, H.J., Lea, D.W., Bijma, J. and Nägler, T.F., 2003. Model for kinetic effects on calcium isotope fractionation ($\delta^{44}\text{Ca}$) in inorganic aragonite and cultured planktonic foraminifera. *Geochimica et Cosmochimica Acta*, 67(7): 1375-1382.
- Harzhauser, M. and Piller, W.E., 2007. Benchmark data of a changing sea -- Palaeogeography, Palaeobiogeography and events in the Central Paratethys during the Miocene. *Palaeogeography, Palaeoclimatology, Palaeoecology*, 253(1-2): 8-31.
- Harzhauser, M., Kroh, A., Mandic, O., Piller, W.E., Göhlich, U., Reuter, M. and Berning, B., 2007. Biogeographic responses to geodynamics: A key study all around the Oligo-Miocene Tethyan Seaway. *Zoologischer Anzeiger - A Journal of Comparative Zoology*, 246(4): 241-256.
- Heikoop, J.M., Tsujita, C.J., Risk, M.J. and Tomascik, T., 1996. Corals as proxy recorders of volcanic activity; evidence from Banda Api, Indonesia. *Palaios*, 11(3): 286-292.
- Hendy, E.J., Gagan, M.K., Lough, J.M., McCulloch, M.T. and deMenocal, P.B., 2007. Impact of skeletal dissolution and secondary aragonite on trace element and isotopic climate proxies in *Porites* corals. *Paleoceanography*, 22: PA4101.
- Hurrell, J.W., 1995. Decadal trends in the North Atlantic Oscillation: regional temperatures and precipitation. *Science*, 269: 676-679.
- Hurrell, J.W. and Van Loon, H., 1997. Decadal variations in climate associated with the North Atlantic Oscillation. *Climatic Change*, 36(3): 301-326.
- Insalaco, E., 1996. The use of Late Jurassic coral growth bands as palaeoenvironmental indicators. *Palaeontology*, 39(2): 413-431.
- Köppen, W., 1931. *Grundriss der Klimakunde*. De Gruyter, Berlin.
- Kouwenhoven, T.J. and van der Zwaan, G.J., 2006. A reconstruction of late Miocene Mediterranean circulation patterns using benthic foraminifera. *Palaeogeography, Palaeoclimatology, Palaeoecology*, 238: 373-385.
- Krijgsman, W., Hilgen, F.J., Raffi, I., Sierro, F.J. and Wilson, D.S., 1999. Chronology, causes and progression of the Messinian salinity crisis. *Nature*, 400: 652-655.
- Land, L.S., 1967. Diagenesis of skeletal carbonates. *Journal of Sedimentary Petrology*, 37: 914-930.
- Land, L.S., Lang, J.C. and Barnes, D.J., 1975. Extension rate: A primary control on the isotopic composition of West Indian (Jamaican) scleractinian reef coral skeletons. *Marine Biology*, 33(3): 221-233.
- LaVigne, M. and Sherrell, R.M., 2006. Sub-Annual Variations of Trace Elements in a *Montastrea* Coral (Martinique, Caribbean) Using a Novel ICP-MS Method: Potential for an Atmospheric Dust Proxy, 13th Ocean Science Meeting, Honolulu, Hawaii.

- Lazar, B., Enmar, R., Schossberger, M., Bar-Matthews, M., Halicz, L. and Stein, M., 2004. Diagenetic effects on the distribution of uranium in live and Holocene corals from the Gulf of Aqaba. *Geochimica et Cosmochimica Acta*, 68(22): 4583-4593.
- Lea, D.W., Heinrich, D.H. and Karl, K.T., 2003. Elemental and Isotopic Proxies of Past Ocean Temperatures, *Treatise on Geochemistry*. Pergamon, Oxford, pp. 1-26.
- Lemarchand, D., Wasserburg, G.J., Papanastassiou, D.A., 2004. Rate-controlled calcium isotope fractionation in synthetic calcite. *Geochimica et Cosmochimica Acta*, 68(22): 4665-4678.
- Lionello, P., Malanotte-Rizzoli, P., Boscolo, R., Alpert, P., Artale, V., Li, L., Luterbacher, J., May, W., Trigo, R., Tsimplis, M., Ulbrich, U., Xoplaki, E., 2006. The Mediterranean climate: An overview of the main characteristics and issues, *Developments in Earth and Environmental Sciences*, 4: 1-26.
- Lough, J.M. and Barnes, D.J., 2000. Environmental controls on growth of the massive coral *Porites*. *Journal of Experimental Marine Biology and Ecology*, 245: 225-243.
- Mai, D.H., 1989. Development and regional differentiation of the European vegetation during the Tertiary. *Plant Systematics and Evolution*, 162(1): 79-91.
- Marriott, C.S., Henderson, G.M., Belshaw, N.S., Tudhope, A.W., 2004. Temperature dependence of $\delta^7\text{Li}$, $\delta^{44}\text{Ca}$ and Li/Ca during growth of calcium carbonate. *Earth and Planetary Science Letters*, 222: 615-624.
- McConnaughey, T., 1989. ^{13}C and ^{18}O isotopic disequilibrium in biological carbonates: I. Patterns. *Geochimica Cosmochimica Acta*, 53: 151-162.
- McCulloch, M., Fallon, S., Wyndham, T., Hendy, E., Lough, J. and Barnes, D., 2003. Coral record of increased sediment flux to the inner Great Barrier Reef since European settlement. *Nature*, 421(6924): 727-730.
- McCulloch, M.T., Gagan, M.K., Mortimer, G.E., Chivas, A.R. and Isdale, P.J., 1994. A high-resolution Sr/Ca and $\delta^{18}\text{O}$ coral record from the Great Barrier Reef, Australia, and the 1982-1983 El Niño. *Geochimica et Cosmochimica Acta*, 58(12): 2747-2754.
- McGregor, H.V. and Gagan, M.K., 2003. Diagenesis and geochemistry of *Porites* corals from Papua New Guinea: Implications for paleoclimate reconstruction. *Geochimica et Cosmochimica Acta*, 67(12): 2147-2156.
- Meibom, A., Yurimoto, H., Cuif, J.P., Domart-Coulon, I., Houlbrèque, F., Brent, C., Dauphin, Y., Tambutté, E., Tambutté, S., Allemand, D., Wooden, J. and Dunbar, R., 2006. Vital effects in coral skeletal composition display strict three-dimensional control. *Geophysical Research Letters*, 33.
- Micheels, A., Bruch, A.A., Uhl, D., Utescher, T. and Mosbrugger, V., 2007. A Late Miocene climate model simulation with ECHAM4/ML and its quantitative validation with terrestrial proxy data. *Palaeogeography, Palaeoclimatology, Palaeoecology*, 253(1-2): 251-270.
- Min, G.R., Edwards, R.L., Taylor, F.W., Recy, J., Gallup, C.D. and Beck, W., 1995. Annual cycles of U/Ca in coral skeletons and U/Ca thermometry. *Geochimica et Cosmochimica Acta*, 59: 2025-2042.
- Mitsuguchi, T., Matsumoto, E., Abe, O., Uchida, T. and Isdale, P.J., 1996. Mg/Ca thermometry in coral skeletons. *Science*, 274(5289): 961-963.
- Munksgaard, N.C., Antwertinger, Y. and Parry, D.L., 2004. Laser ablation ICP-MS analysis of Faviidae corals for environmental monitoring of a tropical estuary. *Environmental Chemistry*, 1(3): 188-196.
- Nägler, T.F., Eisenhauer, A., Müller, A., Hemleben, C. and J., K., 2000. The ^{44}Ca -temperature calibration on fossil and cultured *Globigerinoides sacculifer*: New tool for reconstruction of past sea surface temperatures. *Geochemistry Geophysics Geosystems*, 1: 2000GC000091.

- Naqvi, S.A.S., 1994. Seasonal variation in an annually-banded coral *Porites*: A scanning electron microscopy investigation. *Marine Geology*, 118(3-4): 187-194.
- Neil, D., Newman, S. and Isdale, P., 1994. Long-term records of sediment yield from coral skeletons: results from ion beam analyses. In: Olive, L.J., Loughran, R.J. and Kesby, J.A. (Editors), *Variability in Stream Erosion and Sediment Transport (Proceedings of the Canberra Symposium 1994)*. IAHS Publications 224, pp. 465-472.
- Nürnberg, D., 1995. Magnesium in tests of *Neogloboquarina pachyderma* sinistral from high northern and southern latitudes. *Journal of Foraminiferal Research*, 25: 350-368.
- O'Neil, J.R., Clayton, R.N. and Mayeda, T.K., 1969. Oxygen Isotope Fractionation in Divalent Metal Carbonates. *The Journal of Chemical Physics*, 51(12): 5547-5558.
- Palamarev, E., 1989. Paleobotanical evidences of the Tertiary history and origin of the Mediterranean sclerophyll dendroflora. *Plant Systematics and Evolution*, 162(1): 93-107.
- Prell, W.L. and Kutzbach, J.E., 1992. Sensitivity of the Indian monsoon to forcing parameters and implications for its evolution. *Nature*, 360(6405): 647-652.
- Quade, J., Solounias, N. and Cerling, T.E., 1994. Stable isotopic evidence from paleosol carbonates and fossil teeth in Greece for forest or woodlands over the past 11 Ma. *Palaeogeography, Palaeoclimatology, Palaeoecology*, 108(1-2): 41-53.
- Quinn, T.M. and Sampson, D.E., 2002. A multiproxy approach to reconstructing sea surface conditions using coral skeleton geochemistry. *Paleoceanography*, 17(4).
- Reeder, R.J., Nugent, M., Lamble, G.M., Tait, C.D. and Morris, D.E., 2000. Uranyl incorporation into calcite and aragonite: XAFS and luminescence studies. *Environmental Science & Technology*, 34(4): 638-644.
- Reuter, M., Brachert, T.C. and Kroeger, K.F., 2005. Diagenesis of growth bands in fossil scleractinian corals: Identification and modes of preservation. *Facies*, 51: 155-168.
- Rodwell, M.J. and Hoskins, B.J., 1996. Monsoons and the dynamics of deserts. *Quarterly Journal of the Royal Meteorological Society*, 122(534): 1385-1404.
- Rögl, F., 1998. Palaeogeographic considerations for Mediterranean and Paratethys seaways (Oligocene to Miocene). *Annalen des Naturhistorischen Museums in Wien*, 99 A: 279-310.
- Rosen, B.R., 1999. Paleoclimatic implications of the energy hypothesis from Neogene corals of the Mediterranean region. In: Agusti, J., Rook, L. and Andrews, P. (Editors), *The evolution of Neogene terrestrial ecosystems in Europe*. Cambridge University Press, pp. 309-327.
- Rosenthal, Y., Boyle, E.A. and Slowey, N., 1997. Temperature control on the incorporation of magnesium, strontium, fluorine, and cadmium into benthic foraminiferal shells from Little Bahama Bank: Prospects for thermocline paleoceanography. *Geochimica et Cosmochimica Acta*, 61(17): 3633-3643.
- Sachse, M. and Mohr, B.A.R., 1996. Eine obermiozäne Makro- und Mikroflora aus Südkreta (Griechenland), und deren paläoklimatische Interpretation.- Vorläufige Betrachtungen. *Neues Jahrbuch für Geologie und Paläontologie - Abhandlungen*, 200(1/2): 149-182.
- Schöne, B.R., Oschmann, W., Rössler, J., Freyre Castro, A.D., Houk, S.D., Kröncke, I., Dreyer, W., Janssen, R., Rumohr, H. and Dunca, E., 2003. North Atlantic Oscillation dynamics recorded in shells of a long-lived bivalve mollusk. *Geology*, 31(12): 1037-1040.
- Schrag, D.P., Hampt, G. and Murray, D.W., 1996. Pore fluid constraints on the temperature and oxygen isotopic composition of the glacial ocean. *Science*, 272(5270): 1930-1932.

- Shackleton, N.J., 1974. Attainment of isotopic equilibrium between ocean water and the benthic foraminifera genus *Uvigerina*: isotopic changes in the ocean during the last glacial. In: Labeyrie, L. (Editor), *Les méthodes quantitatives d'étude des variations du climat au cours du Pléistocène*. CNRS, Paris, pp. 203–209.
- Shen, G.T. and Dunbar, R.B., 1995. Environmental controls on uranium in reef corals. *Geochimica et Cosmochimica Acta*, 59(10): 2009-2024.
- Shinn, E.A., 1966. Coral growth-rate, an environmental indicator. *Journal of Paleontology*, 40: 233-240.
- Sinclair, D.J. and McCulloch, M.T., 2004. Corals record low mobile barium concentrations in the Burdekin River during the 1974 flood: evidence for limited Ba supply to rivers? *Palaeogeography, Palaeoclimatology, Palaeoecology*, 214(1-2): 155-174.
- Sinclair, D.J., Kinsley, L.P.J. and McCulloch, M.T., 1998. High resolution analysis of trace elements in corals by laser ablation ICP-MS. *Geochimica et Cosmochimica Acta*, 62(11): 1889-1901.
- Smith, S.V., Buddemeier, R.W., Redalje, R.C. and Houck, J.E., 1979. Strontium-calcium thermometry in coral skeletons. *Science*, 204: 404-407.
- Stoll, H.M. and Schrag, D.P., 1998. Effects of Quaternary sea level cycles on strontium in seawater. *Geochimica et Cosmochimica Acta*, 62(7): 1107-1118.
- Suc, J.-P., 1984. Origin and evolution of the Mediterranean vegetation and climate in Europe. *Nature*, 307: 429-432.
- Suc, J.-P. and Popescu, S.-M., 2005. Pollen records and climatic cycles in the North Mediterranean region since 2.7 Ma. Geological Society, London, Special Publications, 247(1): 147-158.
- Swart, P.K., 1983. Carbon and oxygen isotope fractionation in scleractinian corals: a review. *Earth-Science Reviews*, 19: 51-80.
- Swart, P.K. and Hubbard, J.A.E.B., 1982. Uranium in scleractinian coral skeletons. *Coral Reefs*, 1: 13-19.
- Thompson, D.W.J. and Wallace, J.M., 2001. Regional climate impacts of the Northern Hemisphere Annular Mode. *Science*, 293: 85-89.
- Tudhope, A.W., Chilcott, C.P., McCulloch, M.T., Cook, E.R., Chappell, J., Ellam, R.M., Lea, D.W., Lough, J.M. and Shimmiel, G.B., 2001. Variability in the El Niño-Southern Oscillation through a glacial-interglacial cycle. *Science*, 291: 1511-1517.
- Tzedakis, P.C., 2007. Seven ambiguities in the Mediterranean palaeoenvironmental narrative. *Quaternary Science Reviews*, 26(17-18): 2042-2066.
- Urey, H.C., 1947. The thermodynamic properties of isotopic substances. *Journal of the Chemical Society*: 562 - 581.
- Urey, H.C., Lowenstam, H.A., Epstein, S. and McKinney, C.R., 1951. Measurements of paleotemperatures and temperatures of the Upper Cretaceous of England, Denmark, and the southeastern United States. *Geological Society of America Bulletin*, 62: 399-416.
- van Dam, J.A., 2006. Geographic and temporal patterns in the late Neogene (12 - 3 Ma) aridification of Europe: the use of small mammals as paleoprecipitation proxies. *Palaeogeography, Palaeoclimatology, Palaeoecology*, 238: 190-218.
- van der Zwaan, G.J. and Gudjonsson, L., 1986. Middle Miocene–Pliocene stable isotope stratigraphy and paleoceanography of the Mediterranean. *Marine Micropaleontology*, 10(1-3): 71-90.
- Weber, J.N. and Woodhead, P.M.J., 1970. Carbon and oxygen isotope fractionation in the skeletal carbonate of reef-building corals. *Chemical Geology*, 6: 93-117.
- Weber, J.N. and Woodhead, P.M.J., 1972. Temperature dependence of oxygen-18 concentration in reef coral carbonates. *Journal of Geophysical Research*, 77: 463-473.

- Wefer, G., Berger, W.H., Bijma, J. and Fischer, G., 1999. Clues to ocean history: a brief overview of proxies. In: Fischer, G. and Wefer, G. (Editors), Use of proxies in paleoceanography: examples from the South Atlantic. Springer, Berlin, pp. 1-68.
- Wright, D.H., 1983. Species-energy theory: an extension of species-area theory. *Oikos*, 41(3): 496-506.
- Zachos, J., Pagani, M., Sloan, L., Thomas, E. and Billups, K., 2001. Trends, rhythms, and aberrations in global climate 65 Ma to present. *Science*, 292: 686-693.
- Zhisheng, A., Kutzbach, J.E., Prell, W.L. and Porter, S.C., 2001. Evolution of Asian monsoons and phased uplift of the Himalaya-Tibetan plateau since Late Miocene times. *Nature*, 411(6833): 62-66.
- Zidianakis, G., Mohr, B. and Fassoulas, C., 2004. The Late-Miocene flora of Vrysses, Western Crete - A contribution to the climate and vegetation history, 5th International Symposium on Eastern Mediterranean Geology, Thessaloniki, Greece, pp. 515-518.
- Zidianakis, G., Mohr, B.A.R. and Fassoulas, C., 2007. A late Miocene leaf assemblage from Vrysses, western Crete, Greece, and its paleoenvironmental and paleoclimatic interpretation. *Geodiversitas*, 29(3): 351-377.

2. *Tarbellastraea* (Scleractinia): A new stable isotope archive for Late Miocene paleoenvironments in the Mediterranean

This chapter is published with *Palaeogeography, Palaeoclimatology, Palaeoecology*:

Mertz-Kraus, R., Brachert, T.C. and Reuter, M., 2008. *Tarbellastraea* (Scleractinia): A new stable isotope archive for Late Miocene paleoenvironments in the Mediterranean. *Palaeogeography, Palaeoclimatology, Palaeoecology*, 257(3): 294-307

2.1. Abstract

Geochemical proxy records of sea surface temperature (SST) or sea surface salinity (SSS) variability on intra- and interannual time-scales in corals from geological periods older than Pleistocene are extremely rare due to pervasive diagenetic alteration of coralline aragonite. Very recently, however, stable isotope data ($\delta^{18}\text{O}$, $\delta^{13}\text{C}$) from specimens of *Porites* of Late Miocene age (10 Ma) have been shown to preserve original environmental signatures. In this paper we describe new finds of the zooxanthellate corals *Porites* and *Tarbellastraea* in exceptional aragonite preservation from the island of Crete in sediments of Tortonian (~9 Ma) and Early Messinian (~7 Ma) age. Systematic, comparative stable isotope analysis of massive *Tarbellastraea* and *Porites* sampled from the same beds and localities reveal identical stable isotope fractionation patterns in both genera. Therefore, extinct *Tarbellastraea* represents an additional environmental archive fully compatible and mutually exchangeable with *Porites*. Provided that seasonal variations in $\delta^{18}\text{O}$ reflect SST changes only, seasonal SST contrasts of 7.3°C for the Tortonian and 4.8°C for the Early Messinian are inferred, implying warmer summer and cooler winter SSTs during the Tortonian than during the Messinian. However, reduced $\delta^{18}\text{O}$ seasonality (1.1‰ in the Tortonian and 0.7‰ in the Messinian) and slightly less negative mean $\delta^{18}\text{O}$ in Messinian corals (-2.4‰) compared to Tortonian specimens (-2.7‰) may not necessarily indicate a long-term fall in SSTs, but changes in surface water $\delta^{18}\text{O}$, i.e. global ice build-up or enhanced evaporation during summer or increased precipitation/river discharge during winter and changes in insolation. On the other hand, coral communities of Tortonian and Messinian age in central Crete are identical, and compatible annual extension rates indicate similar average SSTs during the two investigated time periods. In addition, lithological and paleobotanical data from Central Crete document a change from humid to dry climatic conditions during the Late Miocene. Therefore, a likely explanation for the observed shift in coral mean $\delta^{18}\text{O}$ and reduced $\delta^{18}\text{O}$ seasonality from the Tortonian to the Early Messinian is a change in ambient seawater $\delta^{18}\text{O}$ caused by a change in the hydrological balance towards high evaporation/high salinity during summer.

Keywords: *Tarbellastraea*, corals, stable isotopes, SST, sclerochronology, paleoclimate, Late Miocene, Tortonian, Messinian, Crete, Mediterranean

2.2. Introduction

2.2.1. General

Thriving in the shallow zone of the tropical oceans, reefs and reef-building corals are highly sensitive to changes in sea surface temperature (SST), sea surface salinity (SSS) and nutrient supply (Hallock and Schlager, 1986; Schlager, 1992). In frameworks of “modern” reefs, both present and Neogene, the large and long-living scleractinian corals represent the most important group of primary constructors (Fagerstrom, 1987). The rigid coral skeleton composed of CaCO_3 (aragonite) is accretionary and not remodeled once formed. It is, therefore, an excellent climate archive, and geochemical proxy data in sclerochronological records have been used for reconstructions of past environmental variability on sub-annual time scales (Swart, 1983; Druffel, 1997; Gagan et al., 2000). Important prerequisites for sclerochronological analyses, however, are fairly uniform incremental growth and extension rates over the whole coral skeleton. These requirements are met by the genus *Porites*, which is very common, widespread in the tropics and subtropics and has a well-known fossil record (Chevalier, 1961). Therefore, massive *Porites* colonies are commonly used as high-resolution archive of coral reef environments from the Pleistocene to present-day (Grottoli and Eakin, 2007). Because of rather irregular growth patterns usually present in the Atlantic *Porites*, other genera, that have been used for paleoclimatic reconstructions include *Diploria*, *Solenastrea* and *Montastrea* (Fairbanks and Dodge, 1979; Leder et al., 1996; Swart et al., 1996; Cohen et al., 2004).

Oxygen isotope compositions of coral aragonite reflect changes of temperature and isotopic compositions of ambient sea water or a mixed signal (Weber and Woodhead, 1970; Gagan et al., 2000). In regions with low variations in seawater composition coral $\delta^{18}\text{O}$ reflects mainly SST variations. However, in regions with enhanced seasonality in precipitation and/or evaporation which both modify SSS, seasonal $\delta^{18}\text{O}$ records of coral skeletons may be affected by these changes or are even dominated by the evaporation/precipitation effect (Cole et al., 1993; Quinn and Sampson, 2002). Depending on local isotopic composition of rainfall and river water there exist various relationships between $\delta^{18}\text{O}$ and SSS in ocean waters (Corrège, 2006).

Coral aragonite is less stable than calcite and undergoes rapid chemical and microstructural alteration in most diagenetic environments (Land, 1967; Dullo, 1984; Constantz, 1986; Dullo and Mehl, 1989). Although ghost structures of the original skeleton may remain after transformation into calcite (Shinn, 1966; Insalaco, 1996; Reuter et al., 2005; Brachert et al., 2006a), original geochemical proxy records of the environment

become fully reset (Tudhope et al., 2001; McGregor and Gagan, 2003). Reconstructions of pre-Pleistocene seasonal to interannual climate variability from stable isotope records of reef corals are, therefore, still exceedingly rare. Notable exceptions from the Neogene have been described from settings, where preservation of aragonite is linked to a passive diagenetic environment (Roulier and Quinn, 1995; Brachert et al., 2006b). Indeed, preserved pristine skeletons of azooxanthellate corals are not unusual in fine-grained deepwater sediments, and stable isotope sclerochronological records from azooxanthellate corals have been presented from Oligocene (Ivany et al., 2004) and Eocene (Mackenzie et al., 1997) strata. Correspondingly, sites for the retention of the original skeletons of reef corals are expected to occur where displaced into fine-grained sediments (Wendt, 1975; Scherer, 1977; Johnson and Pérez, 2006).

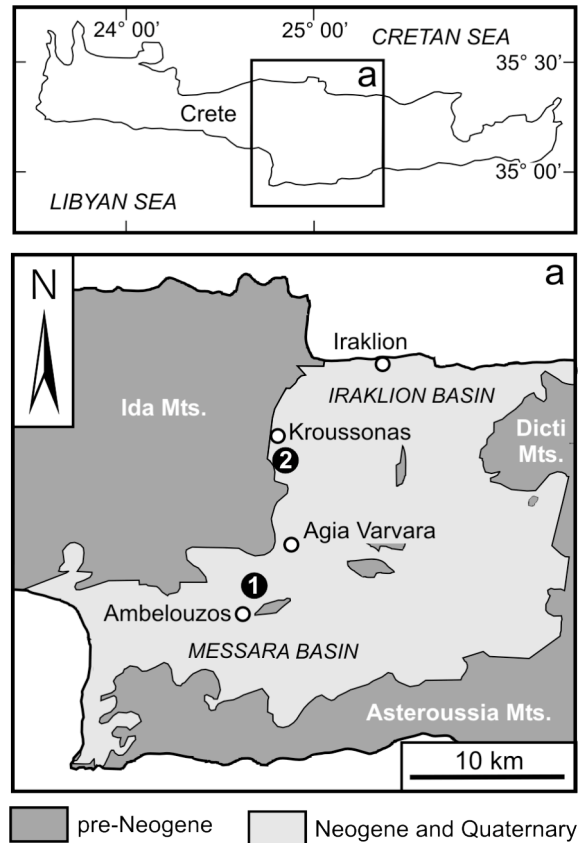


Fig. 2: Simplified geological map of Central Crete, Greece showing sampling sites. (1) Psalidha, Messara Basin, Early Tortonian, (2) Moni Gorgolaini, Western margin of Iraklion Basin, Early Messinian.

This paper presents sub-annually resolved stable isotope time series ($\delta^{18}\text{O}$ and $\delta^{13}\text{C}$) from *Porites* and *Tarbellastraea* corals of Late Miocene age from the island of Crete, Greece. Coral samples described in this study derive from two distinct stratigraphic levels dated ~9 Ma and ~7 Ma. The corals (*Porites*, *Tarbellastraea*) have retained their original skeletal aragonite. Because only trace amounts of secondary calcite cement are present, geochemical proxy data are univocally preserved. The aim of this study is to show that stable isotope data from massive *Tarbellastraea* are fully compatible with those from massive *Porites* recovered from the same beds. Data from *Tarbellastraea* may be used, therefore, where *Porites* fossils are not available for reconstructions of seasonal and interannual variability of SST and SSS during the Neogene within different time slices.

The Mediterranean region formed part of the northern margin of the global reef belt during the Late Miocene (Perrin, 2002). Reef growth occurred almost over the entire Mediterranean region (Esteban, 1979; Pomar, 1991; Martín and Braga, 1994; Reuter et al., 2006), however, reef growth was rather discontinuous and coral faunas were of low diversity and dominated by two genera: *Porites* and *Tarbellastraea* (Pomar, 1991; Brachert et al., 1996; Bosellini, 2006; Reuter et al., 2006). In concert with low extension rates of ~ 4 mm yr⁻¹ in massive *Porites*, this pattern fits suggestions that average winter SSTs were 20 to 21°C and near the lower threshold level for reef coral growth (Brachert et al., 2006a; Reuter et al., 2006). This estimate is in good agreement with distributional patterns of modern coral reefs, which are limited by minimum long-term winter SST $\geq 18^\circ\text{C}$ but allowing for some short excursions below this temperature (Veron and Minchin, 1992; Abram et al., 2001).

Salinity has been shown to have increased in the Mediterranean during the Late Miocene (Santarelli et al., 1998; Kouwenhoven et al., 1999). Terrestrial floras and lignite concentrations from the island of Crete document a warmer and substantially more humid climate than today for the Tortonian with 1000 to 1200 mm of annual precipitation (Sachse and Mohr, 1996; Zidianakis et al., 2004). For the Messinian palaeobotanical records indicate dry conditions with 400 to 500 mm annual precipitation for the early Messinian ending up in an arid environment in the late Messinian (Fauquette et al., 2006).

The first appearance of the scleractinian genus *Tarbellastraea* is reported from the Oligocene in the Mediterranean (Budd et al., 1996). During the Miocene, *Tarbellastraea* was widespread and one of the principal reef builders in the Mediterranean (Esteban, 1979;

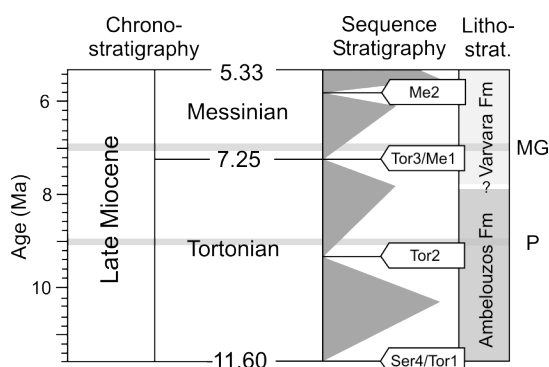


Fig. 3: Chronostratigraphy, lithostratigraphy and age model of Tortonian and Messinian sampling levels at Psalidha (P), Tortonian and Gorgolaini monastery (MG), Early Messinian, Late Miocene, Central Crete, with sequence stratigraphy from Hardenbol et al. (1998) and time scale from Gradstein et al. (2005).

Budd et al., 1996) before it became extinct during the Messinian. Notwithstanding of the importance of *Tarbellastraea* for Miocene Mediterranean reef communities, so far, geochemical signatures of *Tarbellastraea* skeletons have not been used as proxy records of paleoenvironmental variations. *Tarbellastraea* is closely related to the present-day's *Montastraea* and *Solenastraea* (Chevalier, 1961; Budd et al., 1996), and exhibits a strong overall similarity in corallite architecture and growth patterns.

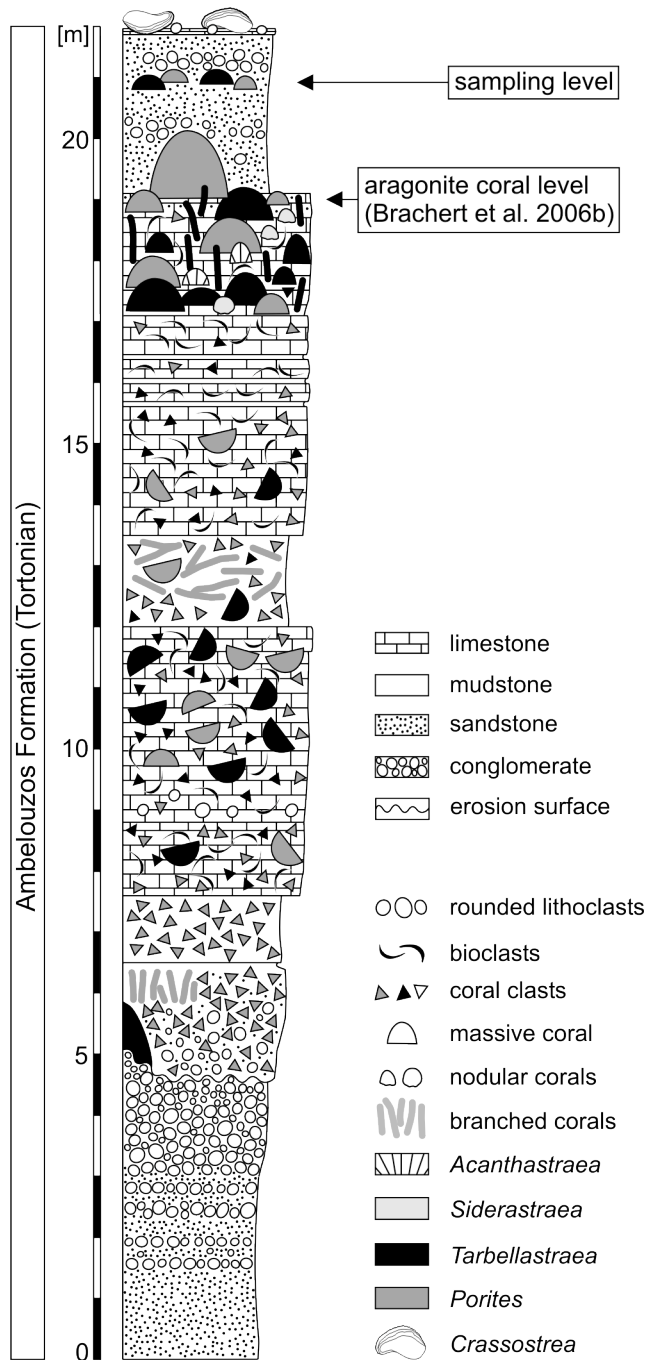


Fig. 4: Geological section of Psalidha sampling sites (Tortonian). Non-altered corals occur in the uppermost part of the reef and intercalated with coarse clastics.

Sampling protocols developed for the two modern corals (Leder et al., 1996; Swart et al., 1996) can, therefore, be adapted to Miocene *Tarbellastraea*.

2.2.2. Geologic setting

Neogene subduction zone roll-back of the Cretan arc caused extension of the former Aegean Land and subsidence of numerous large and small subbasins of the Aegean (Fassoulas, 2001; Meulenkamp and Sissingh, 2003; Rahl, 2004). Intramontane basins of the island of Crete (Southern Greece) formed as a dynamic system of halfgraben and in response with Eastern Mediterranean geodynamic evolution (Fassoulas, 2001; Reuter et al., 2006). Miocene sedimentary rocks of the Iraklion and the Messara Basin in Central Crete (Fig. 2) are attributed to the Ambelouzos Formation of Serravallian to Tortonian age and the Varvara Formation of Late Tortonian to Early Messinian age (Meulenkamp et al., 1979; ten Veen and Postma, 1999) (Fig. 3).

The Ambelouzos Formation represents various clastic sediments formed in brackish-lagoonal, marginally marine and open marine environments. Coral build-ups of the Ambelouzos Formation formed along clastic shorelines, deltas and isolated tectonic horst structures (Reuter et al., 2006; Reuter and Brachert, 2007). The Ambelouzos Formation is

covered by the Varavra Formation comprising shallow marine limestones with corals, and marls with intercalated calciturbidites and debrites deposited in a slope to basin environment. Reef systems of Early Messinian age are present in Central Crete, however, along the western margin of Iraklion Basin they have been removed by erosion (Reuter et al., 2006).

2.2.3. Sampling sites

Sampling sites for corals of Late Miocene age described in this study are located in Central Crete (Fig. 1):

- (1) Psalidha fossil site is a natural outcrop in a coral build-up situated next to the small village of Psalidha (Municipality of Rouvas), and halfway along the public road connecting the towns of Ambelouzos and Gergeri. The Psalidha coral build-up developed in shallow water on a paleogeographically height near the northern margin of Messara Basin. It represents a low mounded structure that is composed of a stack of horizontally bedded coral biostromes and bioclastic beds (Reuter and Brachert, 2007) (Fig. 4) either composed of branching *Porites* or dominated by massive growth forms of *Porites* and *Tarbellastraea*. The build-up is covered by a package of sandstone with intercalated conglomerate and isolated, non-framework forming massive *Porites* in-situ and other marine fauna (mollusks, bryozoans, foraminifers) (Reuter and

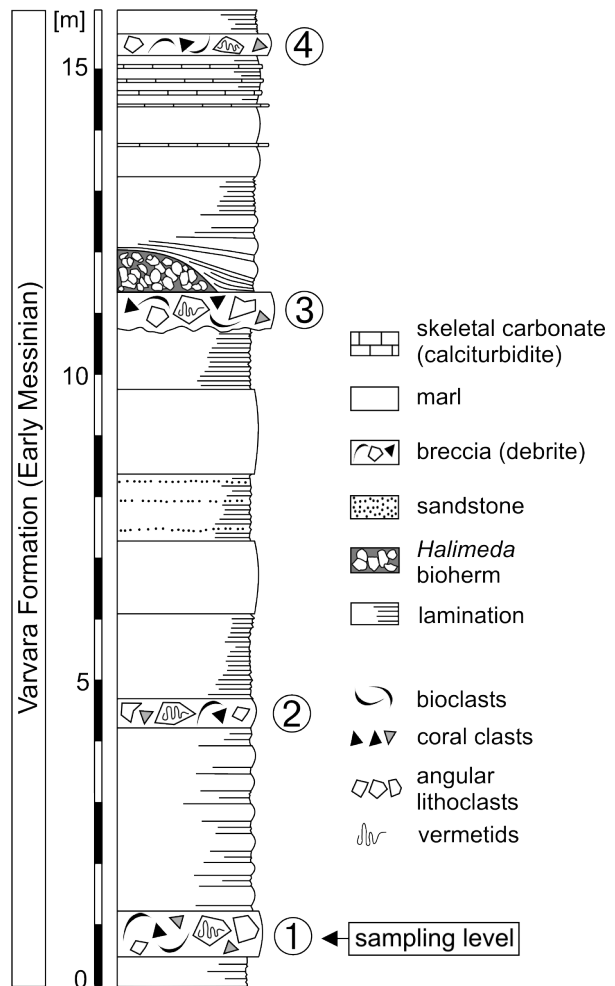


Fig. 5: Geological section of Gorgolaini monastery sampling site (Early Messinian). Corals in pristine preservation, are found within four breccias (1) – (4). Corals described in this study derive from the lowermost of these breccias (1).

Brachert, 2007). The corals described in this study were collected from this unit (Fig. 3) in a nearby olive grove (E 24.96488°, N 35.08682°) from the same stratigraphic unit. On the basis of global oceanic $^{87}\text{Sr}/^{86}\text{Sr}$ chronostratigraphy a coral age of ~9 Ma is derived for the Psalidha sampling level (Mertz-Kraus et al., 2007b). Previous sclerochronological work by Brachert et al. (2006b) is based on samples from the contact of the build-up and overlying sandstone. It was assigned an age of ~10 Ma based on the overall litho- and sequencestratigraphic position (Fig. 4).

- (2) Road section 1 km to the Northwest of Gorgolaini monastery (Municipality of Kroussonas, E 24.9819°, N 35.20535°): At Gorgolaini section bipartite cycles of bedded marl and homogeneous marl with intervening beds of calciturbidites and breccias interpreted as debrites occur, which were deposited in a deeper toe of slope setting at the western margin of Iraklion Basin. Four beds of debrites (Fig. 5) contain various lithoclasts (pre-Neogene basement, Messinian vermetid limestone) and coral fragments including almost complete specimens of *Porites* and *Tarbellastraea* corals (Reuter et al., 2006) ranging in size from a few centimeters up to several decimeters. Some of the coral fragments have retained their original aragonite mineralogy. An early Messinian age is assumed for this sedimentary succession by Reuter et al. (2006) through sequence stratigraphic methods. Consistently, $^{87}\text{Sr}/^{86}\text{Sr}$ ratios from aragonite corals indicate an age of ~7 Ma for the Gorgolaini monastery sampling level (Mertz-Kraus et al., 2007a).

2.3. Material and methods

2.3.1. Sampling techniques

Massive *Tarbellastraea* and *Porites* were sampled from two sections of Psalidha and Gorgolaini monastery outcrops (Figs. 2, 4 and 5). For comparative geochemical analysis both coral genera have been sampled from the same beds. In the field, skeletons with the original aragonite skeleton preserved were identified by their almost white color and very low weight compared to obviously altered (neomorphosed, recrystallized and cemented) corals. The size of the specimens ranges from 5 cm to 20 cm. In the laboratory, coral specimens were split into slabs of ~6 mm thickness parallel to the axis of maximum growth. The slabs (Fig. 6a) were cleaned ultrasonically and with diluted hydrogen peroxide. Contact radiographs (Fig. 6b) of coral slabs were taken using a Faxitron model 805 X-ray unit and

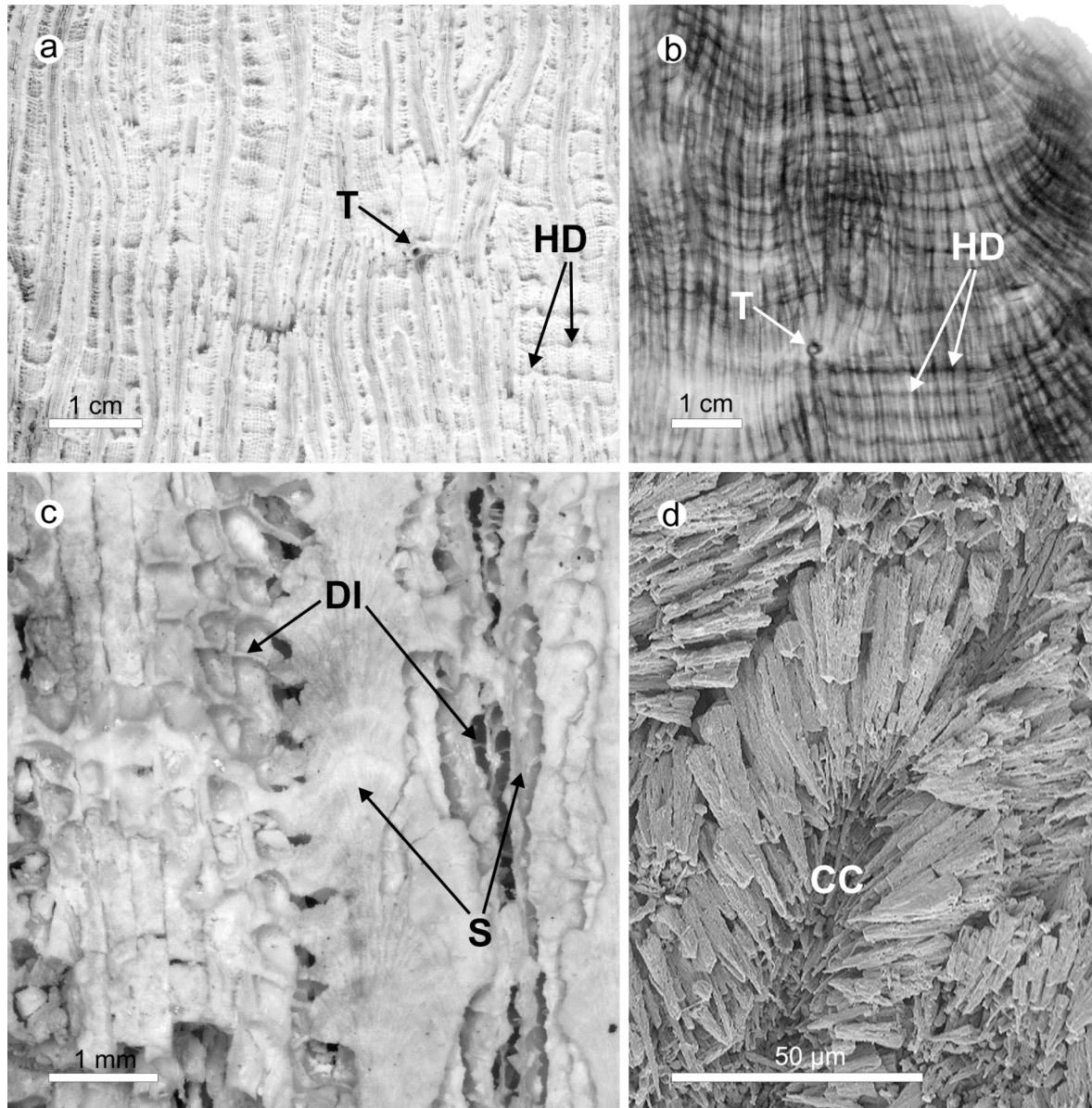


Fig. 6: Photographs from *Tarbellastraea* specimen MG9/2, Early Messinian, used for stable isotope analysis. (a) Slab of massive *Tarbellastraea*. Exothecal dissepiments form buldges related to high density bands (HD). Surface associated with calcareous tubes (T). (b) X-ray image (positive print) showing annual density banding. High density bands (HD) represent the winter and low density bands the summer season. (c) Close up of (a) showing internal structures of the skeleton: Septa (S) and dissepiments (DI). (d) SEM image of fresh fracture. The skeleton is affected by enhanced dissolution at centers of calcification (CC) and between single aragonite fibers, however, aragonite fibers do not show secondary overgrowth.

AGFA Structurix D4 FW Industrial X-ray film. Settings for the X-ray examination were fixed at 3 mA and 45 kV. Exposure time ranged between 6 to 9 minutes, depending on thickness and density of each slab.

X-ray opaque zones on the contact radiographs with unclear or missing density banding were identified as zones of diagenetic alteration (McGregor and Gagan, 2003). Random samples were analyzed by X-ray diffraction (XRD) using a Seifert XRD 3000

diffractometer (2θ ranging from 20° to 60°). Percentages of aragonite and calcite were estimated by comparison to reference samples of known composition. Stereomicroscopic analysis in reflected light (Fig. 6a and 6c) and scanning electron microscopy (Fig 6d) were used to describe the microscopic aspects of the coral skeletons. Areas with secondary infill of carbonate cements, overgrowths or recrystallization were avoided during stable isotope sampling. Only skeletal areas that have retained their original aragonite mineralogy, skeletal porosity and microstructure with no significant secondary crystal growth were accepted for further sample preparation (Table 1).

Coral slabs were mounted on a xy-stage and adjusted below a PROXXON micro miller with a spherical drill bit allowing for precise, equidistant spot sampling at low tournament speeds. Drilling diameter was 0.6 mm, and the distance between sampling spot centers was 0.8 mm. Drilling depth for *Porites* was 1.5 mm. Sampling transects were chosen according to the annual density banding as determined by X-ray photography and in the direction of maximum growth to minimize kinetic stable isotope effects (McConnaughey, 1989). X-ray photography was repeated after sampling to track the sampling path over density bands and potential zones of diagenetic alterations.

In analogy with *Porites*, sampling tracks for *Tarbellastraea* stable isotope data sets followed the growth direction of the theca; however, sampling protocols of *Tarbellastraea* must take into account the large size of corallites ($\varnothing \sim 3$ mm). In order to avoid mixing of material from skeletal elements of unequal age (Leder et al., 1996), sampling concentrated on the thecal wall, following the procedures described for modern *Montastraea* and *Solenastraea* which exhibit a similar corallite organization. However, since the thickness of the fragile thecal wall of *Tarbellastraea* is <1 mm, it was not possible to drill the thecal wall exposed at the surface of the slab between corallites as commonly done for *Montastraea*

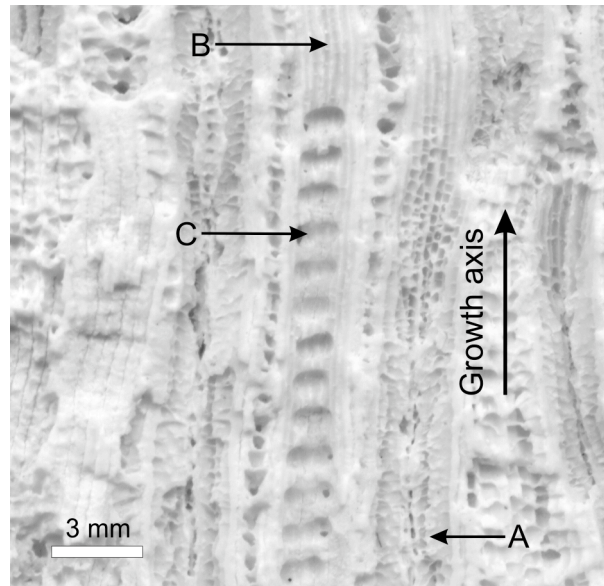


Fig. 7: Close-up of sampling transect in *Tarbellastraea* specimen MG9/2, Early Messinian. (A) Corallite with septa and dissepiments. (B) Corallite with septa removed. Parallel running delicate lines reflect relicts of septae forming the septothecal corallite wall. (C) Drill holes are shallow pits (depth ≤ 1 mm) in the thecal wall, elongated perpendicular to growth axis.

Table 1: Specimen ID, approximate age, genus, length of obtained time series given in years, mean $\delta^{18}\text{O}$ values, mean $\delta^{18}\text{O}$ seasonalities and mean $\delta^{13}\text{C}$ (reported in per mil relative to V-PDB) of the coral specimens discussed this study

Specimen ID	Age [Ma]	Genus	Time series [yr]	Mean $\delta^{18}\text{O}$ [‰]	Mean $\delta^{18}\text{O}$ seasonality [‰]	Mean $\delta^{13}\text{C}$ [‰]
P1	9	<i>Porites</i>	15	-2.76	0.91	-1.54
P3	9	<i>Porites</i>	4	-2.60	1.14	-0.54
P4	9	<i>Porites</i>	11	-2.95	1.16	-0.92
P7	9	<i>Tarbellastraea</i>	10	-2.53	0.99	-1.16
P8	9	<i>Porites</i>	17	-2.70	1.03	-0.26
P9	9	<i>Porites</i>	18	-2.50	1.18	-0.38
MG9/2	7	<i>Tarbellastraea</i>	42	-2.46	0.74	-1.25
MG9/4	7	<i>Porites</i>	—	-2.41	—	-0.87

(Leder et al., 1996). Therefore, prior to sampling all septa in the theca were removed using a hand held micro-drill equipped with a spherical drill bit (\varnothing 1.6 mm). Sampling was performed using the same equipment as in *Porites*. In order to avoid penetration of the thecal wall while obtaining sufficient carbonate powder for stable isotope analyses, elongated sampling spots (~2 mm) were chosen. Elongation of the drill holes was perpendicular to the axis of maximum growth, the depth of the holes amounts only a few tenths of millimeter (Fig. 7). Following this procedure, *Tarbellastraea* as well as *Porites* were sampled for $\delta^{18}\text{O}$ and $\delta^{13}\text{C}$ analyses with a quarterly resolution.

2.3.2. Stable isotopes and data analysis

Oxygen and carbon isotope analyses were carried out in the laboratories of the Institute of Geosciences, University of Frankfurt and of the Department of Geology and Mineralogy, University of Erlangen-Nürnberg (both Germany). Sample amount was >50 μg . Carbon and oxygen isotope analyses of carbonates in the laboratory in Frankfurt were performed using a Gas Bench II connected to a MAT 253 gas source mass spectrometer (both ThermoQuest), according to the setup described by Spötl and Vennemann (2003). An in-house standard (Carrara marble) was analyzed along with the samples, whose isotopic composition has been calibrated against NBS 19 (Fiebig et al., 2005). The internal analytical precision was better than $\pm 0.05\text{‰}$ for $\delta^{13}\text{C}$ and $\pm 0.08\text{‰}$ for $\delta^{18}\text{O}$ (1σ), external reproducibility was $\pm 0.07\text{‰}$ for $\delta^{13}\text{C}$ and $\pm 0.08\text{‰}$ for $\delta^{18}\text{O}$ (1σ). In the laboratory in Erlangen-Nürnberg, carbonate powders were reacted with 100% phosphoric acid at 75°C using a Kiel III online carbonate preparation line connected to a ThermoFinnigan 252 mass spectrometer. All values are reported in per mil relative to V-PDB by assigning a $\delta^{13}\text{C}$ value of $+1.95\text{‰}$ and a $\delta^{18}\text{O}$ value of -2.20‰ to NBS19. Reproducibility was checked by

replicate analysis of laboratory standards and was better than $\pm 0.03\text{‰}$ (1σ). The internal analytic precision was better than $\pm 0.02\text{‰}$ (1σ).

Age models are based on annual density banding combined with stable isotope patterns, with the most positive $\delta^{18}\text{O}$ value in each annual cycle defining minimum winter temperatures used as tie points in the internal chronology. The ages of the other sampling points were interpolated according to their position along the sampling transect. Isolated sample tracks of P7 and MG9/2 were combined into one time series, respectively, by correlation of growth bands and by isotope peak matching. In overlapping sections the values of the most pronounced record were used.

Mean $\delta^{18}\text{O}$ values of each coral specimen were obtained applying the method described by Felis and co-authors (2003), i.e. calculating annual mean $\delta^{18}\text{O}$ values out of a equidistant resampled time series which in turn were used to calculate the mean $\delta^{18}\text{O}$ of the complete time series of one specimen as the average of the annual mean $\delta^{18}\text{O}$ values. A one-way analysis of variance (ANOVA) was performed in order to compare stable isotope data sets of Tortonian *Porites* ($n = 5$) and *Tarbellastraea* ($n = 1$). All values were transformed by $\log_{10}(x+1)$ to satisfy the homogeneity of variance assumptions. The tested null hypothesis H_0 was that there are no statistically significant differences ($p > 0.05$) in the mean $\delta^{18}\text{O}$ values and mean $\delta^{18}\text{O}$ seasonalities, respectively, among Tortonian *Porites* and *Tarbellastraea* specimens against the alternate hypothesis H_1 that there are statistical describable differences ($p < 0.05$). Secondly, the null hypothesis H_0 was tested that there are no statistically significant differences ($p > 0.05$) in the mean $\delta^{18}\text{O}$ values and mean $\delta^{18}\text{O}$ seasonalities, respectively, among Tortonian ($n = 6$) and Messinian ($n = 2$) corals against the alternate hypothesis H_1 that there are statistical describable differences ($p < 0.05$).

For calculating SST variations from $\delta^{18}\text{O}$, the slope (0.15‰ per 1°C) for the relationship between $\delta^{18}\text{O}$ and temperature given by Felis et al. (2004) was used. This value is well within the range of other published calibrations (Gagan et al., 1994; Druffel, 1997; Evans et al., 2000). Stable oxygen isotope compositions were used to calculate salinity according to the equation $S = (\delta^{18}\text{O}_{\text{seawater}} [\text{SMOW}] + 8.9)/0.27$ (Pierre, 1999) where $\delta^{18}\text{O}_{\text{seawater}}$ was calculated making assumptions for water temperatures according to the relationship $\delta^{18}\text{O}_{\text{seawater}} = \delta^{18}\text{O}_{\text{aragonite}} [\text{PDB}] - (20 - T[^\circ\text{C}])/4.42$ (simplified from Böhm et al., 2000).

2.4. Results

2.4.1. Preservation

XRD analyses of coral skeletal materials reveal calcite concentrations <1% (detection limit) and, correspondingly, pure aragonite compositions of stable isotope samples. Under reflected light slabs of *Porites* exhibit a faint dark and light banding pattern, which corresponds to a density banding revealed by X-radiography. Such couplets of high and low density are known from modern corals to reflect annual growth increments (Knutson et al., 1972). Slabs of *Tarbellastraea* (Fig. 6a) show rhythmically thickened exothecal dissepiments in reflected light, which results in a banding of laminae of high and low density visible in X-ray photographs (Fig. 6b). Regular density bandings without conspicuous discontinuities indicate rather continuous growth patterns with growth rates of $\sim 4 \text{ mm yr}^{-1}$. Nonetheless, one specimen of *Tarbellastraea* (MG9/2) shows a distinct surface associated with calcareous tubes, probably serpulids, which may reflect a growth interruption (Fig. 6a, b).

Microscopy under reflected light (Fig. 6c) and scanning electron microscopy (Fig. 6d) reveal for *Porites* as well as for *Tarbellastraea* a trabecular structure composed of radially arranged bundles of aragonite fibers emerging from centers of calcification. Delicate fine scale structures such as dissepiments are preserved. Septa in *Tarbellastraea* exhibit incremental growth patterns in reflected light. Primary skeletal porosity is still open and does not show secondary infill by cryptocrystalline carbonate or carbonate cement. Noticeable alteration of the skeleton is occasional dissolution following the centers of calcification and between single aragonite fibers. However, *Porites* specimens from Gorgolaini monastery (Early Messinian) reveal areas with complete recrystallization adjoining to areas unaffected by diagenesis, therefore, allowing only discontinuous sampling for stable isotope analyses.

2.4.2. Isotope records

Stable isotope ($\delta^{18}\text{O}$ and $\delta^{13}\text{C}$) records were generated from a total of eight colonies. The records cover between 4 and 42 years (Table 1). In order to obtain comparable results from all coral specimens analyzed, sampling resolution was the same for both genera. A minimum of four samples per year which is an effect of the generally low growth rates of $\sim 4 \text{ mm yr}^{-1}$ in both genera reveals quarterly resolved data sets.

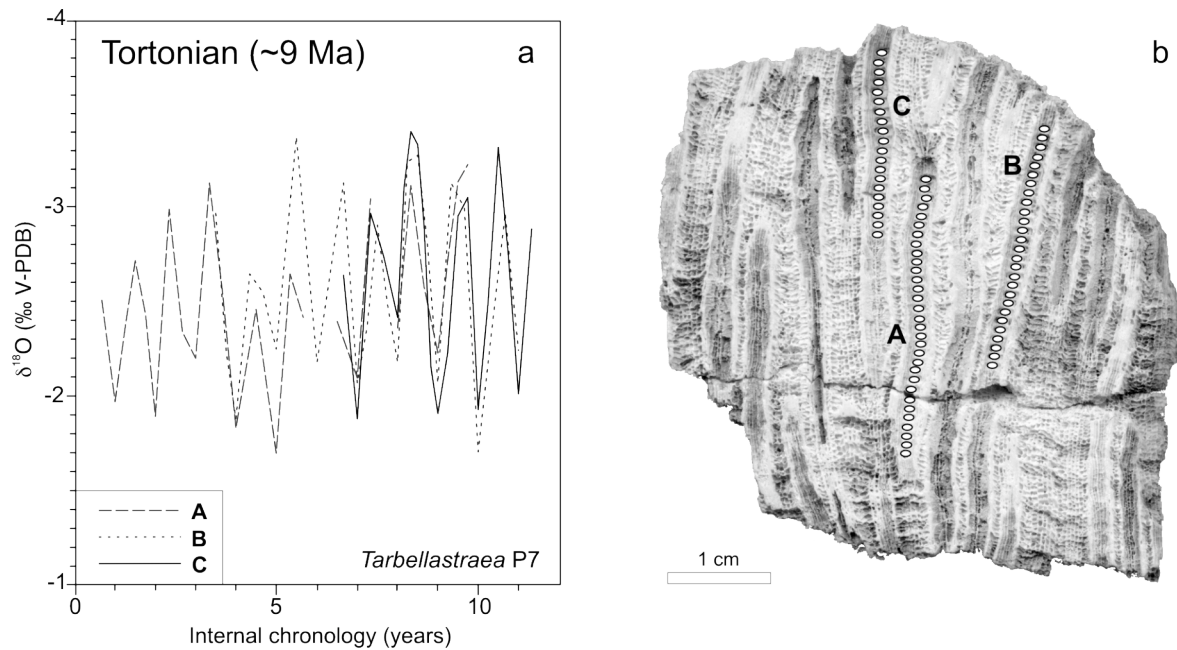


Fig. 8: *Tarbellastraea* specimen P7 (Early Tortonian): (a) $\delta^{18}\text{O}$ records of overlapping sampling tracks from different corallites. (b) Transects A–C cover almost the complete lifetime of the preserved coral fragment.

Tarbellastraea and *Porites* $\delta^{18}\text{O}$ (Figs. 8 to 10) show a sinusoidal pattern corresponding to the density banding visible in X-ray photographs (Fig. 6b). Maxima in $\delta^{18}\text{O}$ coincide with high-density bands, minima with low-density bands.

2.4.3. Tortonian stable isotope records

In a Tortonian *Tarbellastraea* specimen (P7) stable isotope samples were taken at parallel transects following three different corallites (Fig. 8). Overlapping segments of stable isotope time series exhibit consistent patterns in $\delta^{18}\text{O}$ covering 10 years in the lifetime of this specimen. Both, Tortonian (~9 Ma) *Porites* (Fig. 9a) and *Tarbellastraea* (Fig. 9b) show mean $\delta^{18}\text{O}$ values ranging from ca. -2.95‰ to -2.50‰ and mean $\delta^{18}\text{O}$ seasonality of 0.91‰ to 1.18‰ (Table 1).

Tortonian coral $\delta^{13}\text{C}$ is related with density bands as well but systematically phase-shifted relative to $\delta^{18}\text{O}$. The same pattern was observed in previous studies on Miocene coral material (Brachert et al., 2006b). Mean $\delta^{13}\text{C}$ values range from -0.26‰ to -1.54‰ (Table 1).

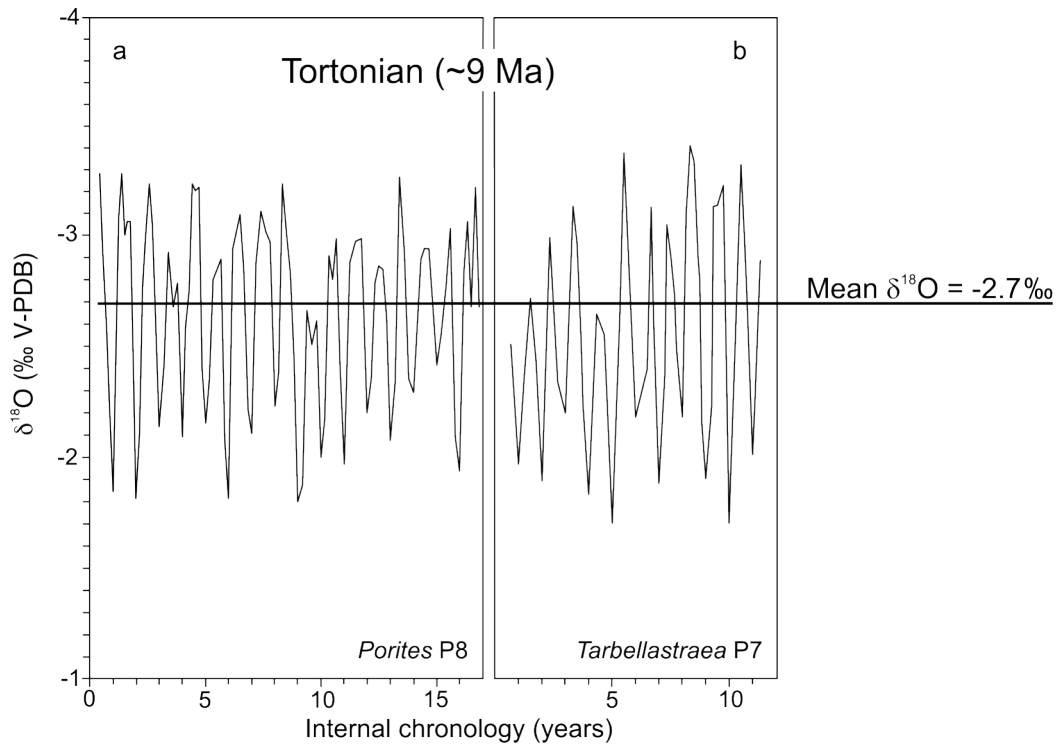


Fig. 9: $\delta^{18}\text{O}$ records of *Porites* specimen P8 and *Tarbellastraea* specimen P7, Early Tortonian. Both genera show mean $\delta^{18}\text{O}$ values at -2.7‰ (horizontal line) and mean seasonality of $\sim 1.1\text{‰}$ on average.

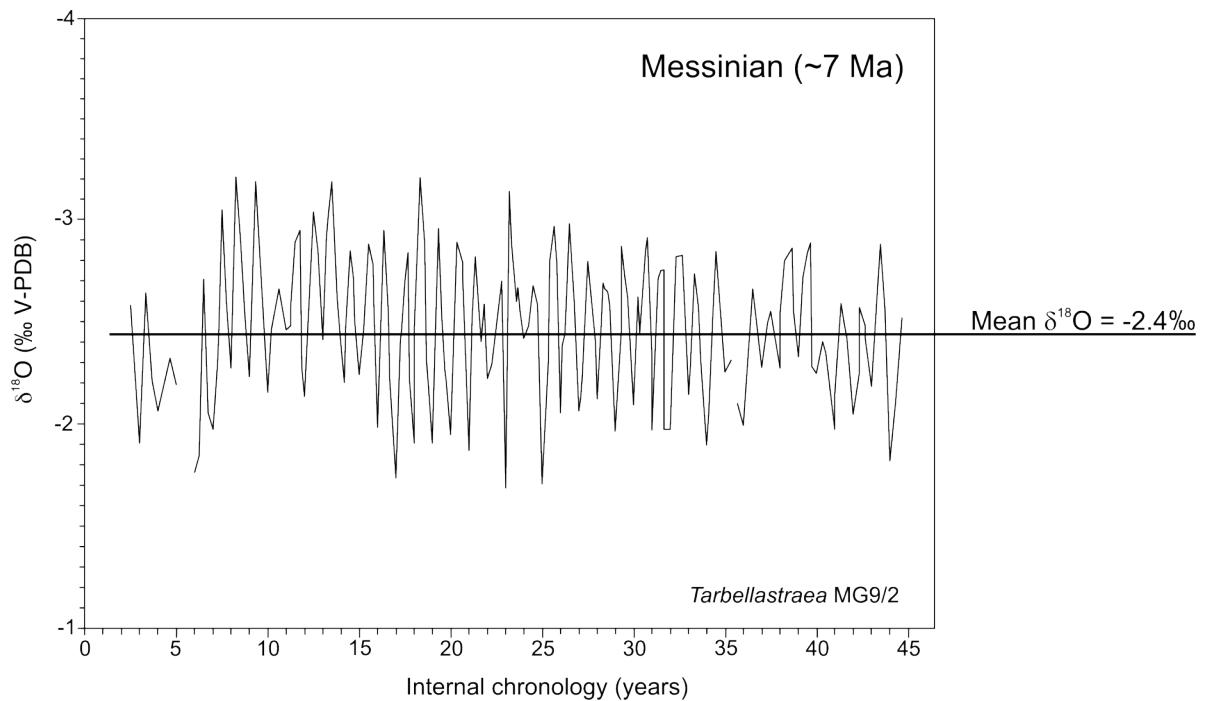


Fig. 10: 42-year $\delta^{18}\text{O}$ record of *Tarbellastraea* specimen MG9/2 (Early Messinian): Mean seasonality is 0.7‰ . Average mean $\delta^{18}\text{O}$ values for the Messinian specimens (*Tarbellastraea* and *Porites*) are -2.4‰ (horizontal line). Mean $\delta^{18}\text{O}$ seasonality between the time periods of year 2 to 16: 0.7‰ , year 17 to 25: 1.0‰ , and year 25 to 44: 0.6‰ .

2.4.4. Early Messinian stable isotope records

An early Messinian (~7 Ma) *Tarbellastraea* (MG9/2) was sampled along nine overlapping sampling tracks and with a quarterly resolution in each transect. Overlapping sections are virtually identical in $\delta^{18}\text{O}$ composition. Therefore, according to correlation of density banding and peak matching the nine transects combine into a 42-year $\delta^{18}\text{O}$ record (Fig. 10). The surface colonized by serpulids in this specimen (Fig. 6a and 6b), has no specific expression in $\delta^{18}\text{O}$ and $\delta^{13}\text{C}$, and stable isotope signatures exhibit a regular cyclic pattern over the entire skeleton. For the Messinian *Tarbellastraea* the mean $\delta^{18}\text{O}$ value is -2.46‰ and the mean $\delta^{18}\text{O}$ seasonality is $\sim 0.74\text{‰}$. However, the record is not uniform but shows varying mean $\delta^{18}\text{O}$ seasonality for distinct time periods: year 2 to 16: 0.7‰ , year 17 to 25: 1.0‰ and year 26 to 45: 0.6‰ .

Early Messinian *Porites* from Gorgolaini section are strongly affected by dissolution and cementation. Correspondingly, sampling transects are short and discontinuous not allowing to construct meaningful time-series. Therefore, analytical data of *Porites* specimen MG9/4 were merged to a mean $\delta^{18}\text{O}$ value of -2.41‰ . However, Messinian *Porites* and *Tarbellastraea* specimens from the same sampling site and bed exhibit comparable mean $\delta^{18}\text{O}$ of averaged -2.44‰ . Messinian coral $\delta^{13}\text{C}$ data exhibit the same phase-shifted pattern relative to $\delta^{18}\text{O}$ as observed in Tortonian specimens (Brachert et al., 2006b). Computed $\delta^{13}\text{C}$ mean values range from -0.87‰ to -1.25‰ .

2.5. Discussion

Porites and *Tarbellastraea* are usually prevailing in Late Miocene coral assemblages of the Mediterranean and adjacent regions. However, some reef communities are clearly dominated by *Tarbellastraea* with minor or missing *Porites* within distinct levels because of slightly different environmental preferences (Pomar et al., 1996; Perrin, 2000; Riegl and Piller, 2000).

Modern *Porites* occur in a rather broad environmental spectrum, and SST and SSS thresholds are well established (Kinsman, 1964; Lough and Barnes, 2000). Proxy records have been derived from localities close to the latitudinal limit of the genus (Fallon et al., 1999; Kuhnert et al., 1999). Little knowledge as to the environmental thresholds exists, however, with regard to extinct *Tarbellastraea*. Therefore, the main objective of this study was to consider if *Tarbellastraea* is successfully applicable as additional stable isotope proxy archive.

Both genera, *Tarbellastraea* as well as *Porites*, show the same patterns with regard to stable isotope data ($\delta^{18}\text{O}$, $\delta^{13}\text{C}$) and density bands known from modern corals. Maxima in $\delta^{18}\text{O}$ correspond with high-density bands, minima with low-density bands reflecting winter and summer season, respectively.

Tarbellastraea skeletons from Psalidha and Gorgolaini monastery sections (Central Crete) analyzed for stable isotope compositions along parallel transects exhibit consistent patterns of variability over time-equivalent density bands. We interpret the minor differences between parallel transects as artifacts of the quarterly sampling resolution and not fully age-concordant sampling. However, the overall pattern clearly shows that incipient leaching of skeletons does not affect the integrity of stable isotope ($\delta^{18}\text{O}$, $\delta^{13}\text{C}$) proxies.

Statistical methods helped to estimate the compatibility of stable isotope records from *Tarbellastraea* and *Porites*. The p -values given by one-way analyses of variance (ANOVA) for the tested Tortonian specimens (*Porites* and *Tarbellastraea*) were 0.39 for mean $\delta^{18}\text{O}$ composition and 0.50 for mean seasonality in $\delta^{18}\text{O}$. Therefore, mean $\delta^{18}\text{O}$ and mean $\delta^{18}\text{O}$ seasonality found in *Tarbellastraea* are indistinguishable statistically from that of massive *Porites* sampled from the same location and identical stratum. In spite of low annual growth rates, the $\delta^{18}\text{O}$ records give no evidence for inter-colony variability due to kinetic isotope effects known from some modern slow growing corals (McConnaughey, 1989; Felis et al., 2003). Therefore, we conclude that *Tarbellastraea* represents a new and paleoenvironmentally meaningful stable isotope proxy archive and data from both genera, *Tarbellastraea* and *Porites*, may be used mutually complimentary in paleoenvironment analyses.

Additionally, another focus of this study concerns a comparative analysis of Tortonian and Messinian stable isotope data. One-way analysis of variance (ANOVA) testing for differences between Tortonian and Messinian data sets reveals p -values of 0.07 for mean $\delta^{18}\text{O}$ and 0.02 for mean $\delta^{18}\text{O}$ seasonality, respectively. These results indicate minor differences in mean $\delta^{18}\text{O}$ but significant variation in $\delta^{18}\text{O}$ seasonality for the Tortonian and Messinian. Observed variation between Tortonian and Messinian data sets, i.e. lower $\delta^{18}\text{O}$ seasonality in the Messinian, may result from insolation changes in response to climatic precession (Santarelli et al., 1998) modifying seasonality in SST and/or SSS in the Mediterranean. The differences in $\delta^{18}\text{O}$ seasonality seen in specimen MG9/2 between distinct time periods do not reflect a pattern due to low sample resolution cutting off highest and lowest values in $\delta^{18}\text{O}$, since all samples of this specimen were gained at the same spatial

resolution. Rather, the differences in $\delta^{18}\text{O}$ seasonality may reflect short-term climatic variability.

Reconstruction of Miocene SST seasonality in the Mediterranean is confronted with the problem of unknown local SST – $\delta^{18}\text{O}$ relationships in coral aragonite. However, due to the similar oceanographic setting (i.e. marginal basin), the modern Red Sea is assumed to be a reasonable analogue to the Eastern Mediterranean during the Late Miocene (Brachert et al., 2006b). This hypothesis is confirmed by a comparison of Late Miocene $\delta^{18}\text{O}$ and phase-shifted $\delta^{13}\text{C}$ records with those of non-altered modern high-latitude *Porites* from the Red Sea (Felis et al., 1998; Rosenfeld et al., 2003) indicating very consistent cyclic patterns in Late Miocene and Red Sea corals, not only arguing for pristine preservation of Late Miocene coral aragonite but also for a Red Sea-type environment. Therefore, consistent $\delta^{18}\text{O}$ signatures in *Porites* suggest that established relationships of SST and $\delta^{18}\text{O}$ in modern *Porites* from the Red Sea (Felis et al., 2004) and Late Miocene *Porites* (Brachert et al., 2006b) are appropriate also for *Tarbellastraea*. On the basis of this assumption and provided that $\delta^{18}\text{O}$ seasonality in the Cretan corals is indeed largely controlled by temperature, seasonal SST variations were 7.3°C during the Tortonian and 4.8°C during the Messinian. Such a reconstruction would imply warmer summer and cooler winter SSTs during the Tortonian at ~9 Ma than during the Messinian at ~7 Ma. However, for three reasons reconstructed SST seasonality may represent only a minimum estimate: (1) quarterly sampling resolution, (2) incomplete documentation of the winter season due to reduced skeletal growth under cool temperatures (Wefer and Berger, 1991; Leder et al., 1996; Omata et al., 2006), or (3) seasonal changes in $\delta^{18}\text{O}$ composition of ambient seawater (Druffel, 1997). Since X-ray photographs of Tortonian and Messinian specimens show a regular density banding over the entire skeleton, we infer a continuous growth over the annual period without significant stillstands. This applies for the Messinian *Tarbellastraea* specimen shown in Fig. 6 as well, since there are no specific expressions in $\delta^{18}\text{O}$ and $\delta^{13}\text{C}$ signatures across the surface associated with calcareous tubes. Since annual growth rates are the same in Tortonian and Messinian *Tarbellastraea*, the reduced seasonality of 0.7‰ in the Messinian $\delta^{18}\text{O}$ records compared to the Tortonian with ~1.1‰ is not an effect of lower sample resolution, but may reflect changes in surface water $\delta^{18}\text{O}$ superimposed on the temperature signal, i.e. enhanced evaporation during summer or increased precipitation during winter. Both factors controlling salinity in the surface waters have the same effect of lowering seasonal $\delta^{18}\text{O}$ variations.

Assuming salinity to be the only factor controlling $\delta^{18}\text{O}$ seasonality and a modern relationship of seawater $\delta^{18}\text{O}$ composition and evaporation, the coral data equal 4.1‰ of SSS seasonality for the Tortonian and 2.7‰ for the Messinian (Pierre, 1999; Böhm et al., 2000). Seasonal SSS data from the present-day Aegean Sea (Eastern Mediterranean), however, are <2‰ at a given locality (Brasseur et al., 1996; Poulos et al., 1997) and corresponding to $\sim 0.5\text{‰}$ seasonality in $\delta^{18}\text{O}_{\text{seawater}}$ based on Pierre (1999). Therefore, since a SSS seasonality of >2‰ is unlikely according to observations in the modern Mediterranean, the main factor causing $\delta^{18}\text{O}$ seasonality in coral aragonite during the Tortonian of the Eastern Mediterranean appears to be SST. However, given that a gradual shift from humid to dry conditions during the Tortonian and the Early Messinian has been reported previously (Zidianakis et al., 2004; Fauquette et al., 2006; Reuter et al., 2006), a mixed signal of SST and SSS seasonality is inferred, especially for the Early Messinian. If accepting average annual SST of 23°C and average winter SST of 18°C for the Mediterranean during the Late Miocene based on vermetid and coral biofacies (Rosen, 1999; Bosellini et al., 2002; Brachert et al., 2006a), then the observed shift in $\delta^{18}\text{O}$ of $\sim 0.3\text{‰}$ to heavier mean $\delta^{18}\text{O}$ values in the Messinian than in the Tortonian data sets confirms the trend to higher annual mean SSS. Based on the modern temperature – $\delta^{18}\text{O}_{\text{seawater}}$ relationship found for modern coralline sponge aragonite (Böhm et al., 2000) and $\delta^{18}\text{O}_{\text{seawater}}$ – salinity relationship (Pierre, 1999) this shift indicates an increase in SSS of >1‰. The assumption that SST is the only factor changing the mean $\delta^{18}\text{O}$ values would imply by 2°C lower annual SST in the Messinian than in the Tortonian. Since the conditions in the Mediterranean are close to the lower threshold of coral reef growth already in the Tortonian and mild winter temperatures in the Messinian reported by Perez-Folgado et al. (2003), such a reduction in SST appears not conclusive. Nonetheless, changes in $\delta^{18}\text{O}_{\text{seawater}}$ due to variations in ice volume, seasonality of SST, freshwater discharge, precipitation and evaporation following insolation changes due to orbital cyclicity (Santarelli et al., 1998) must be taken into account. On the basis of the present data the most plausible explanation for the early Messinian data set is strong summer evaporation and high salinity during summers of the early Messinian with a SSS seasonality of up to 1.5‰ higher than in the Tortonian. This observation is in agreement with the increasing restriction of the Mediterranean region from the Atlantic during the Late Miocene by gradual uplift of the Betic-Rifan orogen in the Western Mediterranean from the Tortonian with conditions that were more open than today into more restricted conditions during the Messinian. This process ended up in the onset of the Messinian Salinity Crisis at 5.96 Ma (Krijgsman et al., 1999).

2.6. Conclusion

This study presents the first stable isotope records of *Tarbellastraea* corals from various time-slices of the Late Miocene from Crete (Greece). X-ray diffraction, petrographic and scanning electron microscopy (SEM) and X-ray photography show that the analyzed corals are preserved with original aragonite skeletons with no significant diagenetic alteration except for some dissolution at centers of calcification and along aragonite fibers. On the basis of a pristine state of preservation, consistent $\delta^{18}\text{O}$ and $\delta^{13}\text{C}$ signatures with *Porites* from the same stratum and modern reefs of the northernmost Red Sea, stable isotope data from *Tarbellastraea* are considered to be significant for paleoenvironmental reconstructions and fully compatible with *Porites*. The stable isotope composition indicates an average SST seasonality of 7.3°C for the Tortonian and 4.8°C for the Messinian if assuming constant seawater compositions. However, enhanced evaporation during summer appears to be a plausible factor during the Messinian, implying that $\delta^{18}\text{O}$ seasonality was not only controlled by temperature, but also by increased seasonal evaporation. Nonetheless, more coral data are needed to rule changing SST seasonality driven by orbital changes in insolation. Apart from seasonal variability, long-term stable isotope records of *Tarbellastraea* have the potential to provide further insights into changes of interannual climate variability during the Late Miocene. Therefore, *Tarbellastraea* is assumed to be an excellent new archive for geochemical proxy analysis of Oligocene and Miocene paleoenvironments, where no suitable materials of *Porites* corals are available.

2.7. References

- Abram, N.J., Webster, J.M., Davies, P.J. and Dullo, W.C., 2001. Biological response of coral reefs to sea surface temperature variation: evidence from the raised Holocene reefs of Kikai-jima (Ryukyu Islands, Japan). *Coral Reefs*, 20: 221-234.
- Böhm, F., Joachimski, M.M., Dullo, W.-C., Eisenhauer, A., Lehnert, H., Reitner, J. and Wörheide, G., 2000. Oxygen isotope fractionation in marine aragonite of coralline sponges. *Geochimica et Cosmochimica Acta*, 64(10): 1695-1703.
- Bosellini, F.R., 2006. Biotic changes and their control on Oligocene-Miocene reefs: A case study from the Apulia Platform margin (southern Italy). *Palaeogeography, Palaeoclimatology, Palaeoecology*, 241(3-4): 393-409.
- Bosellini, F.R., Russo, A. and Vescogni, A., 2002. The Messinian Reef Complex of the Salento Peninsula (Southern Italy): Stratigraphy, facies and Paleoenvironmental Interpretation. *Facies*, 47: 91-112.
- Brachert, T.C., Betzler, C., Braga, J.C. and Martín, J.M., 1996. Record of climatic change in neritic carbonates: Turnovers in biogenic associations and depositional modes (Upper Miocene, southern Spain). *Geologische Rundschau*, 85: 327-337.

- Brachert, T.C., Reuter, M., Kroeger, K.F. and Lough, J., 2006a. Coral growth bands: A new and easy to use paleothermometer in paleoenvironment analysis and paleoceanography (late Miocene, Greece). *Paleoceanography* 21, PA4217.
- Brachert, T.C., Reuter, M., Kroeger, K.F., Felis, T., Lohmann, G., A., M. and Fassoulas, C., 2006b. *Porites* corals from Crete (Greece) open a window into Late Miocene (10 Ma) seasonal and interannual climate variability. *Earth and Planetary Science Letters*, 245: 81-94.
- Brasseur, P., Beckers, J.M., Brankart, J.M. and Schoenauen, R., 1996. Seasonal temperature and salinity fields in the Mediterranean Sea: Climatological analyses of a historical data set. *Deep Sea Research Part I: Oceanographic Research Papers*, 43(2): 159-192.
- Budd, A.F., Bosellini, F.R. and Stemann, T.A., 1996. Systematics of the Oligocene to Miocene reef coral *Tarbellastraea* in the northern Mediterranean. *Palaeontology*, 39(3): 515-560.
- Chevalier, J.P., 1961. Recherches sur les Madréporaires et les formations récifales Miocènes de la Méditerranée occidentale, *Memoir de la Société géologique de France*, pp. 562.
- Cohen, A.L., Smith, S.R., McCartney, M.S. and Etten, J.v., 2004. How brain corals record climate: an integration of skeletal structure, growth and chemistry of *Diploria labyrinthiformis* from Bermuda. *Marine Ecology Progress Series*, 271: 147-158.
- Cole, J.E., Fairbanks, R.G. and Shen, G.T., 1993. Recent Variability in the Southern Oscillation: Isotopic Results from a Tarawa Atoll Coral. *Science*, 260(5115): 1790-1793.
- Constantz, B.R., 1986. The primary surface area of corals and variations in their susceptibility to diagenesis. In: Schroeder, J.H. and Purser, B.H. (Editors), *Reef Diagenesis*. Springer-Verlag, New York, pp. 53-76.
- Corrège, T., 2006. Sea surface temperature and salinity reconstruction from coral geochemical tracers. *Palaeogeography, Palaeoclimatology, Palaeoecology*, 232(2-4): 408-428.
- Druffel, E.R.M., 1997. Geochemistry of corals: Proxies of past ocean chemistry, ocean circulation, and climate. *Proceedings National Academy of Sciences USA*, 94: 8354-8361.
- Dullo, W.-C., 1984. Progressive diagenetic sequence of aragonite structures: Pleistocene coral reefs and their modern counterparts on the eastern Red Sea coast, Saudi Arabia. *Palaeontographica Americana*, 54: 254-160.
- Dullo, W.-C. and Mehl, J., 1989. Seasonal growth lines in Pleistocene scleractinians from Barbados: record potential and diagenesis. *Paläontologische Zeitschrift*, 63(3/4): 207-214.
- Esteban, M., 1979. Significance of the upper Miocene reefs of the western Mediterranean. *Palaeogeography, Palaeoclimatology, Palaeoecology*, 29: 169-188.
- Evans, M.N., Kaplan, A. and Cane, M.A., 2000. Intercomparison of coral oxygen isotope data and historical sea surface temperature (SST): Potential for coral-based SST field reconstructions. *Paleoceanography*, 15: 551-563.
- Fagerstrom, J.A., 1987. *The Evolution of Reef Communities*. John Wiley and Sons, New York, pp. 592.
- Fairbanks, R.G. and Dodge, R.E., 1979. Annual periodicity of the $^{18}\text{O}/^{16}\text{O}$ and $^{13}\text{C}/^{12}\text{C}$ ratios in the coral *Montastrea annularis*. *Geochimica et Cosmochimica Acta*, 43: 1009-1020.
- Fallon, S.J., McCulloch, M.T., van Woesik, R. and Sinclair, D.J., 1999. Corals at their latitudinal limits: laser ablation trace element systematics in *Porites* from Shirigai Bay, Japan. *Earth and Planetary Science Letters*, 172: 221-238.

- Fassoulas, C., 2001. The tectonic development of a Neogene basin at the leading edge of the active European margin: the Heraklion basin, Crete, Greece. *Journal of Geodynamics*, 31: 49-70.
- Fauquette, S., Suc, J.-P., Bertini, A., Popescu, S.-M., Warny, S., Taoufiq, N.B., Villa, M.-J.P., Chikhi, H., Feddi, N., Subally, D., Clauzon, G. and Ferrier, J., 2006. How much did climate force the Messinian salinity crisis? Quantified climatic conditions from pollen records in the Mediterranean region. *Palaeogeography, Palaeoclimatology, Palaeoecology*, 238: 281-301.
- Felis, T., Pätzold, J. and Loya, Y., 2003. Mean oxygen-isotope signatures in *Porites* spp. corals: inter-colony variability and correction for extension-rate effects. *Coral Reefs*, 22: 328-336.
- Felis, T., Pätzold, J., Loya, Y. and Wefer, G., 1998. Vertical water mass mixing and plankton blooms recorded in skeletal stable carbon isotopes of a Red Sea coral. *Journal of Geophysical Research*, 103: 30731-30739.
- Felis, T., Lohmann, G., Kuhnert, H., Lorenz, S.J., Scholz, D., Pätzold, J., Al-Rousan, S.A. and Al-Moghrabi, S.M., 2004. Increased seasonality in Middle East temperatures during the last interglacial period. *Nature*, 429: 164-168.
- Fiebig, J., Schöne, B.R. and Oschmann, W., 2005. High-precision oxygen and carbon isotope analysis of very small (10-30 µg) amounts of carbonates using continuous flow isotope ratio mass spectrometry. *Rapid Communications in Mass Spectrometry*, 19(16): 2355-2358.
- Gagan, M.K., Chivas, A.R. and Isdale, P.J., 1994. High-resolution isotopic records from corals using ocean temperature and mass-spawning chronometers. *Earth and planetary science letters*, 121: 549-558.
- Gagan, M.K., Ayliffe, L.K., Beck, J.W., Cole, J.E., Druffel, E.R.M., Dunbar, R.B. and Schrag, D.P., 2000. New views of tropical paleoclimates from corals. *Quaternary Science Reviews*, 19: 45-64.
- Gradstein, F.M., Ogg, J.G. and Smith, A.G., 2005. *A Geologic Time Scale 2004*. Cambridge University Press, 610 pp.
- Grottoli, A.G. and Eakin, C.M., 2007. A review of modern coral $\delta^{18}\text{O}$ and $\delta^{14}\text{C}$ proxy records. *Earth-Science Reviews*, 81(1-2): 67-91.
- Hallock, P. and Schlager, W., 1986. Nutrient excess and the demise of coral reefs and carbonate platforms. *Palaios*, 1: 389-398.
- Hardenbol, J., Thierry, J., Farley, M.B., Jacquin, T., de Gracianski, P.-C. and Vail, P.R., 1998. Mesozoic and Cenozoic sequence stratigraphic framework of European Basins. In: de Gracianski, P.-C., Hardenbol, J., Thierry, J. and Vail, P.R. (Editors), *Mesozoic and Cenozoic sequence stratigraphy of European Basins*. SEPM Special Publication. Society for Sedimentary Geology, Tulsa, pp. 3-14.
- Insalaco, E., 1996. The use of Late Jurassic coral growth bands as palaeoenvironmental indicators. *Palaeontology*, 39(2): 413-431.
- Ivany, L.C., Peters, S.C., Wilkinson, B.H., Lohmann, K.C. and Reimer, B.A., 2004. Composition of the early Oligocene ocean from coral stable isotope and elemental chemistry. *Geobiology*, 2: 97-106.
- Johnson, K.G. and Pérez, M.E., 2006. Skeletal extension rates of Cenozoic Caribbean reef corals. *Palaios*, 21: 262-271.
- Kinsman, D.J.J., 1964. Reef coral tolerance of high temperatures and salinities. *Nature*, 202: 1280-1282.
- Knutson, D.W., Buddemeier, R.W. and Smith, S.V., 1972. Coral chronometers: seasonal growth bands in reef corals. *Science*, 177: 270-272.
- Kouwenhoven, T.J., Seidenkrantz, M.-S. and van der Zwaan, G.J., 1999. Deep-water changes: the near-synchronous disappearance of a group of benthic foraminifera from

- the Late Miocene Mediterranean. *Palaeogeography, Palaeoclimatology, Palaeoecology*, 152: 259-281.
- Krijgsman, W., Hilgen, F.J., Raffi, I., Sierro, F.J. and Wilson, D.S., 1999. Chronology, causes and progression of the Messinian salinity crisis. *Nature*, 400: 652-655.
- Kuhnert, H., Pätzold, J., Hatcher, B., Wyrwoll, K.-H., Eisenhauer, A., Collins, L.B., Zhu, Z.R. and Wefer, G., 1999. A 200-year coral stable isotope record from a high-latitude reef off Western Australia. *Coral Reefs*, 18: 1-12.
- Land, L.S., 1967. Diagenesis of skeletal carbonates. *Journal of Sedimentary Petrology*, 37: 914-930.
- Leder, J.J., Swart, P.K., Szmant, A.M. and Dodge, R.E., 1996. The origin of variations in the isotopic record of scleractinian corals: I. Oxygen. *Geochimica et Cosmochimica Acta*, 60(15): 2857-2870.
- Lough, J.M. and Barnes, D.J., 2000. Environmental controls on growth of the massive coral *Porites*. *Journal of Experimental Marine Biology and Ecology*, 245: 225-243.
- Mackenzie, G., Veauvy, C.M. and Swart, P.K., 1997. Climatic variation in the Early to Middle Eocene using the stable isotopic composition of coral skeletons. Geological Society of America Annual Meeting, Salt Lake City, Abstracts with Programs, 29: A-395.
- Martín, J.M. and Braga, J.C., 1994. Messinian events in the Sorbas basin in southeastern Spain and their implications in the recent history of the Mediterranean. *Sedimentary Geology*, 90: 257-268.
- McConnaughey, T., 1989. ^{13}C and ^{18}O isotopic disequilibrium in biological carbonates: I. Patterns. *Geochimica Cosmochimica Acta*, 53: 151-162.
- McGregor, H.V. and Gagan, M.K., 2003. Diagenesis and geochemistry of *Porites* corals from Papua New Guinea: Implications for paleoclimate reconstruction. *Geochimica et Cosmochimica Acta*, 67(12): 2147-2156.
- Mertz-Kraus, R., Brachert, T.C. and Reuter, M., 2007a. *Tarbellastraea*: a new archive for paleoenvironmental research, EGU General Assembly 2007. *Geophysical Research Abstracts*, 9: 03390.
- Mertz-Kraus, R., Brachert, T.C., Galer, S.J.G., Stoll, B. and Jochum, K.P., 2007b. Seasonal element and Sr isotope ratio variations in Late Miocene corals from Crete, Eastern Mediterranean. *Geochimica et Cosmochimica Acta*, 71(15, Supplement 1): A656.
- Meulenkamp, J.E. and Sissingh, W., 2003. Tertiary palaeogeography and tectonostratigraphic evolution of the Northern and Southern Peri-Tethys platforms and the intermediate domains of the African-Eurasian convergent plate boundary zone. *Palaeogeography, Palaeoclimatology, Palaeoecology*, 196(1-2): 209-228.
- Meulenkamp, J.E., Dermitzakis, M., Georgiadou-Dikeoulia, E., Jonkers, H.A. and Böger, H., 1979. Field guide to the Neogene of Crete, University of Athens, Athens.
- Omata, T., Suzuki, A., Kawahata, H., Nojima, S., Minoshima, K. and Hata, A., 2006. Oxygen and carbon stable isotope systematics in *Porites* coral near its latitudinal limit: The coral response to low-thermal temperature stress. *Global and Planetary Change*, 53(1-2): 137-146.
- Perez-Folgado, M., Sierro, F.J., Barcena, M.A., Flores, J.A., Vazquez, A., Utrilla, R., Hilgen, F.J., Krijgsman, W. and Filippelli, G.M., 2003. Western versus eastern Mediterranean paleoceanographic response to astronomical forcing: a high-resolution microplankton study of precession-controlled sedimentary cycles during the Messinian. *Palaeogeography Palaeoclimatology Palaeoecology*, 190: 317-334.
- Perrin, C., 2000. Changes of palaeozonation patterns within Miocene coral reefs, Gebel Abu Shaar, Gulf of Suez, Egypt. *Lethaia*, 33(4): 253-268.

- Perrin, C., 2002. Tertiary: The emergence of modern reef ecosystems. In: Kiessling, W. and Flügel., E. (Editors), Phanerozoic reef patterns. SEPM Special Publication. Society for Sedimentary Geology, Tulsa, pp. 587-621.
- Pierre, C., 1999. The oxygen and carbon isotope distribution in the Mediterranean water masses. *Marine geology*, 153: 41-55.
- Pomar, L., 1991. Reef geometries, erosion surfaces and high-frequency sea-level changes, upper Miocene reef complex, Mallorca, Spain. *Sedimentology*, 38: 243-270.
- Pomar, L., Ward, W.C. and Green, D.G., 1996. Upper Miocene reef complexes of the Lluçmajor area, Mallorca, Spain. In: Franseen, E.K., Esteban, M., Ward, W.C. and Rouchy, J.-M. (Editors), Models for carbonate stratigraphy from Miocene reef complexes of Mediterranean regions. Concepts in Sedimentology and Paleontology. Society for Sedimentary Geology, Tulsa, pp. 191-225.
- Poulos, S.E., Drakopoulos, P.G. and Collins, M.B., 1997. Seasonal variability in sea surface oceanographic conditions in the Aegean Sea (Eastern Mediterranean): an overview. *Journal of Marine Systems*, 13(1-4): 225-244.
- Quinn, T.M. and Sampson, D.E., 2002. A multiproxy approach to reconstructing sea surface conditions using coral skeleton geochemistry. *Paleoceanography*, 17(4).
- Rahl, J.M., 2004. Exhumation of high-pressure metamorphic rocks within an active convergent margin, Crete, Greece. Field-trip guide book., 32nd International Geological Congress, Florence, Italy, pp. 36.
- Reuter, M. and Brachert, T.C., 2007. Freshwater discharge and sediment dispersal - control on growth, ecological structure and geometry of Late Miocene shallow-water coral ecosystems (Early Tortonian, Crete/Greece). *Palaeogeography, Palaeoclimatology, Palaeoecology*.
- Reuter, M., Brachert, T.C. and Kroeger, K.F., 2005. Diagenesis of growth bands in fossil scleractinian corals: Identification and modes of preservation. *Facies*, 51: 155-168.
- Reuter, M., Brachert, T.C. and Kroeger, K.F., 2006. Shallow-marine carbonates of the tropical - temperate transition zone: effects of hinterland climate and basin physiography (Late Miocene, Crete/Greece). In: Pedley, H.M. and Carannante, S. (Editors), Cool-Water Carbonates. Geological Society of London, Special Publication. Geological Society of London, London, pp. 157-178.
- Riegl, B. and Piller, W.E., 2000. Biostromal coral facies - A Miocene example from the Leitha Limestone (Austria) and its actualistic interpretation. *Palaios*, 15(5): 399-413.
- Rosen, B.R., 1999. Paleoclimatic implications of the energy hypothesis from Neogene corals of the Mediterranean region. In: Agusti, J., Rook, L. and Andrews, P. (Editors), The evolution of Neogene terrestrial ecosystems in Europe. Cambridge University Press, pp. 309-327.
- Rosenfeld, M., Yam, R., Shemesh, A. and Loya, Y., 2003. Implication of water depth on stable isotope composition and skeletal density patterns in a *Porites lutea* colony: results from a long-term translocation experiment. *Coral Reefs*, 22(4): 337-345.
- Roulier, L.M. and Quinn, T.M., 1995. Seasonal- to decadal-scale climatic variability in southwest Florida during the middle Pliocene: Inferences from a coralline stable isotope record. *Paleoceanography*, 10(3): 429-443.
- Sachse, M. and Mohr, B.A.R., 1996. Eine obermiozäne Makro- und Mikroflora aus Südkreta (Griechenland), und deren paläoklimatische Interpretation.- Vorläufige Betrachtungen. *Neues Jahrbuch für Geologie und Paläontologie - Abhandlungen*, 200(1/2): 149-182.
- Santarelli, A., Brinkhuis, H., Hilgen, F.J., Lourens, L.J., Versteegh, G.J.M. and Visscher, H., 1998. Orbital signatures in a Late Miocene dinoflagellate record from Crete (Greece). *Marine Micropaleontology*, 33: 273-297.

- Scherer, M., 1977. Preservation, alteration and multiple cementation of aragonitic skeletons from the Cassian Beds (U. Triassic, southern Alps). *Neues Jahrbuch für Geologie und Paläontologie, Abhandlungen*, 154: 213-262.
- Schlager, W., 1992. Sedimentology and sequence stratigraphy of reefs and carbonate platforms, a short course. The American Association of Petroleum Geologists, Continuing Education Course Note Series, 34: 1-71.
- Shinn, E.A., 1966. Coral growth-rate, an environmental indicator. *Journal of Paleontology*, 40: 233-240.
- Spötl, C. and Vennemann, T.W., 2003. Continuous-flow isotope ratio mass spectrometric analysis of carbonate minerals. *Rapid Communications in Mass Spectrometry*, 17(9): 1004-1006.
- Swart, P.K., 1983. Carbon and oxygen isotope fractionation in scleractinian corals: A review. *Earth-Science Reviews*, 19: 51-80.
- Swart, P.K.H., G.F., Dodge, R.E., Kramer, P., Hudson, J.H., Halley, R.B. and Robblee, M.B., 1996. The stable oxygen and carbon isotopic record from a coral growing in Florida Bay: a 160 year record of climatic and anthropogenic influence. *Palaeogeography, Palaeoclimatology, Palaeoecology*, 123: 219-237.
- ten Veen, J.H. and Postma, G., 1999. Neogene tectonics and basin fill patterns in the Hellenic outer-arc (Crete, Greece). *Basin Research*, 11(3): 223-242.
- Tudhope, A.W., Chilcott, C.P., McCulloch, M.T., Cook, E.R., Chappell, J., Ellam, R.M., Lea, D.W., Lough, J.M. and Shimmield, G.B., 2001. Variability in the El Niño-Southern Oscillation through a glacial-interglacial cycle. *Science*, 291: 1511-1517.
- Veron, J.E.N. and Minchin, P.R., 1992. Correlations between sea surface temperature, circulation patterns and the distribution of hermatypic corals of Japan. *Continental Shelf Research*, 12(7): 835-857.
- Weber, J.N. and Woodhead, P.M.J., 1970. Carbon and oxygen isotope fractionation in the skeletal carbonate of reef-building corals. *Chemical Geology*, 6: 93-117.
- Wefer, G. and Berger, W.H., 1991. Isotope paleontology: growth and composition of extant calcareous species. *Marine Geology*, 100: 207-248.
- Wendt, J., 1975. Aragonitische Stromatoporen aus der alpinen Obertrias. *Neues Jahrbuch für Geologie und Paläontologie, Abhandlungen*, 150: 111-125.
- Zidianakis, G., Mohr, B. and Fassoulas, C., 2004. The Late-Miocene flora of Vrysses, Western Crete - A contribution to the climate and vegetation history, 5th International Symposium on Eastern Mediterranean Geology, Thessaloniki, Greece, pp. 515-518.

3. Late Miocene sea surface salinity variability and paleoclimate conditions in the Eastern Mediterranean inferred from coral aragonite $\delta^{18}\text{O}$

This chapter is in press with Chemical Geology:

Mertz-Kraus, R., Brachert, T.C., Reuter, M., Galer, S.J.G., Fassoulas, C. and Iliopoulos, G., 2009. Late Miocene sea surface salinity variability and paleoclimate conditions in the Eastern Mediterranean inferred from coral aragonite $\delta^{18}\text{O}$. Chemical Geology, doi:10.1016/j.chemgeo.2009.01.010.

3.1. Abstract

Coral skeletons are archives of chemical proxies which enable paleoenvironmental reconstructions to be made at subannual resolution. Stable oxygen isotope ($\delta^{18}\text{O}$) ratios of these archives reflect sea surface temperature (SST) as well as the $\delta^{18}\text{O}$ composition of ambient seawater. The $\delta^{18}\text{O}_{\text{seawater}}$ composition is not only controlled by global ice build-up, but river discharge and the hydrological balance of evaporation and precipitation, all influencing sea surface salinity (SSS), also play an important role in marginal seas. New sub-annually resolved coral $\delta^{18}\text{O}$ data were measured and evaluated together with published data from reef coral communities of Late Miocene age from Crete (Eastern Mediterranean). This time-window is of particular importance for the paleoceanographic evolution of the Mediterranean Sea, because it covers the successive closure of the marine gateways connecting the Mediterranean with the Atlantic Ocean, which culminated in the onset of the Messinian salinity crisis (MSC) at 5.96 Ma. Corals were recovered from eight time-slices dated by $^{87}\text{Sr}/^{86}\text{Sr}$ chronostratigraphy and cover a time-window from ~ 10 to ~ 7 Ma to monitor pre-MSC environmental changes. The oxygen isotope composition of the reef corals *Porites* and *Tarbellastraea* document significant changes in mean annual $\delta^{18}\text{O}$ as well as in mean $\delta^{18}\text{O}$ seasonality during the Late Miocene. Tortonian and Messinian coral mean annual $\delta^{18}\text{O}$ values differ by up to 1.72‰ and exhibit substantial variability. Since SSTs can be considered rather constant over the Late Miocene according to lithological, paleobotanical and geochemical evidence, the mean annual $\delta^{18}\text{O}$ variations in the corals appear to result from changing SSS during the Late Miocene prior to the MSC. This result is in contrast to earlier concepts that, despite increasing isolation of the Mediterranean basin starting at about 9 Ma ago, SSS did not change until only 300 kyr prior to the deposition of the first MSC evaporites. Mean seasonal $\delta^{18}\text{O}$ amplitudes are lower by 0.4‰ in the Messinian compared to those of the Tortonian corals, which may be due to enhanced summer evaporation. Spectral analyses of Tortonian and Messinian coral $\delta^{18}\text{O}$ records indicate significant interannual variability with periods of 2-3 and 4-5 years. Such variability is similar to that found in modern records. In the modern case, the Iceland Low and Azores High pressure centers influence climate in the Circum-Mediterranean region. Combined with evidence from other studies, the coral records of this study suggest that a similar pressure field system was already in existence in the early Late Miocene.

Keywords: Paleoclimate, $\delta^{18}\text{O}$, sea surface salinity, sea surface temperature, corals, Messinian, Tortonian, Crete, Eastern Mediterranean

3.2. Introduction

The Late Miocene sedimentary record of the Mediterranean region heralds one of the most profound geological events of the Cenozoic: increasing Mediterranean restriction, partial desiccation and marine refilling during the Messinian salinity crisis (MSC) ~6 Ma ago (Hsü et al., 1977). Although many problems regarding “the chronology, causes and progression of the MSC” (Krijgsman et al., 1999) remain, a consistent pattern has started to emerge (Rouchy and Caruso, 2006). According to Sr isotope data from foraminifera, the Atlantic - Mediterranean water mass exchange started to be increasingly severed about 9 Ma ago, 3 Myr earlier than accumulation of the first evaporites of the MSC. However, salinity is usually believed to have remained essentially constant and marine in the Mediterranean basin during this pre-evaporite period because evaporation was balanced by deep brine outflow and freshwater discharge and/or precipitation (Flecker and Ellam, 1999; 2006). The geological expression of this situation is an omnipresent suite of conspicuous marl - sapropel cycles because freshwater input was not constant but strongly pulsed at precessional time-scales (Hilgen et al., 1995; Schenau et al., 1999). Associated salinity and/or water temperature changes are well documented in various stable isotope and micropaleontological data sets from the Circum-Mediterranean region. Typically, $\delta^{18}\text{O}$ values of Late Miocene microfossils from different sedimentary sections within the Mediterranean region show enhanced variations in the course of the Late Miocene compared to the Late Miocene open ocean (Kouwenhoven et al., 1999; Perez-Folgado et al., 2003; Santarelli et al., 1998; Sierro et al., 2003). As a consequence of continual restriction, hinterland climate (including remote precipitation of the African monsoon) played an increasingly significant role in Mediterranean hydrography and as a pacemaker of the geological record (Rohling et al., 2008; Tzedakis, 2007). However, on the basis of vegetational data, it is generally thought that modern Mediterranean climate with hot, dry summers and mild, wet winters did not develop before 3.6 Ma (Suc, 1984; Suc and Popescu, 2005) whereas winter precipitation has been reinforced during Pleistocene episodes of sapropel formation (Wijmstra et al., 1990). Subannually resolved stable isotope data from reef corals (*Porites*) of Late Miocene age and climate model results, however, suggest the

modern climatic system appeared earlier in the course of the Tertiary or before (Brachert et al., 2006a).

Despite detailed knowledge of pelagic and terrestrial high-frequency ecosystem change in response to climatic fluctuations and Mediterranean restriction, very little is known about its effects on shallow water benthic ecosystems. Previous studies focused on sedimentary facies analysis and sea-level signatures in reefs and carbonate platforms (Esteban, 1996; Pomar, 1991). For the Western Mediterranean region, sea-level change was found to be in phase with sea surface temperatures (SSTs) causing rhythmic reef demise and turnover in carbonate-producing biotic associations (Brachert et al., 1996; Martín and Braga, 1994). This fits more recent findings of pronounced glacial control on sea-level fluctuations during the Neogene (Billups and Schrag, 2003; Sánchez-Almazo et al., 2007; Westerhold et al., 2005) and stable isotope data, therefore, represent excellent proxy sets of Neogene sea level (Miller et al., 2005). In the Eastern Mediterranean region, cold Atlantic spells have not been clearly documented in Late Miocene SSTs (Kroeger et al., 2006), however, pulsed freshwater influx and sediment discharge, possibly responding to astronomical forcing, have been shown to be an important factor in controlling coral reef distribution during the Tortonian (Reuter and Brachert, 2007). A recent account of Mediterranean reef distribution during the Late Miocene is given by Brachert et al. (2006b). Usually, geochemical proxy records of the Neogene based on deep sea sedimentary successions resolve thousands of years and fail to reveal climate variability on interannual and seasonal timescales.

In this paper we show how geochemical coral data can be of particular significance to Neogene paleoclimatology. Usually, massive reef corals grow to large size in tropical – subtropical shallow-water environments and are especially sensitive to sea level, SST and sea surface salinity (SSS); however, aragonite saturation and nutrient concentrations are also important for coral growth (Kleypas et al., 1999). The massive skeletons, composed of CaCO₃ (aragonite), exhibit annual incremental growth and, therefore, represent excellent time-calibrated paleoenvironment archives (Druffel, 1997). Time-series of geochemical proxy data from the aragonite skeletons are extremely useful for describing environmental variability on subannual to decadal time scales for both, instrumental and pre-instrumental time periods (e.g., Druffel, 1997). Stable oxygen isotope ratios ($\delta^{18}\text{O}$) represent the most widely used coral geochemical proxy. However, its use as a paleothermometer is limited, because the $\delta^{18}\text{O}$ signal represents both SST and SSS, and ambient seawater $\delta^{18}\text{O}$ may vary in time and space as a result of local evaporation/precipitation and patterns of river

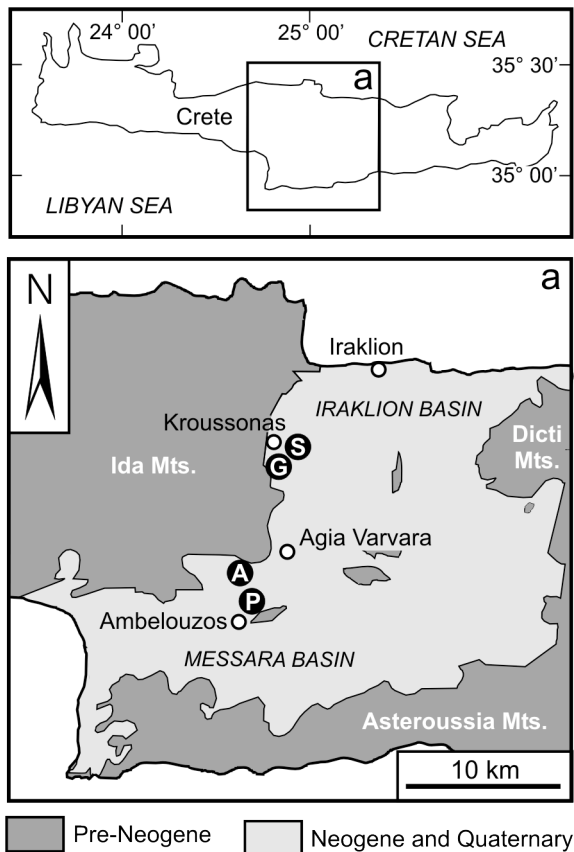


Fig. 11: Simplified geological map of Central Crete, Greece. (P) Psalidha, Early Tortonian and (A) Apomarma, Early Messinian, Messara Basin; (G) Gorgolaini Monastery and (S) Sarhos, Early Messinian, western margin of Iraklion Basin.

discharge (Weber and Woodhead, 1972). SST calibrations from $\delta^{18}\text{O}$, therefore, require additional, independent geochemical proxy data (i.e. Sr/Ca) (Gagan et al., 2000). For geological time, however, such SST reconstructions remain problematic because of glacial changes in $\delta^{18}\text{O}$ of global sea water and secular variations in trace element ratios (Lear et al., 2003; Zachos et al., 2001). In order to overcome the problem of seawater effects on the $\delta^{18}\text{O}$ thermometer and other geochemical proxy data during the late Neogene, the statistically significant relationship between SST and annual extension or growth rate for certain reef corals (Lough and Barnes, 2000; Slowey and Crowley, 1995) can be applied (Brachert et al., 2006b).

Coral skeletons (*Porites*, *Tarbellastraea*) of Late Miocene age (Tortonian and Messinian) from the island of Crete (Eastern Mediterranean) were recovered from two areas representing eight time-slices covering the period from ~10 to ~7 Ma. The ~3 Myr-period covered by our sampling falls in the time of increasing restriction of the Mediterranean modulated by climatic changes on subannual to geological time scales. We compare our new data to published coral stable isotope time-series (Brachert et al., 2006a; Mertz-Kraus et al., 2008) in terms of average $\delta^{18}\text{O}$ composition and seasonal $\delta^{18}\text{O}$ variability in order to separate long-term effects of global sea level from Eastern Mediterranean evaporation/precipitation systems and freshwater discharge or salinity and seasonal SST changes. Our observations substantially complement views about the hydrological balance or freshwater discharge with climatic precession and seasonal distribution of precipitation/evaporation and can therefore help in completing our picture of Neogene Mediterranean climate dynamics and hydrography.

3.3. Geological context

Basins of Neogene age are scattered over the island of Crete and were formed following extensional geodynamic processes in the Aegean region during the Middle Miocene (Fassoulas, 2001; Meulenkamp and Sissingh, 2003). In this study, we focus on

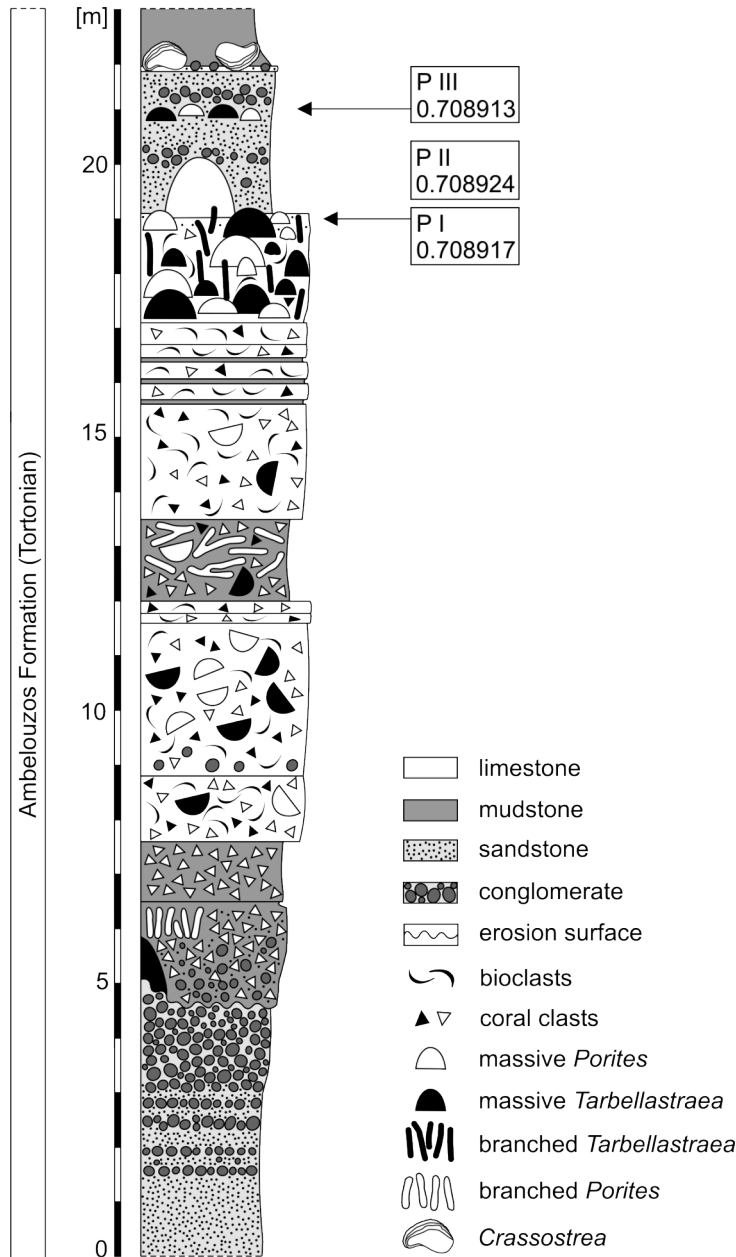


Fig. 12: Geological section at Psalidha with sampling sites P I, P II and P III (Tortonian) indicated, and respective mean $^{87}\text{Sr}/^{86}\text{Sr}$ values. P I is equivalent to CL 1.2 of Brachert et al. (2006b).

material sampled from Miocene sediments of the Iraklion and Messara Basins in Central Crete (Fig. 11). These sediments can be subdivided into two stratigraphic units: (1) the Ambelouzos Formation of Serravallian to Tortonian age, and (2) the Varvara Formation of Late Tortonian to Early Messinian age (Meulenkamp et al., 1979; ten Veen and Postma, 1999). The Ambelouzos Formation consists of clastic sediments, which have been attributed to brackish-lagoonal, marginally marine and open marine depositional environments where the climate was humid. Coral constructions representing both, biostromes and bioherms, are associated with coarse-grained delta

deposits and marine clastics (Faranda et al., 2007; Reuter and Brachert, 2007).

Sediments of the Varvara Formation overlay those of the Ambelouzos Formation, and comprise shallow marine limestones with reef corals (Pirgos Member), as well as deeper marine marls, with

intercalated calciturbidites and debris flow deposits, and evaporites. The change from shallow marine clastics to carbonates, and finally evaporites reflects increasing sediment starvation of the basin with time. Such changes were most likely a consequence of structural rejuvenations of the basin, long-term relative rise of sea level, and climatic aridification which took place during the course of the Late Miocene (Fassoulas, 2001; Reuter et al., 2006). In addition to long-term changes, Tortonian coral constructions reflect high-frequency variability of freshwater input and sediment discharge, possibly in response to climatic precession (Reuter and Brachert, 2007).

Stratal architectures and stacking patterns of seven unconformity-bound depositional units (or “Coral levels”, CL of Brachert et al. (2006b)) were grouped into three larger-scale depositional sequences. They represent the backbone for the age model for Late Miocene shallow-water deposits of Western Iraklion Basin in central Crete (Brachert et al., 2006b; Reuter et al., 2006). Units 1 to 3 represent the Early Tortonian sea-level cycle, Units 4 to 6 the Late Tortonian, and Unit 7 the Early Messinian eustatic cycles of Hardenbol et al. (1998), respectively. Since outcrops are isolated in most basins it is difficult to establish a stratigraphic framework on a larger geographical scale. Thus, it should be borne in mind that some corals described in this study cannot be placed univocally within the stratigraphy of the Western Iraklion Basin.

3.4. Sampling sites

The coral samples are from two areas in central Crete which are at the northern margin of the Messara Basin and at the western margin of the Iraklion Basin, respectively (Fig. 11). In the northern Messara Basin, corals were sampled at three sites near the abandoned town of Psalidha just north of the town of Ambelouzos (Fig. 11). Psalidha coral sites are within the lower segment of the Tortonian Ambelouzos Formation (Fig. 12) at the top of a coral build-up (thickness 15 m) and within the overlying unit of coarse clastics (thickness 3 m). The build-up exhibits prominent horizontal, parallel bedding resulting from the stacking of coral biostromes and bioclastic carbonates. *Porites* and *Tarbellastraea* are the dominant coral genera. A detailed sedimentological and paleoecological analysis is reported in Reuter and Brachert (2007).

Sampling site P I (E 24.96094°, N 35.08424°), identical with section B of Reuter and Brachert (2007), is located along the contact surface of the topmost biostrome with overlying sandstone and conglomerate. This site can be considered equivalent to the top of

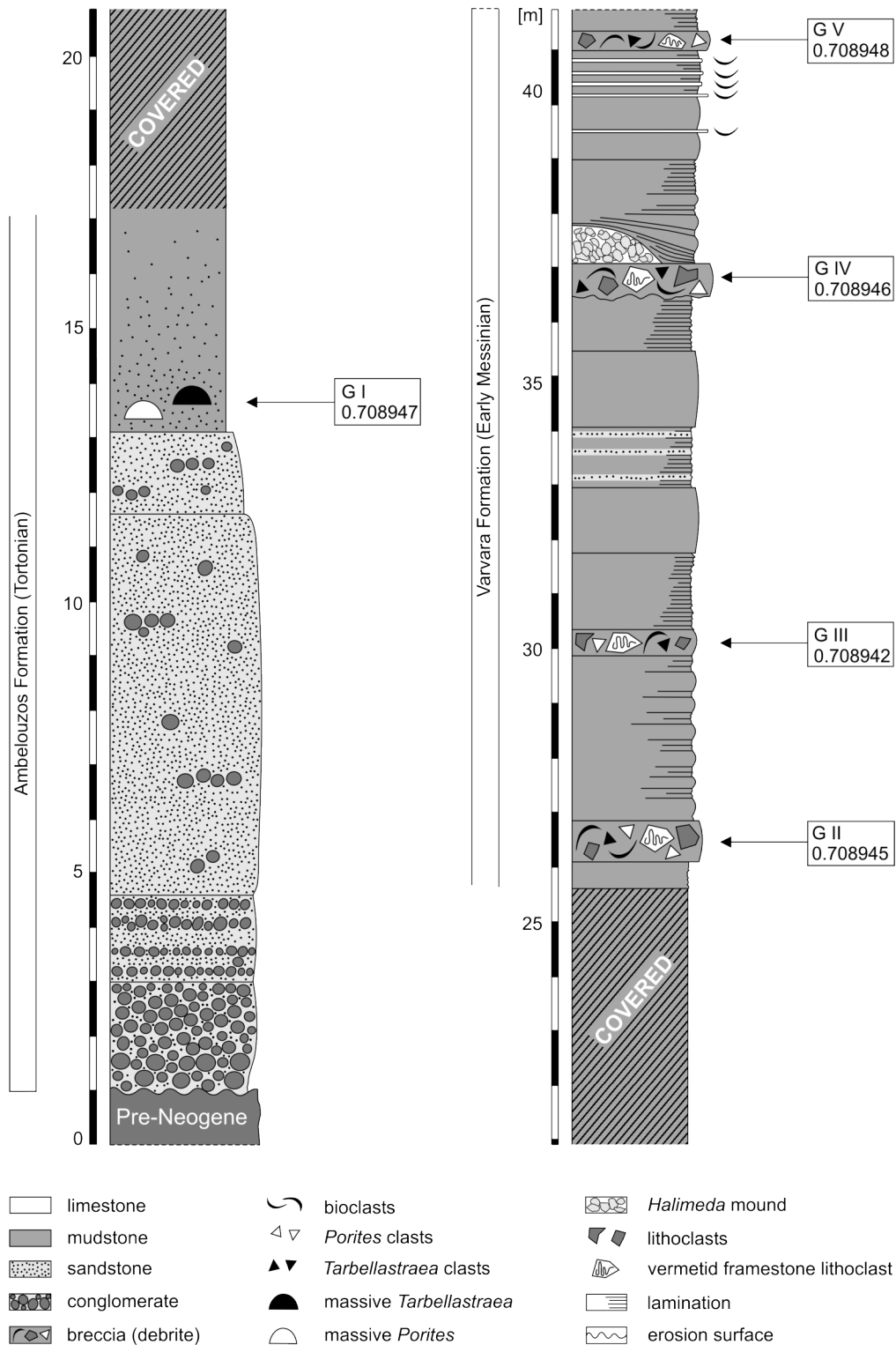


Fig. 13: Geological section at Gorgolaini Monastery including sampling sites G I (CL 4) of Tortonian age, G II (CL 7.1), G III, G IV (CL 7.2) and G V (CL 7.3) from the Early Messinian and respective mean $^{87}\text{Sr}/^{86}\text{Sr}$ values. CL nomenclature of Brachert et al. (2006b).

stratigraphic Unit 1 of the Western Iraklion chronostratigraphic succession. Some of the corals along the contact are extremely large up to a height of ca. 1 m and dominated by massive *Porites* still in life position. This gives the stratigraphic surface a strongly undulating shape, with some of the corals being almost fully encased by cross-stratified sandstone or conglomerate. According to coral zonation patterns in Late Miocene reefs of the Mediterranean, water depth was <20 m. Site P III lies stratigraphically above and within the sandstone unit. It represents a small patch of massive, non framework-forming *Porites* (decimeter size) in life position (E 24.96038°, N 35.08498°). An oyster bed composed of *Crassostrea* sp. shells forms the top of the sandstone unit and indicates a very shallow, marginal marine environment (Kirby, 2001). It marks an abrupt transition into fine-grained sediments of the Ambelouzos Formation and final drowning of Psalidha reef site (Fig. 12). Site P II, congruent with section C of Reuter and Brachert (2007), is located in a nearby olive grove (linear distance ~550 m, E 24.96488°, N 35.08682), which is situated within the unit of coarse clastics on top of the build-up. Because of poor outcrop, corals were collected from soil, which obscures their exact stratigraphic position. However, the similarity in Sr isotope composition to that of corals from P I (Mertz-Kraus et al., 2008) suggests that P II lies stratigraphically between that of P I and P III, or perhaps is identical with P I. Combined lithostratigraphic and biostratigraphic data suggest an age of ~10 Ma for coral site P I (Brachert et al., 2006a; Faranda et al., 2007; Frydas et al., 2008) and an age of ~9 to 10 Ma for sites P II (Mertz-Kraus et al., 2007) based on $^{87}\text{Sr}/^{86}\text{Sr}$ chronostratigraphy.

The second set of sampling sites is located at the western margin of the Iraklion Basin, to the northwest of Gorgolaini Monastery (Fig. 11). The Gorgolaini section is 40 m thick and formed of sediments of Tortonian and Early Messinian age onlapping Pre-Neogene basement. Corals crop out in distinct stratigraphic levels and have been collected at sites G I, G II, G III, G IV and G V (Fig. 13). The lowermost sampling level G I (E 25.63861°, N 35.34819°) lies on top of a thick conglomerate and is composed of sandy marl containing coarse sand-granular lithoclasts and decimeter-sized corals in life position. Lithostratigraphically, this sampling level is located near the top of the Ambelouzos Formation and, in terms of sequence stratigraphy, is equivalent to Unit 4 (or CL 4) of Late Tortonian age (Brachert et al., 2006b). The section continues after ~8.5 m covered by vegetation and slope debris with a succession of bipartite cycles of laminated marl and homogeneous marl with thin intervening beds of calciturbidites and four thick beds of breccia interpreted as debrites (Fig. 13). These debrites contain lithoclasts of Pre-Neogene basement, Messinian vermetid limestone, and coral fragments, including almost complete

specimens of *Porites* and *Tarbellastraea*. Coral size ranges from a few centimeters to several decimeters. Some of the corals have fully or partially retained their original aragonite mineralogy.

The upper part of the Gorgolaini section belongs to the lower Varvara Formation which has been assigned an Early Messinian biostratigraphic age (Meulenkamp et al., 1979). According to the sequence stratigraphic framework of the Western Iraklion Basin, this section also corresponds to Unit 7 (CL 7), which correlates to the Early Messinian eustatic sea-level cycle (Hardenbol et al., 1998). The sampling sites G II, G IV and G V (E 24.9819°, N 35.20535°) of our study are equivalent to coral levels CL 7.1, CL 7.2 and CL 7.3 (Brachert et al., 2006b). A section of the Varvara Formation, with intercalated volcanic ash layers and base of slope deposits (turbidites) in Northern Messara Basin (Kastelli), was dated at 6.8 to 6.9 Ma (Hilgen et al., 1997; ten Veen and Postma, 1999), which is in agreement with an Early Messinian age for sites G II to G V. Distinct cycles of homogeneous marl and dark gray laminated marl within the Gorgolaini section might be equivalent to a conspicuous bipartite marl – sapropelite succession described from various locations on Crete, which reflect precession-driven climatic change (Krijgsman et al., 1995; Santarelli et al., 1998). On this basis, the top of the section at site G V might only be some hundreds of kyr younger than that of site G II.

3.5. Material and methods

3.5.1. Sample preparation

In the field, only almost white-colored coral specimens with relatively low density were selected, because from personal sampling experience such specimens have proven to most likely represent corals having retained their primary aragonitic skeleton and porosity, respectively. In contrast, specimens not suitable for geochemical analyses have signs of neomorphosis, recrystallization and cementation, resulting in higher density.

In the laboratory, slabs of ~6 mm thickness were sliced out of each coral specimen parallel to the axis of maximum growth. After cleaning the slabs with a solution of hydrogen peroxide (<1%), contact radiographs were obtained using a Faxitron model 805 X-ray unit (3 mA, 45 kV, exposure time 6 to 9 minutes) and AGFA Structurix D4 FW Industrial X-ray film. X-ray diffraction (XRD), reflected light stereomicroscopic analysis and scanning electron microscopy (SEM) were performed on random samples in order to check for diagenetical alteration prior to preparation for radiogenic and stable isotope

Table 2: Specimen number, sampling site code (P = Psalidha, G = Gorgolaini Monastery), mean $^{87}\text{Sr}/^{86}\text{Sr}$ ratios of each sampling site (2σ analytical error <0.000008), genus, length of obtained time series, mean $\delta^{18}\text{O}$ values, average $\delta^{18}\text{O}$ minima (summer) as well as maxima (winter), mean $\delta^{18}\text{O}$ amplitudes (seasonality) and average annual growth rate of the analyzed corals. ^x Brachert et al. (2006a), ⁺ Mertz-Kraus et al. (2008)

Specimen	Sampling level	$^{87}\text{Sr}/^{86}\text{Sr}$	Genus	Time series [years]	Mean $\delta^{18}\text{O}$ [‰]	Average $\delta^{18}\text{O}$ minima [‰]	Average $\delta^{18}\text{O}$ maxima [‰]	Mean $\delta^{18}\text{O}$ amplitudes [‰]	Annual growth rate [mm y^{-1}]	
P2 ^x	P I	0.708917	<i>Porites</i>	66.7	-2.68	-3.11	-2.16	0.95	3.6	Tortonian
P16	P I		<i>Porites</i>	20.8	-2.74	-3.20	-2.07	1.08	3.4	
P1 ^x	P II	0.708924	<i>Porites</i>	15.0	-2.76	-3.11	-2.20	0.91	4.9	
P3 ^x	P II		<i>Porites</i>	3.7	-2.60	-3.08	-1.94	1.14	5.8	
P4 ^x	P II		<i>Porites</i>	11.2	-2.95	-3.44	-2.28	1.16	4.5	
P7 ⁺	P II		<i>Tarbellastraea</i>	10.3	-2.53	-3.02	-2.03	0.99	3.3	
P8 ⁺	P II		<i>Porites</i>	16.6	-2.70	-3.08	-2.05	1.03	5.0	
P8B	P II		<i>Porites</i>	20.5	-2.44	-2.90	-1.75	1.15	5.7	
P9 ⁺	P II		<i>Porites</i>	17.8	-2.50	-3.00	-1.82	1.18	3.6	
P12	P III	0.708913	<i>Porites</i>	18.2	-3.42	-3.88	-2.67	1.21	5.3	
P14	P III		<i>Porites</i>	14.7	-3.23	-3.71	-2.46	1.25	4.7	
SF1	G I	0.708947	<i>Tarbellastraea</i>	15.0	-1.79	-1.98	-1.40	0.58	2.0	
SF2	G I		<i>Tarbellastraea</i>	10.0	-1.52	-1.70	-1.31	0.39	1.9	
SF3	G I		<i>Tarbellastraea</i>	—	-1.59	—	—	—	—	
SF4	G I		<i>Tarbellastraea</i>	—	-1.60	—	—	—	—	
SF5	G I		<i>Tarbellastraea</i>	—	-1.68	—	—	—	—	
MG9/2 ⁺	G II	0.708945	<i>Tarbellastraea</i>	42.2	-2.46	-2.82	-2.08	0.74	3.4	Messinian
MG9/4	G II		<i>Porites</i>	—	-2.41	—	—	—	—	
MG9/6	G II		<i>Tarbellastraea</i>	—	-2.35	—	—	—	3.0	
MG10-11/1	G III	0.708942	<i>Porites</i>	—	-2.53	—	—	—	3.0	
MG10-11/2	G III		<i>Porites</i>	—	-2.76	—	—	—	—	
MG10-11/3	G III		<i>Porites</i>	—	-2.21	—	—	—	3.8	
MG10-11/4	G III		<i>Porites</i>	2.0	-2.64	-2.96	-2.35	0.61	3.0	
MG10-11/5	G III		<i>Porites</i>	—	-2.70	—	—	—	—	
MG16/1	G IV	0.708946	<i>Porites</i>	—	-2.33	—	—	—	4.0	
MG16/2	G IV		<i>Tarbellastraea</i>	—	-2.44	—	—	—	—	
MG24/2	G V	0.708948	<i>Porites</i>	19.6	-1.65	-2.01	-1.35	0.66	4.3	
MG24/3	G V		<i>Tarbellastraea</i>	—	-1.56	—	—	—	3.1	

analysis. Based on the results of the outlined quality monitoring, only skeletal material with preservation of the original aragonite mineralogy was used further (Table 2) resulting in an about 20% rejection of specimens considered to be suitable during field sampling.

3.5.2. Radiogenic strontium isotope analyses

For bulk Sr isotope analyses approximately 150 µg of coral aragonite from each sampling site was reacted with 200 µl ultra-pure 1M acetic acid. Additionally, 10 mg of gypsum from a locality (E 24.94829°, N 35.09817°) close to Apomarma north of Psalidha where laminated evaporites, interfinger with the Messinian Varvara Formation (Reuter et al., 2005) and from a locality close to Sarhos (E 25.00198°, N 35.22118°) east of Kroussonas (Fig. 11), respectively, were dissolved with 1 ml ultra-pure 2.0 N HCl. Solutions were separated from residues by centrifugation, evaporated and redissolved in 200 µl 3N HNO₃ and dried down again. Strontium was separated from the samples using EiChrom® Sr-spec resin, a Sr-selective extraction chromatographic resin (Horwitz et al., 1992). Teflon shrink columns (100 µl) packed with Sr-spec resin were preconditioned with 500 µl of 3N HNO₃ and the samples loaded in 100 µl 3N HNO₃. The samples were then washed in with three portions of 100 µl of 3N HNO₃ followed by 3 ml of 3N HNO₃. Sr was eluted with 1 ml of MilliQ water. The eluate was evaporated, transformed into a nitrate by adding 1 drop of concentrated HNO₃ and dried down. The Sr recovered (~100 ng) was loaded onto previously outgassed W single filaments together with a tantalum fluoride activator (Birck, 1986). The isotopic compositions were measured on a Triton TIMS instrument (ThermoFisher, Bremen) at the Max Planck-Institut für Chemie at Mainz. Regular measurements of the NIST SRM 987 Sr standard, measured in static mode, range from 0.710230 to 0.710259 ($n = 32$) and are 0.710244 on average (2SD = 0.000013). In dynamic mode values range from 0.710245 to 0.710269 ($n = 17$) and are 0.710257 on average (2SD = 0.000012). Measured sample ⁸⁷Sr/⁸⁶Sr ratios were corrected to the NIST SRM 987 value of 0.710248 (McArthur et al., 2001). For all samples the internal analytical error is $\leq \pm 0.000008$ (2σ). Age estimations are based on Sprovieri et al. (2003) and Flecker et al. (2002).

3.5.3. Stable isotope analyses and data processing

Sample preparation for stable isotope analyses was done using a PROXXON micro miller equipped with a spherical bit (Ø 0.6 mm) operating at low speed. Equidistant sampling spots (distance of centers 0.8 mm) in *Porites* were aligned along the axis of maximum growth, as indicated by X-ray images. The drilling depth was kept constant at 1.5 mm. The sampling profile for *Tarbellastraea* followed the growth direction of one single corallite according to the method described in Mertz-Kraus et al. (2008). The sampling

procedure provides an average of ≥ 4 samples per year due to the average annual growth rate of 3-5 mm (Brachert et al., 2006b, Table 2). Stable oxygen and carbon isotope ratios were measured at the Institute of Geosciences, University of Frankfurt and at the Department of Geology and Mineralogy, University of Erlangen-Nürnberg (Germany). All values are reported in per mil relative to V-PDB. The internal analytical precision and external reproducibility was better than $\pm 0.08\%$ for $\delta^{18}\text{O}$ and $\delta^{13}\text{C}$ (1σ).

Annual density banding patterns visible in X-ray images are the basis for the age models of the $\delta^{18}\text{O}$ time series presented. The most positive $\delta^{18}\text{O}$ value in each annual cycle was considered to define the “winter” and was assigned as a tie point in the internal age model. The ages of the other sampling points between the winters were calculated by linear interpolation according to their position along the sampling transect. Mean seasonal $\delta^{18}\text{O}$ amplitudes of each coral were estimated as the average of the differences of all annual minima and maxima.

For each coral, an evenly spaced $\delta^{18}\text{O}$ time series was resampled at a bimonthly resolution, matching best with the original record, using the AnalySeries 2.0 software package (Paillard et al., 1996). Additionally, each time series was detrended linearly and normalized to unit variance. Spectral analysis of the coral $\delta^{18}\text{O}$ data was performed with the kSpectra Toolkit 2.7 (SpectraWorks: <http://www.kspectraworks.com>) (Ghil et al., 2002). We applied the multi-taper method (MTM) (Thomson, 1982) with number of tapers set to 3, a bandwidth parameter of 2, and a red noise null hypothesis.

Mean annual $\delta^{18}\text{O}$ values were calculated as the average of six bimonthly interpolated values for a single year. The mean $\delta^{18}\text{O}$ value of one individual coral specimen is taken as the average of all annual mean values of this specimen. For estimation of SST variations from coral $\delta^{18}\text{O}$, we made use of the relationship between $\delta^{18}\text{O}_{\text{aragonite}}$ and temperature (0.15‰ per 1°C) discussed by Felis et al. (2004). Additionally, the relationship between SSS and $\delta^{18}\text{O}_{\text{seawater}}$ is given by Pierre (1999) as:

$$\text{SSS} = (\delta^{18}\text{O}_{\text{seawater}} + 8.9) / 0.27 \quad (1)$$

which allows us to estimate differences in salinity (ΔSSS) between two samples A and B from:

$$\Delta\text{SSS} = (\delta^{18}\text{O}_{\text{seawater A}} - \delta^{18}\text{O}_{\text{seawater B}}) / 0.27 \quad (2)$$

where $\delta^{18}\text{O}_{\text{seawater}}$ in equations (1) and (2) is expressed relative to SMOW. Applying the relationship between SST, $\delta^{18}\text{O}_{\text{seawater}}$ and $\delta^{18}\text{O}_{\text{aragonite}}$ given by Felis et al. (2004)

$$\text{SST} = 5.291 - 6.605 \times (\delta^{18}\text{O}_{\text{aragonite}} - \delta^{18}\text{O}_{\text{seawater}}) \quad (3)$$

and the relationship between PDB and SMOW units (Coplen et al., 1983), as well as the $\delta^{18}\text{O}_{\text{aragonite}}$ -independent SST estimation based on the relationship between annual mean SST and annual growth rates (G), calculated using unpublished data provided by Janice Lough (Australian Institute of Marine Science, Townsville, Australia):

$$\text{SST} = 0.2683 \times G + 22.775 \quad (4)$$

we can transform equation (2) into

$$\Delta\text{SSS} = 3.818 \times (\delta^{18}\text{O}_{\text{aragonite A-B}} + 0.2683 \times G_{\text{A-B}} / 6.605) \quad (5)$$

which expresses the salinity difference as a function of the difference in coral $\delta^{18}\text{O}$ and growth rates in two samples. $\delta^{18}\text{O}_{\text{aragonite A-B}}$ and $G_{\text{A-B}}$ are the absolute values of the differences of the parameters $\delta^{18}\text{O}_{\text{aragonite}}$ and G, respectively, between the two samples A and B. $\delta^{18}\text{O}_{\text{aragonite A-B}}$ is expressed relative to PDB.

A one-way analysis of variance (ANOVA) has been performed in order to compare the mean $\delta^{18}\text{O}$ values of corals from the eight sampling sites P I to G V. All values were transformed by $\log_{10}(x+1)$ to satisfy the homogeneity of variance assumptions. The tested null hypothesis H_0 was that there are no statistically significant differences ($p > 0.05$) in the mean $\delta^{18}\text{O}$ values among the different sampling sites against the alternate hypothesis H_1 that there are statistical describable differences ($p < 0.05$).

3.6. Results

3.6.1. Radiogenic strontium isotope ratios

Sr isotope compositions of the coral aragonite were assigned to two different groups: The coral specimens analyzed from Tortonian sites P I, P II and P III have $^{87}\text{Sr}/^{86}\text{Sr}$ ratios ranging from 0.708900 to 0.708940 ($n = 55$). Values from sites G I, G II, G III, G IV and G V differ clearly from the Tortonian values of P I to P III and range from 0.708932 to

0.708958 ($n = 26$). In Table 2, Fig. 12 and Fig. 13, Tortonian and Messinian mean $^{87}\text{Sr}/^{86}\text{Sr}$ ratios of the coral aragonite for each sampling site are shown together with the respective stratigraphic positions within the sections. The gypsum samples analyzed have a mean $^{87}\text{Sr}/^{86}\text{Sr}$ value of 0.708956.

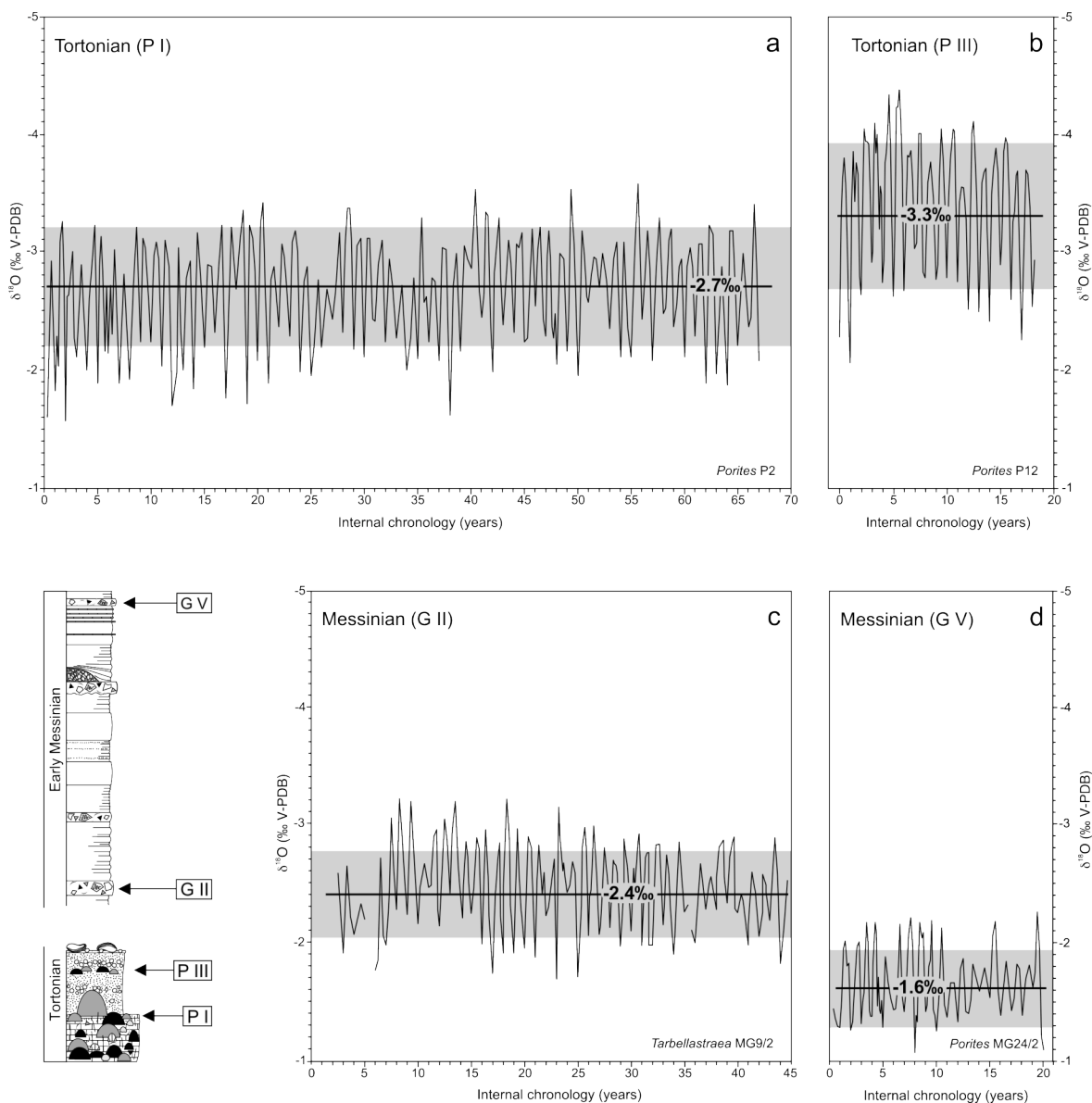


Fig. 14: Coral $\delta^{18}\text{O}$ records of the four sampling sites P I and P III (Tortonian) as well as G II and G V (Messinian). All $\delta^{18}\text{O}$ records show cyclic signals. Mean $\delta^{18}\text{O}$ values (horizontal line) differ between different sampling levels: (a) P I: -2.7‰ , (b) P III: -3.3‰ , (c) G II: -2.4‰ and (d) G V: -1.6‰ . Mean seasonal $\delta^{18}\text{O}$ amplitudes (grey shading) are also variable, and vary between 1.23‰ (site P III) and 0.66‰ (site G V). In the bottom left-hand corner the geological section illustrates the stratigraphic position of the four sampling sites.

3.6.2. Stable oxygen isotope ratios

Oxygen isotope variations of corals from eight Late Miocene stratigraphic levels of Tortonian age (P I, P II, P III and G I) and Early Messinian age (G II, G III, G IV and G V) were compared. The data comprise 28 specimens of *Tarbellastraea* as well as *Porites*. Table 2 shows the analytical results of the new specimens along with results from previous publications. Oxygen isotope compositions of *Tarbellastraea* and *Porites* within a given coral level are statistically indistinguishable, and thus both genera represent compatible proxy archives (Mertz-Kraus et al., 2008). A minimum of four samples per year were taken, so that the resolution is at least quarterly. Unless otherwise noted, the sampling resolution was the same for all coral specimens analyzed. The sampled records represent 2 to 67 years of coral growth (Table 2). All corals analyzed yielded cyclic $\delta^{18}\text{O}$ signals corresponding to the annual density bands visible in X-ray images. For all sampling sites apart from G I, $\delta^{13}\text{C}$ is systematically phase-shifted relative to $\delta^{18}\text{O}$. Maxima in $\delta^{18}\text{O}$ coincide with high-density bands and minima with low-density bands. This yearly cyclicity was observed independent of the stratigraphic position of the sample; further in terms of statistics, values from corals that derive from the same stratigraphic level are identical. There are, however, significant differences in mean $\delta^{18}\text{O}$ values and mean seasonal $\delta^{18}\text{O}$ amplitudes in corals taken from different stratigraphic levels. Statistical evaluation of the mean $\delta^{18}\text{O}$ values was done applying ANOVA. The resulting p -values are indicated in Table 3.

Table 3: p -values of one-way analysis of variance (ANOVA) on mean $\delta^{18}\text{O}$ values of corals from eight different sampling sites (see Table 1).

	Sampling level							
	P I	P II	P III	G I	G II	G III	G IV	G V
P I	–							
P II	0.59 ^{NS}	–						
P III	0.023 ^S	0.0022 ^S	–					
G I	0.000081 ^S	0.00000022 ^S	0.000018 ^S	–				
G II	0.0080 ^S	0.056 ^{NS}	0.0013 ^S	0.000040 ^S	–			
G III	0.43 ^{NS}	0.53 ^{NS}	0.010 ^S	0.000016 ^S	0.28 ^{NS}	–		
G IV	0.037 ^S	0.088 ^{NS}	0.012 ^S	0.00042 ^S	0.73 ^{NS}	0.33 ^{NS}	–	
G V	0.0029 ^S	0.000037 ^S	0.0030 ^S	0.72 ^{NS}	0.00062 ^S	0.0012 ^S	0.0081 ^S	–

NS: no significant difference ($p > 0.05$) between corresponding sites.

S: significant difference ($p < 0.05$) between corresponding sites.

3.6.2.1. Psalidha sampling sites

Site P I

On average, the annual $\delta^{18}\text{O}$ minima are -3.16‰ and the maxima -2.12‰ , respectively, at sampling site P I. Mean $\delta^{18}\text{O}$ values range from -2.74‰ to -2.68‰ with an average of -2.71‰ . Mean seasonal $\delta^{18}\text{O}$ amplitudes vary between 0.95‰ and 1.08‰ , and average 1.02‰ . The 67-year record from *Porites* P2 (Fig. 14a) was obtained from the P I site in an earlier study, and these data have already been used for spectral analysis (Brachert et al., 2006a). However, to ensure compatible data processing, this multidecadal data set was reanalyzed for interannual variability. Significant spectral peaks were identified at periods of 2.2 and 4.7 years (Fig. 15a).

Site P II

At site P II, $\delta^{18}\text{O}$ data were obtained for seven coral specimens. On average, the annual $\delta^{18}\text{O}$ minima are -3.09‰ and the maxima -2.01‰ , respectively. Mean $\delta^{18}\text{O}$ values range from -2.95‰ to -2.50‰ with an average of -2.64‰ . Mean seasonal $\delta^{18}\text{O}$ amplitudes vary between 0.91‰ and 1.18‰ , and average 1.08‰ .

Site P III

Two *Porites* specimens from site P III yielded $\delta^{18}\text{O}$ records 18 (Fig. 14b) and 15 years long, respectively (see Table 1), with an average of all $\delta^{18}\text{O}$ minima of -3.80‰ and of all $\delta^{18}\text{O}$ maxima of -2.57‰ . Mean $\delta^{18}\text{O}$ values range from -3.42 to -3.23‰ (-3.33‰ on average). Mean seasonal $\delta^{18}\text{O}$ amplitudes vary between 1.21‰ and 1.25‰ , with an average value of 1.23‰ .

3.6.2.2. Gorgolaini Monastery sampling sites

Site G I

Two *Tarbellastraea* specimens (SF1 and SF2) from G I gave discontinuous transects of ca. 15 and 10 years, respectively. The mean seasonal $\delta^{18}\text{O}$ amplitudes vary between 0.58‰ and 0.39‰ , with an average of 0.49‰ . The average of all $\delta^{18}\text{O}$ minima is -1.84‰ and of all $\delta^{18}\text{O}$ maxima is -1.36‰ . Together with three other discontinuously sampled *Tarbellastraea* specimens a mean $\delta^{18}\text{O}$ value of -1.64‰ was calculated for G I from the mean $\delta^{18}\text{O}$ values of the single specimens ranging from -1.52‰ to -1.79‰ .

Site G II

Well-preserved *Porites* skeletal material within the lowermost Messinian level is present only within limited skeletal domains of one specimen. The resulting sampling transect is therefore short and discontinuous. For this reason, the mean $\delta^{18}\text{O}$ value (-2.41‰) was calculated by averaging the measured values of the *Porites* (MG9/4) analyzed. By analogy, for another coral specimen (*Tarbellastraea* MG9/6) a mean $\delta^{18}\text{O}$ value of -2.33‰ was obtained. From *Tarbellastraea* MG9/2 a 42-year record was reported previously (Mertz-Kraus et al., 2008) with an average of -2.82‰ for the minima and -2.08‰ for the maxima. The mean seasonal $\delta^{18}\text{O}$ amplitude is 0.74‰ (Fig. 14c). The mean $\delta^{18}\text{O}$ value of the G II data sets is -2.41‰ . Significant spectral peaks exist at 2.3 and 5.1 years (Fig. 15b).

Site G III

A short 2-year transect of a *Porites* specimen (MG10-11/4) gives a mean seasonal $\delta^{18}\text{O}$ amplitude of 0.61‰ and an average of -2.96‰ for the $\delta^{18}\text{O}$ minima and -2.35‰ for the $\delta^{18}\text{O}$ maxima. From

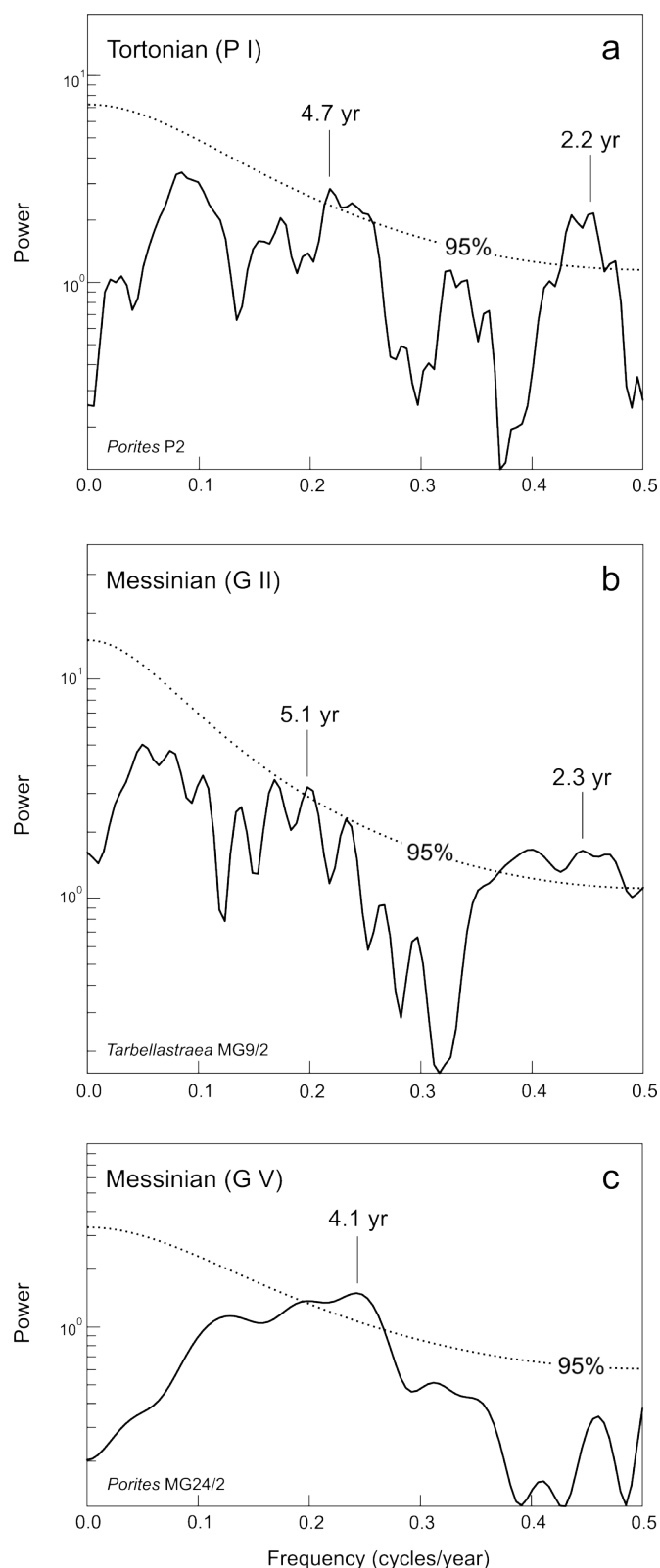


Fig. 15: Power spectra (MTM) of the Late Miocene coral $\delta^{18}\text{O}$ time series. (a) *Porites* P2 (67-year record, site P I, age ~ 10 Ma, Tortonian), (b) *Tarbellastraea* MG9/2 (42-year record, site G II, age ~ 7 Ma, Messinian), and (c) *Porites* MG24/2 (20-year record, site G V, age ~ 7 Ma, Messinian). Dotted lines indicate a 95% significance level. Significant periods are marked

additional discontinuous sampling of four other *Porites* specimen mean $\delta^{18}\text{O}$ values were obtained, ranging from -2.76 to -2.21‰ , with an average of -2.57‰ .

Site G IV

In common with the G I site, the G IV site provided little well preserved skeletal material. Sampling transects at G IV are short and discontinuous, and only allow mean $\delta^{18}\text{O}$ values from one *Porites* and one *Tarbellastraea* specimen to be obtained. Mean $\delta^{18}\text{O}$ values range from -2.44 to -2.33‰ , while the average is -2.39‰ .

Site G V

The uppermost sampling level yielded a 20-year record of *Porites* (specimen MG24/2) (Fig. 14d). The mean $\delta^{18}\text{O}$ value of this data set is -1.65‰ and the mean seasonal $\delta^{18}\text{O}$ amplitude is 0.66‰ . The average of the minima is -2.01‰ , while the average of the maxima is -1.35‰ . Discontinuous sampling of a *Tarbellastraea* specimen (MG24/3) provided a mean $\delta^{18}\text{O}$ value of -1.56‰ . Notwithstanding the relatively short 20-year chronology of MG24/2 available, spectral analysis of this record identified a significant peak at ~ 4 years (Fig. 15c).

3.7. Discussion

3.7.1 Radiogenic strontium isotope ratios

$^{87}\text{Sr}/^{86}\text{Sr}$ values from diagenetically unaltered biogenic carbonates are widely used to estimate ages of sedimentary successions based on the well-documented time-evolution of the Sr isotope composition of seawater (e.g., McArthur et al., 2001). The isotopic composition of Neogene seawater is well documented (e.g., Hodell et al., 1989) and allows successful application of this technique in restricted basins if there is sufficient mixing with the open ocean (Flecker et al., 2002; Flecker and Ellam, 2006). However, the chronostratigraphic resolution of the $^{87}\text{Sr}/^{86}\text{Sr}$ seawater curve for the Late Miocene is low because there are only small changes in $^{87}\text{Sr}/^{86}\text{Sr}$ over time (McArthur et al., 2001).

All $^{87}\text{Sr}/^{86}\text{Sr}$ values measured from Psalidha corals fall within the range of Tortonian Mediterranean seawater (e.g., Sprovieri et al., 2003) and are consistent with their relative stratigraphic position (Reuter et al., 2005). Therefore, an age of around 10 to 9 Ma is considered for the Psalidha sampling sites (P I to P III).

$^{87}\text{Sr}/^{86}\text{Sr}$ data from corals of the Gorgolaini section cluster around 0.708946 and are consistent with published ranges from astronomically calibrated foraminifera samples from

the island of Gavdos south of Crete that are assumed to reflect open Messinian ocean water (Flecker et al., 2002).

The Sr isotope ratios of the gypsum samples from the Varvara Formation at Apomarma and Sarhos, assigned to the Early Messinian (Meulenkamp et al., 1979), fit well with published values of the Lower Evaporites, which have a Sr isotope signature of Messinian open ocean water (Flecker et al., 2002). Since the Apomara evaporites interfinger with sediments of the Varvara Formation, a Messinian age for the debrites of the Varvara Formation at Gorgolaini Monastery appears conclusive. Therefore, the measured Sr isotope ratios imply an age of around 6.5 to 7.5 Ma for the Gorgolaini section. In combination with lithological evidences an Early Messinian age is assigned to the debrites (sites G II to G V) and a Late Tortonian age to the sampling site G I.

3.7.2. Mean annual $\delta^{18}\text{O}$ compositions

Average annual stable oxygen isotope compositions of corals (*Porites*, *Tarbellastraea*) show considerable variation among the eight sampling levels (Fig. 16). One-way analysis of variance yield statistically significant differences ($p < 0.05$) between the mean $\delta^{18}\text{O}$ values of coral sampling sites, e.g., between P I/P II and P III, P I/P II and G I, P I/P II and G V, P III and G I, as well as P III and G V (Table 3). There are also statistically indistinguishable sampling sites ($p > 0.05$) which are not considered in deriving SST or SSS variations.

Intermediate mean $\delta^{18}\text{O}$ compositions were found at levels P I and P II of Psalidha section (-2.71‰ and -2.64‰), and G II through G IV of Moni Gogolaini section (-2.41‰ , -2.57‰ and -2.39‰). Substantial excursions, however, exists at P III representing the most negative composition (-3.33‰) and G I and G V representing the most positive values (-1.64‰ and -1.61‰), respectively. The difference in mean $\delta^{18}\text{O}$ between Tortonian P I and the uppermost Messinian G V on average is 1.10‰ , and has a maximum of 1.72‰ between P III and G V (Table 2, Fig. 16). Between P I and P III the difference is 0.62‰ , between P II and P III 0.69‰ , and 1.69‰ between P III and G I.

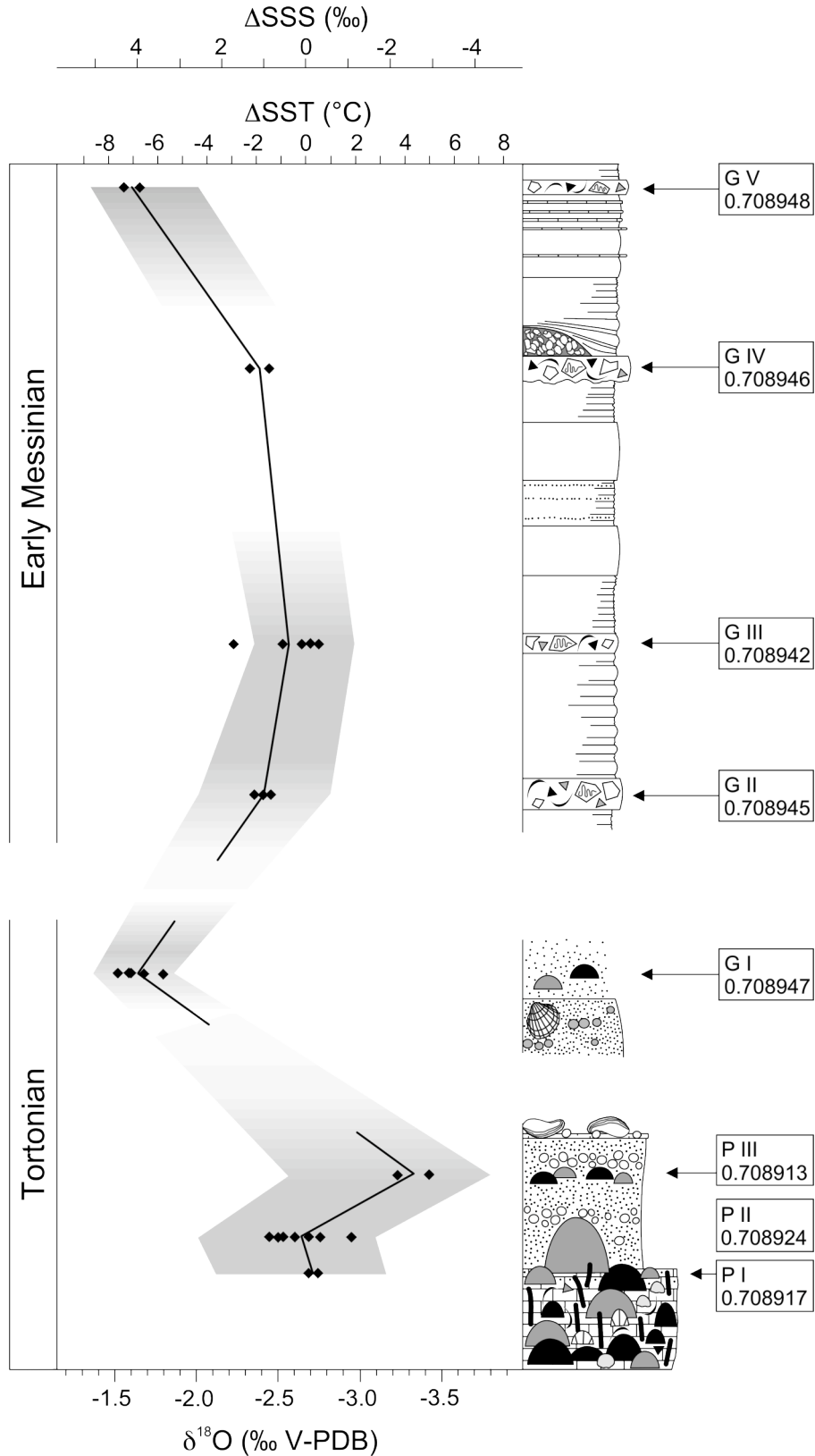


Fig. 16: Average of the mean $\delta^{18}\text{O}_{\text{coral}}$ values (black line) and averaged mean seasonal $\delta^{18}\text{O}_{\text{coral}}$ amplitudes (gray shading) of the eight sampling sites (P I to P III and G I to G V). The border of the shading illustrates the average $\delta^{18}\text{O}_{\text{coral}}$ maxima (winter) and minima (summer) values of each sampling site. Calculated SST and SSS variations are given relative to sampling site P I (chosen arbitrarily as zero point on the SST and SSS scale) and assume no global $\delta^{18}\text{O}_{\text{seawater}}$ change. Black diamonds represent mean $\delta^{18}\text{O}_{\text{coral}}$ values (Table 2) of the analyzed specimens. Mean $^{87}\text{Sr}/^{86}\text{Sr}$ values of each sampling site are indicated at the respective part of the section.

In modern corals, variations in SST are usually derived using a local, empirical relationship between SST and $\delta^{18}\text{O}_{\text{aragonite}}$. Such relationships are not well known for ancient corals. For this reason, we have used the SST – $\delta^{18}\text{O}$ relationship published for modern *Porites* from the Red Sea (Felis et al., 2004) for the Late Miocene Mediterranean corals. This appears to be justified because the oceanographic setting of the current Red Sea and Late Miocene Eastern Mediterranean Sea are comparable.

If we assume SST to control exclusively the variations in coral $\delta^{18}\text{O}$, the shift of 0.62‰ or 0.69‰ between the Tortonian sampling sites P I and P III, or P II and P III, respectively, would imply a SST increase of 4.1°C or 4.6°C within a few meters of the geological section. The more positive values from P III to G I imply a SST decrease of 11.2°C. Additionally, the general shift to more positive mean $\delta^{18}\text{O}$ values implies a decrease in SST of 7.3°C from the Tortonian P I to the Messinian G V, or 11.4°C from the Tortonian P III to the Messinian G V (Fig. 16). Such implied temperature changes are extreme and unfounded. For this reason, we do not consider that the long-term variations in coral $\delta^{18}\text{O}$ can be simply related to changes in SST. Below, we consider the arguments in more detail.

Although reef growth occurred in the Late Miocene almost over the entire Mediterranean region (e.g., Esteban, 1979; Reuter et al., 2006), it was rather discontinuous. The coral fauna was of low diversity and dominated by two genera: *Porites* and *Tarbellastraea* (Bosellini and Perrin, 2008; Brachert et al., 1996). In concert with low growth rates of ~3 to 5 mm yr⁻¹ in massive *Porites*, the distribution and diversity fit suggestions that average winter SSTs were near the lower threshold for reef coral growth in the Tortonian as well as in the Messinian (Brachert et al., 2006a). This estimate is in agreement with the distributional patterns of modern coral reefs, which are limited by minimum long-term winter SST <18°C, though some short excursions below this temperature may occur (Abram et al., 2001; Veron and Minchin, 1992). Average annual SSTs of 23°C and average winter SST around 20°C for the Eastern Mediterranean during the Late Miocene were derived from coral growth rates (Brachert et al., 2006b). However, biofacies analysis has revealed SST below the critical threshold temperature during some stratigraphic intervals without coral growth (Kroeger et al., 2006). SST estimates based on the taxonomic richness of coral reef assemblages at a given locality (Rosen, 1999) also imply constant winter SSTs around 19°C since the number of coral genera is almost unchanged in the Mediterranean sampling sites of Tortonian and

Messinian age (Bosellini and Perrin, 2008). Another important line of evidence is that foraminiferal assemblages indicate mild winter temperatures in the Messinian (Perez-Folgado et al., 2003). Therefore, severely increasing SSTs during the Tortonian as well as drastically decreasing SSTs towards the Messinian appear questionable considering the stratigraphic intervals containing coral assemblages.

One might argue, therefore, that measured mean $\delta^{18}\text{O}_{\text{aragonite}}$ variability is caused by compositional changes in $\delta^{18}\text{O}$ of global ocean water, such as in response to changing ice volume. On balance, this appears a much more promising explanation of our results. However, a 0.1‰ change in global ocean water $\delta^{18}\text{O}$ can be considered equivalent to a ~10 m eustatic change (Miller et al., 2005) or 60 to 70 m of sea-level rise from P I/P II to P III or a 160 m sea-level fall from P III to G I. Such drastic changes in sea level are not supported by sedimentary facies analysis. There is no correspondence in the compositional changes in $\delta^{18}\text{O}$ of global ocean water to the more negative $\delta^{18}\text{O}_{\text{aragonite}}$ between P I and P III, or P II and P III, respectively. Nonetheless, the change in $\delta^{18}\text{O}_{\text{aragonite}}$ between the Tortonian P III and G I to more positive values coincides with an observed increase in $\delta^{18}\text{O}_{\text{seawater}}$ of around 0.5‰ at 8.2 Ma (Miller et al., (2005). However, this increase in $\delta^{18}\text{O}_{\text{seawater}}$ is small compared to the coral aragonite data – the change from P III to G I in $\delta^{18}\text{O}_{\text{aragonite}}$ is higher by at least a factor of 3 than the change at 8.2 Ma in global mean $\delta^{18}\text{O}_{\text{seawater}}$. Furthermore, the reported shift in the global mean $\delta^{18}\text{O}_{\text{seawater}}$ record is of quite short duration and shows no long-term trend towards more positive $\delta^{18}\text{O}_{\text{seawater}}$ values during the Late Miocene.

The G I dataset with more positive $\delta^{18}\text{O}_{\text{aragonite}}$ values and to some extent in-phase $\delta^{13}\text{C}$ patterns can be explained following Rosenfeld et al. (2003) as a coral community growing in deeper water. This assumption is confirmed by sandy marls indicating greater water depths, and low coral growth rates of <2.3 mm on average (Brachert et al., 2006b). The growth rate can be attributed therefore to low-light conditions (water depth and turbidity). Therefore the G I corals appear not to correspond with the pattern shown by the other sampling sites which are all associated with shallow waters.

For the coarse-grained delta deposits above P I we assume the changes towards more negative $\delta^{18}\text{O}_{\text{aragonite}}$ values in the Tortonian section (P I to P III) are more likely to reflect variability in local freshwater discharge and salinity of the ambient seawater, instead of substantial SST increase and global mean $\delta^{18}\text{O}_{\text{seawater}}$ variations. Using Equation (5) of Section 3.5.3., the measured difference between P I and P III, or P II and P III in mean $\delta^{18}\text{O}_{\text{aragonite}}$ corresponds with an SSS decrease of 2.6‰ or 2.7‰,

respectively. Such differences in SSS have been reported from sampling sites with open marine compared to estuarine-coastal environments (Akagi et al., 2004). Additionally, a major positive shift of 0.78‰ in coral mean $\delta^{18}\text{O}$ occurred at ~7 Ma (between G IV and G V), for which no equivalent excursion exists in the record of Miller et al. (2005). If this change could be related to eustatic sea-level change, a fall of about 70 m from G IV to G V or even 170 m from P III to G V would be the consequence. This has no equivalent in the sedimentary succession. Rather a long-term sea-level rise is assumed during the Late Miocene (Miller et al., 2005, André W. Droxler (Rice University, Houston), personal communication 2006). Therefore, ice volume change appears not to be the exclusive cause for the decrease of coral $\delta^{18}\text{O}$ from P I and P II to P III or the increase from P I to G V.

Increasingly positive, and also more variable $\delta^{18}\text{O}$ values starting at 6.7 (Blanc-Valleron et al., 2002) and 7.1 Ma (Kouwenhoven et al., 1999) have been reported and interpreted to be related to the uplift in the Betic Corridor area (Southern Spain). On the basis of progressive isolation of the Mediterranean basin, we assume that changing $\delta^{18}\text{O}$ values of sea surface water due to variable precipitation, river discharge and evaporation seem to be the predominant cause of the variability of $\delta^{18}\text{O}$ in the corals.

Paleobotanical and sedimentological data indicate a gradual shift from humid conditions (Reuter and Brachert, 2007), with annual precipitation rates of 1000 to 1200 mm (Sachse and Mohr, 1996; Zidianakis et al., 2004), to drier conditions, with annual precipitation rates of 400 to 500 mm (Fauquette et al., 2006) from the Tortonian to the Messinian. This observation, together with results from fossil mammal communities (Eronen et al., submitted) and almost constant growth rates in *Porites* and *Tarbellastraea* as well as non-variable coral diversity are all consistent with uniform SST during periods of coral growth (Bosellini and Perrin, 2008; Brachert et al., 2006b; Rosen, 1999). Thus, overall, our $\delta^{18}\text{O}_{\text{aragonite}}$ data appear to reflect predominantly effects of changes in salinity. Based on a modern Mediterranean $\delta^{18}\text{O}_{\text{seawater}}$ – salinity relationship (Pierre, 1999), and using Equation (5) of Section 3.5.3. we suggest the $\delta^{18}\text{O}$ data of the Late Miocene corals to indicate a minimum long-term salinity build-up in the marine Neogene Basins of Crete prior to the MSC of 2.3‰. Here, we have considered the ~0.5‰ change in $\delta^{18}\text{O}_{\text{seawater}}$ at 8.2 Ma reported by Miller et al. (2005) and subtracted this from the measured $\delta^{18}\text{O}$ shift of the Tortonian and Messinian corals. Alternatively, the salinity increase might have been as large as 6.8‰ (Fig. 16) if the ice-volume effect is considered to be only of subordinate relevance, and if we use the maximum difference of the $\delta^{18}\text{O}_{\text{aragonite}}$ values

between P III and G V as a basis of the calculation. A difference of around 6‰ corresponds to that of SSS values of the modern northern Red Sea (~41‰) compared to open ocean waters (~35‰).

3.7.3. Mean seasonal $\delta^{18}\text{O}$ amplitudes

The lower mean seasonal $\delta^{18}\text{O}_{\text{aragonite}}$ amplitudes of 0.66‰ to 0.74‰ in the Messinian records compared to 0.91‰ to 1.25‰ in the Tortonian records (Table 2, Fig. 14 and Fig. 16) cannot be explained as an artifact of lower sampling resolution in the Messinian corals. The reason for this is that annual growth rates were similar in Tortonian and Messinian corals and sampling procedures were the same for all corals analyzed.

Early Tortonian mean seasonal $\delta^{18}\text{O}$ amplitudes in *Porites* and *Tarbellastraea* at Psalidha (P I to P III) correspond to 6.3 to 8.3°C (7.2°C on average) seasonal SST change (Fig. 16). Such SST seasonality is in agreement with modern SST seasonality of ca. 8 to 9°C for the present-day Eastern Mediterranean (Brasseur et al., 1996; Poulos et al., 1997).

Rosenfeld et al. (2003) observed increasing seasonal $\delta^{18}\text{O}$ amplitudes in *Porites* growing in deep water caused by kinetic fractionation resulting in a correlation of $\delta^{18}\text{O}$ and $\delta^{13}\text{C}$ due to low extension rates. This pattern is not detectable in the stable isotope data of G I. Therefore, we explain the low seasonal $\delta^{18}\text{O}$ amplitudes of the corals from this level possibly as a result of the low annual extension rate of <2 mm which do not permit an appropriate sample resolution for defining the full range of seasonality between summer and winter in deeper water. Alternatively, seasonal differences in water temperature are less pronounced in deeper waters. Summarizing, the seasonal $\delta^{18}\text{O}$ amplitudes of G I corals do not provide reasonable information on seasonal variations in sea surface conditions.

Early Messinian mean seasonal $\delta^{18}\text{O}$ amplitudes (0.61‰ to 0.74‰) found in corals from the Gorgolaini Monastery section (G II, G III and G V) are substantially smaller than those of the Psalidha section. The amplitudes translate into a 4°C to 5°C seasonal SST change (Fig. 16), assuming the seasonal $\delta^{18}\text{O}_{\text{aragonite}}$ variability was exclusively controlled by temperature. If the estimated seasonal SST variations were the sole origin for observed seasonal $\delta^{18}\text{O}_{\text{aragonite}}$ changes, winter SSTs would have been cooler during the Tortonian (10 to 9 Ma) compared to those in the Messinian (~7 Ma). However, enhanced evaporation during summer or increased precipitation during winter, also influence surface water $\delta^{18}\text{O}$. Thus, the reduced mean seasonal $\delta^{18}\text{O}_{\text{aragonite}}$ amplitudes in the Messinian are most probably related to salinity changes.

Lowering the mean seasonal $\delta^{18}\text{O}$ amplitudes by increased precipitation during the Messinian winters would cause a shift of the mean $\delta^{18}\text{O}$ to more negative values which is in contrast to the measured Messinian data with more positive mean $\delta^{18}\text{O}$ compared to the Tortonian. In fact, the $\delta^{18}\text{O}$ values of the winter month are less affected than the summer $\delta^{18}\text{O}$ values. If disregarding the $\delta^{18}\text{O}$ values of P III, which we assume to reflect substantial freshwater input, and G I, the average winter $\delta^{18}\text{O}$ values from P I to G II are almost constant; only the summer $\delta^{18}\text{O}$ values are more positive by 0.3‰. From G II to G V the winter values are also more positive by 0.7‰, while the summer values continue to become more positive by 0.8‰. Therefore, we conclude that the Tortonian climate was generally more humid compared to the Messinian. Enhanced summer evaporation started in the earliest Messinian and intensified in the course of the Early Messinian when winters also became less humid in comparison to the Tortonian. Consequently, the shift to more positive mean $\delta^{18}\text{O}_{\text{aragonite}}$ coupled with lower seasonal $\delta^{18}\text{O}_{\text{aragonite}}$ amplitudes is mainly caused by enhanced summer evaporation.

If mean seasonal $\delta^{18}\text{O}$ amplitudes of Late Miocene coral aragonite were only influenced by seasonal salinity change, we estimate the average SSS seasonality to have been 4.2‰ during the Tortonian (P I to P III) and 2.8‰ or 2.3‰ during the Messinian (G III and G V), respectively (Equation (5) of section 3.5.3.) (Fig. 16). In the present-day Aegean Sea, seasonal SSS variations at a given locality are $\leq 2\%$ (Brasseur et al., 1996; Poulos et al., 1997) and far less than we infer for the Tortonian. Note that modern Aegean SSS variations correspond to seasonal $\delta^{18}\text{O}_{\text{seawater}}$ variations of $\sim 0.5\%$ (Equation (2) of Section 3.5.3.). For this reason, a SSS seasonality in the Tortonian of $>4\%$ appears unlikely. Instead, we conclude that Tortonian mean seasonal $\delta^{18}\text{O}_{\text{aragonite}}$ amplitudes were mainly controlled by seasonal SST variability, with only minor contribution related to SSS seasonality. Recent climate modeling of the Late Miocene summer precipitation anomaly (model ECHAM4/ML) (G. Lohmann and A. Micheels, personal communication) has shown enhanced summer drought over the Mediterranean region. Thus, we suggest that the mean seasonal $\delta^{18}\text{O}_{\text{aragonite}}$ amplitudes present a mixed signal of SST and SSS, and especially so in the Early Messinian. This is in agreement with assumptions that the Mediterranean-type climate with dry summers occurred already in the Late Miocene in response to the uplift of the Himalaya-Tibetan plateau above a critical threshold (Tzedakis, 2007). Strong evaporation and thus high salinity during Eastern Mediterranean summers appear to account for the lower mean seasonal $\delta^{18}\text{O}_{\text{aragonite}}$ amplitudes at constant annual mean SST and Tortonian-like SST seasonality during the Early Messinian. Seasonality in SSS might be

1.5‰ higher (0.4‰ difference in mean seasonal $\delta^{18}\text{O}_{\text{aragonite}}$ amplitudes between Tortonian and Messinian data) in the Messinian than in the Tortonian assuming constant SST seasonality. This conclusion is consistent with increasing restriction of the Mediterranean during the Late Miocene, leading to the onset of the MSC at 5.96 Ma (Krijgsman et al., 1999).

The occurrence of increasing mean annual salinity together with pronounced SSS seasonality from the Tortonian to the Early Messinian is also supported by $\delta^{18}\text{O}$ data from marine inorganic aragonite precipitates (Brachert et al., 2007). These $\delta^{18}\text{O}$ data imply short events of enhanced salinity (>50‰) followed by the return to normal marine conditions suitable for coral reef growth. Brachert et al. (2007) concluded that salinity was highly variable more than 1 Myr prior to the MSC, and most likely the restricted basin structure intensified the patterns of precipitation, evaporation and therefore salinity distribution. Strong changes in water balance caused by isolation of the Mediterranean basin were similarly inferred to have taken place from foraminiferal stable oxygen isotope data by Sánchez-Almazo et al. (2007).

3.7.4. Spectral analysis

Data from three corals have $\delta^{18}\text{O}$ chronologies of sufficient length and resolution for analyzing interannual variability by spectral analysis. Multi-taper method (MTM) spectral analyses of these $\delta^{18}\text{O}$ time series show significant peaks at periods of 2-3 years and 4-5 years (Fig. 15). Identical spectral patterns have been found in a Late Pliocene coral $\delta^{18}\text{O}$ record from Florida (Roulier and Quinn, 1995). Likewise, Middle Miocene tree-ring data from Germany possess similar spectral peaks (Kurths et al., 1993). Additionally, last interglacial, late Holocene and modern proxy records of *Porites* from the Middle East (Felis et al., 2004) show similar peaks to those found in our data sets. Felis et al. (2004; 2000) inferred that the observed ~2 and ~5 year periods in *Porites* were related to fluctuations in the El Niño-Southern Oscillation (ENSO) and the North Atlantic Oscillation/Arctic Oscillation (NAO/AO).

Previous time series spectra from a Late Miocene coral (Brachert et al., 2006a) are confirmed by the MTM analysis here. On the basis of the spectral similarities, 10 Ma Tortonian and present-day atmospheric pressure fields are considered to be comparable comprising an Icelandic Low-type and an Azores High-type pressure center. These two pressure centers then control NAO/AO indices, though they would be located farther southward in the Tortonian (Brachert et al., 2006a). In the Tortonian, atmospheric

variability of the pressure fields over the Northern Hemisphere influenced temperature as well as the hydrological balance: During periods with a positive NAO-type index, warm and humid air masses from the Atlantic reached the Mediterranean, whereas during periods with a negative NAO-type index, dry continental air came in from Northern Arabia. Our new time-series spectra of $\delta^{18}\text{O}$ show that the atmospheric variability during the Messinian at 7 Ma and the Tortonian at 10 Ma also was broadly similar. Interannual variation in $\delta^{18}\text{O}_{\text{aragonite}}$ in all the analyzed data sets shows peaks around 2 and 5 years. This indicates that a NAO-type interannual atmospheric variability is a rather stable and geologically old climate phenomenon, already occurring continuously or episodically during the Late Miocene.

3.8. Conclusions

Late Miocene corals from Crete (Eastern Mediterranean) show a significant change in mean annual $\delta^{18}\text{O}_{\text{aragonite}}$ values as well as in mean seasonal $\delta^{18}\text{O}_{\text{aragonite}}$ amplitudes during the time period from the Tortonian (10 - 9 Ma) to the Early Messinian (~7 Ma).

Mean $\delta^{18}\text{O}$ compositions of the Tortonian corals are up to 1.7‰ more negative than those from the uppermost Early Messinian sampling level, with a major shift to more positive values occurring at around 7 Ma ago. The change in mean $\delta^{18}\text{O}$ could be explained solely by a 7 to 11°C decrease in SST. However, such a massive temperature decrease is not reasonable compared to other Late Miocene data from previous studies which document almost constant SSTs for Late Miocene episodes of coral growth. Furthermore, such a reconstruction would imply that during the Early Messinian the lower threshold SST of 18°C for coral reef growth would have been clearly undercut by such a drastic SST decrease. The $\delta^{18}\text{O}$ records of the Late Miocene corals are, therefore, responding primarily to signals other than SST, such as $\delta^{18}\text{O}$ composition of seawater. The influence of ice-volume induced change in global $\delta^{18}\text{O}_{\text{seawater}}$ and sea-level change is not conclusive. The difference in mean $\delta^{18}\text{O}_{\text{coral}}$ of 1.7‰ would be equivalent to a sea-level fall of ~170 m from the Tortonian (site P III) to the Messinian (site G V). Lithological, paleobotanical and geochemical evidence supports $\delta^{18}\text{O}$ variation in the corals to result from SSS changes during the Late Miocene as a prelude to the MSC.

Mean seasonal $\delta^{18}\text{O}_{\text{aragonite}}$ amplitudes are 1.1‰ on average at 10 - 9 Ma and 0.7‰ at ~7 Ma. Since summer and winter $\delta^{18}\text{O}$ values are affected differently, we conclude that enhanced summer evaporation during the Early Messinian was the essential reason for lower $\delta^{18}\text{O}$ amplitudes and consequently more positive mean $\delta^{18}\text{O}$ indicating an $\geq 2\%$ increase of annual mean SSS from the Tortonian to the Messinian.

Spectral analyses (MTM) of the Tortonian and the Messinian $\delta^{18}\text{O}$ chronological records indicate significant interannual variability with periods of 2-3 years and 4-5 years. Similarities in period compared to time series analyses of modern and other fossil proxy archives suggest an overall response to atmospheric forcing, in particular effects similar to the modern NAO/AO. This implies an atmospheric pressure field system with Iceland Low-type and Azores High-type pressure centers influencing climate conditions in the Circum-Mediterranean region at 10 - 9 Ma and ~ 7 Ma as much as at present-day. Our new $\delta^{18}\text{O}$ data from corals, therefore, suggest that the NAO/AO-type atmospheric pressure field phenomenon has been a robust feature over geologically significant periods of time.

3.9. References

- Abram, N.J., Webster, J.M., Davies, P.J. and Dullo, W.C., 2001. Biological response of coral reefs to sea surface temperature variation: evidence from the raised Holocene reefs of Kikai-jima (Ryukyu Islands, Japan). *Coral Reefs*, 20: 221-234.
- Akagi, T., Hashimoto, Y., Fu, F.-F., Tsuno, H., Tao, H. and Nakano, Y., 2004. Variation of the distribution coefficients of rare earth elements in modern coral-lattices: species and site dependencies. *Geochimica et Cosmochimica Acta*, 68(10): 2265-2273.
- Billups, K. and Schrag, D.P., 2003. Application of benthic foraminiferal Mg/Ca ratios to questions of Cenozoic climate change. *Earth and Planetary Science Letters*, 209: 181-195.
- Birck, J.-L., 1986. Precision K-Rb-Sr isotopic analysis: application to Rb-Sr chronology. *Chemical Geology*, 56: 73-83.
- Blanc-Valleron, M.-M., Pierre, C., Caulet, J.P., Caruso, A., Rouchy, J.M., Cespuglio, G., Sprovieri, R., Pestra, S. and di Stefano, E., 2002. Sedimentary, stable isotope and micropaleontological records of paleoceanographic change in the Messinian Tripoli Formation (Sicily, Italy). *Palaeogeography, Palaeoclimatology, Palaeoecology*, 185: 255-286.
- Bosellini, F.R. and Perrin, C., 2008. Estimating Mediterranean Oligocene-Miocene sea-surface temperatures: An approach based on coral taxonomic richness. *Palaeogeography Palaeoclimatology Palaeoecology*, 258(1-2): 71-88.
- Brachert, T.C., Betzler, C., Braga, J.C. and Martín, J.M., 1996. Record of climatic change in neritic carbonates: Turnovers in biogenic associations and depositional modes (Upper Miocene, southern Spain). *Geologische Rundschau*, 85: 327-337.
- Brachert, T.C., Reuter, M., Felis, T., Kroeger, K.F., Lohmann, G., Micheels, A. and Fassoulas, C., 2006a. *Porites* corals from Crete (Greece) open a window into Late Miocene (10 Ma) seasonal and interannual climate variability. *Earth and Planetary Science Letters*, 245: 81-94.
- Brachert, T.C., Reuter, M., Kroeger, K.F. and Lough, J., 2006b. Coral growth bands: A new and easy to use paleothermometer in paleoenvironment analysis and paleoceanography (late Miocene, Greece). *Paleoceanography* 21, PA4217.
- Brachert, T.C., Vescogni, A., Bosellini, F.R., Reuter, M. and Mertz-Kraus, R., 2007. High salinity variability during the early Messinian revealed by stable isotope signatures from vermetid and *Halimeda* reefs of the Mediterranean region. *Geologica Romana*, 40: 1-16.

- Brasseur, P., Beckers, J.M., Brankart, J.M. and Schoenauen, R., 1996. Seasonal temperature and salinity fields in the Mediterranean Sea: Climatological analyses of a historical data set. *Deep Sea Research Part I: Oceanographic Research Papers*, 43(2): 159-192.
- Coplen, T.B., Kendall, C. and Hopple, J., 1983. Comparison of stable isotope reference standards. *Nature*, 302: 236-238.
- Druffel, E.R.M., 1997. Geochemistry of corals: Proxies of past ocean chemistry, ocean circulation, and climate. *Proceedings National Academy of Sciences USA*, 94: 8354-8361.
- Eronen, J.T., Mirzaie, M., Karne, A., Micheels, A., Bernor, R.L. and Fortelius, M., submitted. Distribution History and Climatic Controls of the Late Miocene Pikermian Chronofauna. *PNAS*.
- Esteban, M., 1979. Significance of the upper Miocene reefs of the western Mediterranean. *Palaeogeography, Palaeoclimatology, Palaeoecology*, 29: 169-188.
- Esteban, M., 1996. An overview of Miocene reefs from Mediterranean areas: General trends and facies models. In: E.K. Franseen, Esteban, M., Ward, W.C., Rouchy, J.-M. (Editor), *Models for carbonate stratigraphy from the Miocene reef complexes of Mediterranean regions. Concepts in Sedimentology and Paleontology*. Society for Sedimentary Geology, Tulsa, pp. 3-54.
- Faranda, C., Cipollari, P., Cosentino, D., Gliozzi, E. and Pipponzi, G., 2007. Late Miocene ostracod assemblages from eastern Mediterranean coral-reef complexes (central Crete, Greece). *Revue de Micropaléontologie*: 1-22.
- Fassoulas, C., 2001. The tectonic development of a Neogene basin at the leading edge of the active European margin: the Heraklion basin, Crete, Greece. *Journal of Geodynamics*, 31: 49-70.
- Fauquette, S., Suc, J.-P., Bertini, A., Popescu, S.-M., Warny, S., Taoufiq, N.B., Villa, M.-J.P., Chikhi, H., Feddi, N., Subally, D., Clauzon, G. and Ferrier, J., 2006. How much did climate force the Messinian salinity crisis? Quantified climatic conditions from pollen records in the Mediterranean region. *Palaeogeography, Palaeoclimatology, Palaeoecology*, 238: 281-301.
- Felis, T., Lohmann, G., Kuhnert, H., Lorenz, S.J., Scholz, D., Pätzold, J., Al-Rousan, S.A. and Al-Moghrabi, S.M., 2004. Increased seasonality in Middle East temperatures during the last interglacial period. *Nature*, 429: 164-168.
- Felis, T., Pätzold, J., Loya, Y., Fine, M., Nawar, A.H. and Wefer, G., 2000. A coral oxygen isotope record from the northern Red Sea documenting NAO, ENSO, and North Pacific teleconnections on Middle East climate variability since the year 1750. *Paleoceanography*, 15: 679-694.
- Flecker, R., De Villiers, S. and Ellam, R.M., 2002. Modelling the effect of evaporation on the salinity - $^{87}\text{Sr}/^{86}\text{Sr}$ relationship in modern and ancient marginal-marine systems: the Mediterranean Messinian Salinity Crisis. *Earth and Planetary Science Letters*, 203: 221-233.
- Flecker, R. and Ellam, R.M., 1999. Distinguishing climatic and tectonic signals in the sedimentary successions of marginal basins using Sr isotopes: An example from the Messinian salinity crisis, Eastern Mediterranean. *Journal of the Geological Society*, 156(4): 847-854.
- Flecker, R. and Ellam, R.M., 2006. Identifying Late Miocene episodes of connection and isolation in the Mediterranean–Paratethyan realm using Sr isotopes. *Sedimentary Geology*, 188-189: 189-203.
- Frydas, D., Keupp, H. and Bellas, S., 2008. Stratigraphical investigations based on calcareous and siliceous phytoplankton assemblages from the upper Cenozoic deposits of Messara Basin, Crete, Greece. *Zeitschrift der Deutschen Gesellschaft für Geowissenschaften*, 159(3): 415-437.

- Gagan, M.K., Ayliffe, L.K., Beck, J.W., Cole, J.E., Druffel, E.R.M., Dunbar, R.B. and Schrag, D.P., 2000. New views of tropical paleoclimates from corals. *Quaternary Science Reviews*, 19: 45-64.
- Ghil, M., Allen, M.R., Dettinger, M.D., Ide, K., Kondrashov, D., Mann, M.E., Robertson, A.W., Saunders, A., Tian, Y., Varadi, F. and Yiou, P., 2002. Advanced spectral methods for climatic time series. *Reviews of Geophysics*, 40: doi:10.1029/2001RG000092.
- Hardenbol, J., Thierry, J., Farley, M.B., Jacquin, T., de Gracianski, P.-C. and Vail, P.R., 1998. Mesozoic and Cenozoic sequence stratigraphic framework of European Basins. In: P.-C. de Gracianski, J. Hardenbol, J. Thierry and P.R. Vail (Editors), *Mesozoic and Cenozoic sequence stratigraphy of European Basins*. SEPM Special Publication. Society for Sedimentary Geology, Tulsa, pp. 3-14.
- Hilgen, F.J., Krijgsman, W., Langereis, C.G., Lourens, L.J., Santarelli, A. and Zachariasse, W.J., 1995. Extending the astronomical (polarity) time scale into the Miocene. *Earth and Planetary Science Letters*, 136(3-4): 495-510.
- Hilgen, F.J., Krijgsman, W. and Wijbrans, J.R., 1997. Direct comparison of astronomical and $^{40}\text{Ar}/^{39}\text{Ar}$ ages of ash beds: Potential implications for the age of mineral dating standards. *Geophysical Research Letters* 24(16): 2043-2046.
- Hodell, D.A., Mueller, P.A., McKenzie, J.A. and Mead, G.A., 1989. Strontium isotope stratigraphy and geochemistry of the late Neogene ocean. *Earth and Planetary Science Letters*, 92: 165-178.
- Horwitz, E.P., Chiarizia, R. and Dietz, M.L., 1992. A novel strontium-selective extraction chromatographic resin. *Solvent Extraction and Ion Exchange*, 10(2): 313-336.
- Hsü, K.J., Montadert, L., Bernoulli, D., Cita, M.B., Ericson, A., Garrison, R.E., Kidd, R.B. and others, 1977. History of the Mediterranean salinity crisis. *Nature*, 267: 399-403.
- Kirby, M.X., 2001. Differences in growth rate and environment between Tertiary and Quaternary *Crassostrea* oysters. *Paleobiology*, 27(1): 84-103.
- Kleypas, J.A., McManus, J.W. and Menez, L.A.B., 1999. Environmental limits to coral reef development. Where do we draw the line? *American Zoologist*, 39(146-159).
- Kouwenhoven, T.J., Seidenkrantz, M.-S. and van der Zwaan, G.J., 1999. Deep-water changes: the near-synchronous disappearance of a group of benthic foraminifera from the Late Miocene Mediterranean. *Palaeogeography, Palaeoclimatology, Palaeoecology*, 152: 259-281.
- Krijgsman, W., Hilgen, F.J., Langereis, C.G., Santarelli, A. and Zachariasse, W.J., 1995. Late Miocene magnetostratigraphy, biostratigraphy and cyclostratigraphy in the Mediterranean. *Earth and Planetary Science Letters* 136(3-4): 475-494.
- Krijgsman, W., Hilgen, F.J., Raffi, I., Sierro, F.J. and Wilson, D.S., 1999. Chronology, causes and progression of the Messinian salinity crisis. *Nature*, 400: 652-655.
- Kroeger, K.F., Reuter, M. and Brachert, T.C., 2006. Palaeoenvironmental reconstruction based on non-geniculate coralline red algal assemblages in Miocene limestone of central Crete. *Facies*, 52(3): 381-409.
- Kurths, J., Spiering, C., Müller-Stoll, M. and Striegler, U., 1993. Search for periodicities in Miocene tree ring widths. *Terra Nova*, 5: 359-363.
- Lear, C.H., Elderfield, H. and Wilson, P.A., 2003. A Cenozoic seawater Sr/Ca record from benthic foraminiferal calcite and its application in determining global weathering fluxes. *Earth and Planetary Science Letters*, 208: 69-84.
- Lough, J.M. and Barnes, D.J., 2000. Environmental controls on growth of the massive coral *Porites*. *Journal of Experimental Marine Biology and Ecology*, 245: 225-243.
- Martín, J.M. and Braga, J.C., 1994. Messinian events in the Sorbas basin in southeastern Spain and their implications in the recent history of the Mediterranean. *Sedimentary Geology*, 90: 257-268.

- McArthur, J.M., Howarth, R.J. and Bailey, T.R., 2001. Strontium Isotope Stratigraphy: LOWESS Version 3. Best-fit line to the marine Sr-isotope curve for 0 to 509 Ma and accompanying look-up table for deriving numerical age. *Journal of Geology*, 109: 155-170.
- Mertz-Kraus, R., Brachert, T.C., Galer, S.J.G., Stoll, B. and Jochum, K.P., 2007. Seasonal element and Sr isotope ratio variations in Late Miocene corals from Crete, Eastern Mediterranean. *Geochimica et Cosmochimica Acta*, 71(15, Supplement 1): A656.
- Mertz-Kraus, R., Brachert, T.C. and Reuter, M., 2008. *Tarbellastraea* (Scleractinia): A new stable isotope archive for Late Miocene paleoenvironments in the Mediterranean. *Palaeogeography, Palaeoclimatology, Palaeoecology*, 257(3): 294-307.
- Meulenkamp, J.E., Dermitzakis, M., Georgiadou-Dikeoulia, E., Jonkers, H.A. and Böger, H., 1979. Field guide to the Neogene of Crete, University of Athens, Athens.
- Meulenkamp, J.E. and Sissingh, W., 2003. Tertiary palaeogeography and tectonostratigraphic evolution of the Northern and Southern Peri-Tethys platforms and the intermediate domains of the African-Eurasian convergent plate boundary zone. *Palaeogeography, Palaeoclimatology, Palaeoecology*, 196(1-2): 209-228.
- Miller, K.G., Kominz, M.A., Browning, J.V., Wright, J.D., Mountain, G.S., Katz, M.E., Sugarman, P.J., Cramer, B.S., Christie-Blick, N. and Pekar, S.F., 2005. The Phanerozoic Record of Global Sea-Level Change. *Science*, 310(5752): 1293-1298.
- Paillard, D., Labeyrie, L. and Yiou, P., 1996. Macintosh program performs time-series analysis. *EOS Transactions of the American Geophysical Union*, 77(39): 379.
- Perez-Folgado, M., Sierro, F.J., Barcena, M.A., Flores, J.A., Vazquez, A., Utrilla, R., Hilgen, F.J., Krijgsman, W. and Filippelli, G.M., 2003. Western versus eastern Mediterranean paleoceanographic response to astronomical forcing: a high-resolution microplankton study of precession-controlled sedimentary cycles during the Messinian. *Palaeogeography, Palaeoclimatology, Palaeoecology*, 190: 317-334.
- Pierre, C., 1999. The oxygen and carbon isotope distribution in the Mediterranean water masses. *Marine Geology*, 153: 41-55.
- Pomar, L., 1991. Reef geometries, erosion surfaces and high-frequency sea-level changes, upper Miocene reef complex, Mallorca, Spain. *Sedimentology*, 38: 243-270.
- Poulos, S.E., Drakopoulos, P.G. and Collins, M.B., 1997. Seasonal variability in sea surface oceanographic conditions in the Aegean Sea (Eastern Mediterranean): an overview. *Journal of Marine Systems*, 13(1-4): 225-244.
- Reuter, M. and Brachert, T.C., 2007. Freshwater discharge and sediment dispersal - Control on growth, ecological structure and geometry of Late Miocene shallow-water coral ecosystems (early Tortonian, Crete/Greece). *Palaeogeography, Palaeoclimatology, Palaeoecology*, 255: 308-328.
- Reuter, M., Brachert, T.C. and Kroeger, K.F., 2005. Diagenesis of growth bands in fossil scleractinian corals: Identification and modes of preservation. *Facies*, 51: 155-168.
- Reuter, M., Brachert, T.C. and Kroeger, K.F., 2006. Shallow-marine carbonates of the tropical - temperate transition zone: effects of hinterland climate and basin physiography (Late Miocene, Crete/Greece). In: H.M. Pedley and S. Carannante (Editors), *Cool-Water Carbonates*. Geological Society of London, Special Publication. Geological Society of London, London, pp. 157-178.
- Rohling, E.J., Abu-Zied, R.H., Casford, J.S.L., Hayes, A. and Hoogakker, B.A.A., 2008. The Mediterranean Sea: present and past. In: J.C. Woodward (Editor), *The Physical Geography of the Mediterranean*. Oxford University Press, Oxford, UK.
- Rosen, B.R., 1999. Paleoclimatic implications of the energy hypothesis from Neogene corals of the Mediterranean region. In: J. Agusti, L. Rook and P. Andrews (Editors), *The evolution of Neogene terrestrial ecosystems in Europe*. Cambridge University Press, pp. 309-327.

- Rosenfeld, M., Yam, R., Shemesh, A. and Loya, Y., 2003. Implication of water depth on stable isotope composition and skeletal density patterns in a *Porites lutea* colony: results from a long-term translocation experiment. *Coral Reefs*, 22(4): 337-345.
- Rouchy, J.M. and Caruso, A., 2006. The Messinian salinity crisis in the Mediterranean basin: A reassessment of the data and an integrated scenario. *Sedimentary Geology*, 188-189: 35-67.
- Roulier, L.M. and Quinn, T.M., 1995. Seasonal- to decadal-scale climatic variability in southwest Florida during the middle Pliocene: Inferences from a coralline stable isotope record. *Paleoceanography*, 10(3): 429-443.
- Sachse, M. and Mohr, B.A.R., 1996. Eine obermiozäne Makro- und Mikroflora aus Südkreta (Griechenland), und deren paläoklimatische Interpretation.- Vorläufige Betrachtungen. *Neues Jahrbuch für Geologie und Paläontologie - Abhandlungen*, 200(1/2): 149-182.
- Sánchez-Almazo, I.M., Braga, J.C., Dinarès-Turell, J. and Martín, J.M., 2007. Palaeoceanographic controls on reef deposition: the Messinian Cariatiz reef (Sorbas Basin, Almería, SE Spain). *Sedimentology*, 54: 637-660.
- Santarelli, A., Brinkhuis, H., Hilgen, F.J., Lourens, L.J., Versteegh, G.J.M. and Visscher, H., 1998. Orbital signatures in a Late Miocene dinoflagellate record from Crete (Greece). *Marine Micropaleontology*, 33: 273-297.
- Schenau, S.J., Antonarakou, A., Hilgen, F.J., Lourens, L.J., Nijenhuis, I.A., van der Weijden, C.H. and Zachariasse, W.J., 1999. Organic-rich layers in the Metochia section (Gavdos, Greece): evidence for a single mechanism of sapropel formation during the last 10My. *Marine Geology*, 153: 117-135.
- Sierro, F.J., Flores, J.A., Francés, G., Vazquez, A., Utrilla, R., Zamarreno, I., Erlenkeuser, H. and Barcena, M.A., 2003. Orbitally controlled oscillations in planktic communities and cyclic changes in western Mediterranean hydrography during the Messinian. *Paleogeography, Paleoclimatology, Paleoecology*, 190: 289-316.
- Slowey, N.C. and Crowley, T.J., 1995. Interdecadal variability of Northern Hemisphere circulation recorded by Gulf of Mexico corals. *Geophysical Research Letters*, 22(17): 2345-2348.
- Sprovieri, M., Barbieri, M., Bellanca, A. and Neri, R., 2003. Astronomical tuning of the Tortonian $^{87}\text{Sr}/^{86}\text{Sr}$ curve in the Mediterranean basin. *Terra Nova*, 15: 29-35.
- Suc, J.P., 1984. Origin and evolution of the Mediterranean vegetation and climate in Europe. *Nature*, 307: 429-432.
- Suc, J.-P. and Popescu, S.-M., 2005. Pollen records and climatic cycles in the North Mediterranean region since 2.7 Ma. *Geological Society, London, Special Publications*, 247(1): 147-158.
- ten Veen, J.H. and Postma, G., 1999. Neogene tectonics and basin fill patterns in the Hellenic outer-arc (Crete, Greece). *Basin Research*, 11(3): 223-242.
- Thomson, D.J., 1982. Spectrum estimation and harmonic analysis. *Procc. IEEE*, 70: 1055-1096.
- Tzedakis, P.C., 2007. Seven ambiguities in the Mediterranean palaeoenvironmental narrative. *Quaternary Science Reviews*, 26(17-18): 2042-2066.
- Veron, J.E.N. and Minchin, P.R., 1992. Correlations between sea surface temperature, circulation patterns and the distribution of hermatypic corals of Japan. *Continental Shelf Research*, 12(7): 835-857.
- Weber, J.N. and Woodhead, P.M.J., 1972. Temperature dependence of oxygen-18 concentration in reef coral carbonates. *Journal of Geophysical Research*, 77: 463-473.
- Westerhold, T., Bickert, T. and Rohl, U., 2005. Middle to late Miocene oxygen isotope stratigraphy of ODP site 1085 (SE Atlantic): new constraints on Miocene climate

- variability and sea-level fluctuations. *Palaeogeography, Palaeoclimatology, Palaeoecology*, 217(3-4): 205-222.
- Wijmstra, T.A., Young, R., Witte, H.J.L. and 1990, 1990. An evaluation of the climatic conditions during the Late Quaternary in northern Greece by means of multivariate analysis of palynological data and comparison with recent phytosociological and climatic data. *Geologie en Mijnbouw*, 69: 243-251.
- Zachos, J., Pagani, M., Sloan, L., Thomas, E. and Billups, K., 2001. Trends, rhythms, and aberrations in global climate 65 Ma to present. *Science*, 292: 686-693.
- Zidianakis, G., Mohr, B. and Fassoulas, C., 2004. The Late-Miocene flora of Vrysses, Western Crete - A contribution to the climate and vegetation history, 5th International Symposium on Eastern Mediterranean Geology, Thessaloniki, Greece, pp. 515-518.

4. LA-ICP-MS analyses on coral growth increments reveal heavy winter rain in the Eastern Mediterranean at 9 Ma

This chapter is published with *Palaeogeography, Palaeoclimatology, Palaeoecology*:

Mertz-Kraus, R., Brachert, T.C., Jochum, K.P., Reuter, M., Stoll, B., 2009. LA-ICP-MS analyses on coral growth increments reveal heavy winter rain in the Eastern Mediterranean at 9 Ma. *Palaeogeography, Palaeoclimatology, Palaeoecology*, doi:10.1016/j.palaeo.2008.11.015.

4.1. Abstract

Sediment particles incorporated into coral skeletons reflect variation in composition and amount of suspended material in ambient water during coral growth. They can be used to identify periods of enhanced storm frequency and associated freshwater discharge. Tortonian (Late Miocene) *Porites* corals from Crete (Aegean Sea, Eastern Mediterranean) show pronounced annual density bands in X-ray photographs. $\delta^{18}\text{O}$ compositional variability reflects the annual banding equivalent with a $\sim 7^\circ\text{C}$ annual sea surface temperature (SST) cycle over a seven-year period. Fine sediment particles are concentrated in layers with skeletal porosity parallel to growth increments. Variations in the chemical composition of coral skeletons can result from changes in the environment. Therefore, variations in element concentrations with a spatial resolution of $\sim 500\ \mu\text{m}$ along a transect perpendicular to growth increments were measured using laser ablation inductively coupled plasma mass spectrometry (LA-ICP-MS). Complementary X-ray diffraction, X-ray fluorescence and scanning electron microscope analytical techniques were applied in order to characterize the sediment particles.

Besides Sr/Ca and U/Ca variability indicating SST seasonality, the alternation of layers of pure aragonite and layers of aragonite coated with sediment particles (e.g., kaolinite, montmorillonite, quartz) is reflected in systematic variations in major and trace element concentrations. This element pattern results from a seasonal environmental mechanism where periodically enhanced input of sediment particles into the coral reef environment causes high concentrations of non-lattice bound elements (e.g., Al, Mn, Mg). Potential sources for the non-lattice bound elements (i.e., elements related to the clay minerals) such as airborne Saharan dust, Nile-derived sediment suspension as well as volcanic ash fall can be excluded on the basis of chemical, mineralogical or geological evidence. In contrast, normalized element patterns indicate that the clay minerals represent weathering products of local rocks, e.g., ophiolites, which at present crop out on Crete in mountainous areas, and formed islands exposed to erosion during the Late Miocene.

High concentrations of the non-lattice bound elements correlate with low SSTs of the winter months. The discrepancy in SST estimations between $\delta^{18}\text{O}$ and Sr/Ca seasonality suggests that fresh water originating from intense winter rain caused a reduction of the annual $\delta^{18}\text{O}$ amplitudes and transported suspended material to the near-shore reef. Thus, we relate the seasonality in non-lattice bound element concentrations to climate variations in the Eastern Mediterranean region during the Late Miocene. Our results indicate that the present-day Mediterranean-type climate with a strong seasonality of precipitation and heavy

winter rainfall events may have occurred at least temporarily during the Late Miocene at ~9 Ma in the Eastern Mediterranean.

Keywords: LA-ICP-MS, coral, *Porites*, Sr/Ca, U/Ca, trace element composition, SST, river discharge, heavy winter rain, Mediterranean-type climate, Late Miocene

4.2. Introduction

The subtropical climate in the Mediterranean region during the Tortonian (Late Miocene) appears to have been warmer and more humid than today with annual precipitation rates of 1000 to 1200 mm (Sachse and Mohr, 1996; Zidianakis et al., 2004). Recently, based on precipitation estimates from herpetofaunal assemblages, the Tortonian climate of large parts of Europe at around 9 and 10 Ma has been described as “washhouse climate” characterized by global warm conditions and up to several times more precipitation than present-day (Böhme et al., 2008). Recent annual precipitation for Crete and Greece ranges from about 300 to 900 mm and 300 to 1300 mm, respectively, with the majority of precipitation during the period from October until March (National Data Bank of Hydrological & Meteorological Information (NDBHMI), Greece, <http://ndbhmi.chi.civil.ntua.gr>). In contrast to the suggested “washhouse climate”, terrestrial Tortonian paleoflora of Crete indicate annual precipitation rates of approximately 700 to 1000 mm (Bruch et al., 2006) comparable to present-day conditions. For the Late Miocene, little is known on the temporal distribution of the precipitation over the year. However, the modern climate in the Mediterranean region with strong seasonality of precipitation causing hot and dry summers and mild and wet winters is assumed to have been established during the early Late Pliocene at ca. 3.6 Ma on the basis of palynological data (Suc, 1984; Suc and Popescu, 2005). In contrast, Tzedakis (2007) compiled evidence that the modern Mediterranean-type climate developed pre-Pliocene: (1) The evergreen sclerophylls dominating modern Mediterranean-type climates already appeared during the Oligocene and Miocene (Mai, 1989; Palamarev, 1989); (2) $\delta^{13}\text{C}$ of soil carbonates and mammalian tooth enamel indicate over the past 11 Ma a domination of C_3 over C_4 plants in the Eastern Mediterranean region (Greece, Turkey) in woodland settings in a winter rainfall regime with mean annual rainfall of 300 to 1000 mm (Quade et al., 1994); (3) Pressure field modeling tested with a multidecadal $\delta^{18}\text{O}$ time series from a Tortonian coral yield similarity to the modern pressure field systems of the Northern Hemisphere (Brachert et al., 2006b); (4) The

onset of the Indian monsoon which contributes to the intensification of seasonal precipitation contrasts in the Mediterranean, occurred ~9 Ma ago in response to uplift of the Himalayan-Tibetan plateau (Prell and Kutzbach, 1992; Zhisheng et al., 2001). Also, a pre-Pliocene development of the Mediterranean-type climate is supported by Akgün et al. (2007) postulating a warm temperate climate with dry seasons in the Late Miocene in Anatolia (Turkey) based on vegetational changes. Similarly, the increase of xeromorphic taxa within a Tortonian plant assemblage from northwestern Crete indicates the beginning development of summer drought (Zidianakis et al., 2007).

Additional analytical evidence for seasonal climate conditions is provided by seasonally resolved chemical proxy records. Variations in the chemical composition of, e.g., coral aragonite (CaCO_3) result from changes in environmental parameters such as sea surface temperature (SST), sea surface salinity (SSS) and seawater composition. High growth rates of several mm per year enable corals to record variations on a subannual scale. Beside stable isotope ratios, trace elements are used to monitor such variations. Incorporation of chemical elements into the aragonite skeleton of corals follows different pathways:

- (1) Bivalent cations like Sr^{2+} substitute Ca^{2+} on the basis of an ion-exchange reaction ($\text{CaCO}_3 + \text{X}^{2+} = \text{XCO}_3 + \text{Ca}^{2+}$) and are lattice-bound within the aragonite (Amiel et al., 1973b; Ramos et al., 2004). However, there is some controversy whether Sr^{2+} simply replaces Ca^{2+} in the aragonite lattice or resides in discrete strontianite (SrCO_3) domains (Gregor et al., 1997). The incorporation of Sr into the lattice is regarded to be mainly temperature dependent (Smith et al., 1979; Beck et al., 1992) but also controlled by the Sr/Ca composition of the ambient seawater (de Villiers et al., 1994; McCulloch et al., 1994; Alibert and McCulloch, 1997). Additionally, biological and kinetic effects (Allison et al., 2005) as well as growth and calcification rates (Goodkin et al., 2007) affect the incorporation process. Besides Sr, other elements (e.g., Ba, Mn, Zn, Pb, Y) substituting Ca in the aragonite have the potential to provide subannual information on sediment flux and river runoff (McCulloch et al., 2003; Sinclair, 2005), soil erosion (Fleitmann et al., 2007; Lewis et al., 2007), mining (Fallon et al., 2002; David, 2003) and pollution (Hanna and Muir, 1990; Munksgaard et al., 2004).
- (2) U also can replace Ca in the aragonite lattice (Amiel et al., 1973a). However, dissolved U in seawater most frequently occurs as complexed uranyl carbonate ions (Djogic et al., 1986; Reeder et al., 2000). Their charge and ionic radius argue against a substitution of single Ca^{2+} cations in the aragonite lattice (Shen and Dunbar, 1995;

Lazar et al., 2004) and substitution of complete CaCO_3 groups in the aragonite lattice by $\text{UO}_2(\text{CO}_3)_2^{2-}$ appears more plausible (Swart and Hubbard, 1982; Shen and Dunbar, 1995). Beside temperature (Min et al., 1995), secondary influences on the U incorporation into the coral skeleton are SSS, pH and the carbonate concentration of the oceans (Shen and Dunbar, 1995; Sinclair et al., 1998).

- (3) Chemical elements can also be incorporated as non-lattice bound components of the coral skeleton in terms of constituents of detrital particles becoming trapped in skeletal porosity – e.g., taken up by feeding (Fallon et al., 2002) or passed through paracellular pathways between cells in the calicoblastic epithelium opening and closing due to polyp movement (Erez and Braun, 2007). Such inorganic sediment particles in coral skeletons were assumed to indicate spatial and temporal variations in composition and amount of suspended material in ambient water (Barnard et al., 1974; Naqvi, 1994; Neil et al., 1994). Furthermore, non-lattice bound elements in corals were used to trace volcanic activity (Heikoop et al., 1996a) and dust deposition into the ocean (LaVigne and Sherrell, 2006).

Adopting the terminology of LaVigne and Sherrell (2006), we use the term “lattice-bound elements” for Sr and U in the following, even if both elements to a certain degree are enriched in non-aragonitic phases as outlined above as long as they are secreted by the coral. Accordingly, elements incorporated into the skeleton following the mechanism described in (3) are termed “non-lattice bound elements”.

There are numerous sources and transportation modes of particles supplied to the present-day Mediterranean Sea. These particles can be characterized chemically providing information of their provenance. In combination with a possible transportation mechanism and a temporal pattern conclusions to climatic conditions are possible. The major portion of present-day sediment to the Eastern Mediterranean Sea can be assigned to airborne Saharan dust supplied mainly during the summer and to a lower part to riverine transported material from the Nile and other rivers.

In this study, Tortonian (Late Miocene) *Porites* from Crete (South Aegean Sea, Eastern Mediterranean) growing close to a fresh-water influenced deltaic environment (Reuter and Brachert, 2007) are examined. These corals are preserved with their original aragonitic skeleton and have provided seasonally-resolved $\delta^{18}\text{O}$ records (Brachert et al., 2006b). The corals show variable concentrations of detrital inorganic particles incorporated into their skeletons. A specific rhythmicity in concentration changes arranged parallel to the

annual density banding is macroscopically indicated by vague darker and lighter colors on cut surfaces of the coral specimen and reproduces systematic changes in environmental conditions on subannual scale. The aim of this study is to resolve subannual environmental changes by measuring small-scale chemical variations in the rhythmically structured coral skeleton and incorporated particles using laser ablation inductively coupled plasma mass spectrometry (LA-ICP-MS) together with complementary analytical techniques for chemical and mineralogical characterization. Combined Sr/Ca, U/Ca and $\delta^{18}\text{O}$ data allow to reconstruct seasonal changes in SST and SSS. Subannually resolved element records of the non-lattice bound elements provide a temporal pattern on the supply of terrigenous detritus into the reef environment. Additionally, the provenance of these particles can be resolved by a chemical characterization of the detritus trapped within the coral skeleton. A combination of these aspects provides reconstruction of the development of the Late Miocene paleoclimate in the Eastern Mediterranean.

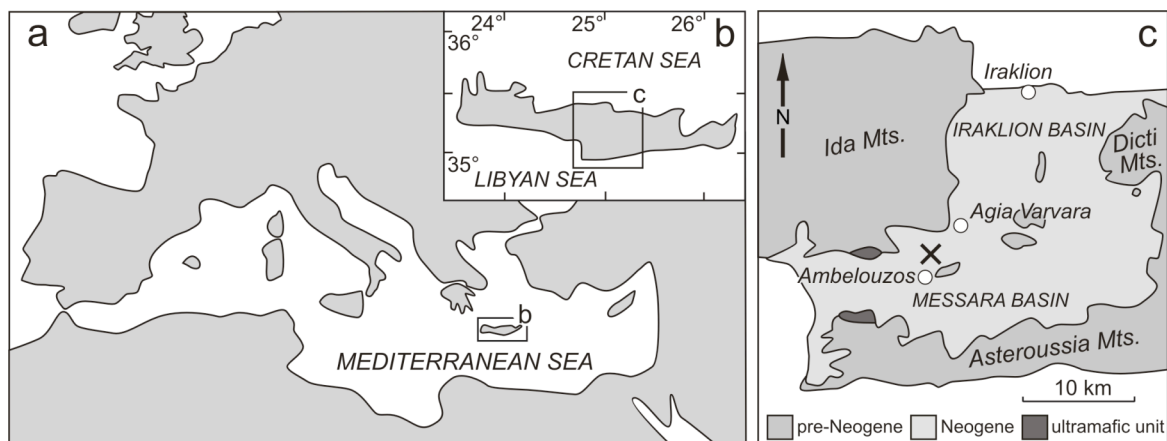


Fig. 17: (a) Outline map of the Mediterranean Basin. (b) The inset shows the island of Crete, Greece. (c) Simplified geological map of Central Crete modified from Bonneau et al. (1977) and Fassoulas (1998). Psalidha sampling site (Messara Basin, Early Tortonian) is indicated by a cross.

4.3. Geological setting and sampling site

The Neogene Basins of Crete formed in response to extensional geodynamic processes in the Aegean region during the late Middle Miocene (Fassoulas, 2001; Meulenkamp and Sissingh, 2003). Large uplifted blocks composed of pre-Neogene sediments (limestones, sandstones, mudstones), metamorphites (phyllite, quartzite) and ultramafic rocks (ophiolites) separate these basins and form the present-day mountains of Crete (e.g., Ida Mountains, Asteroussia Mountains) (ten Veen and Postma, 1999). During the Late Miocene these blocks formed islands (Welter-Schultes, 2000) undergoing erosion while within the basins siliciclastic fluvial, brackish and marine sediments were

accumulated (Reuter et al., 2006; Reuter and Brachert, 2007). The Neogene basin fill is essentially composed of conglomerates, sandstones, mudstones, marls, carbonates and evaporites.

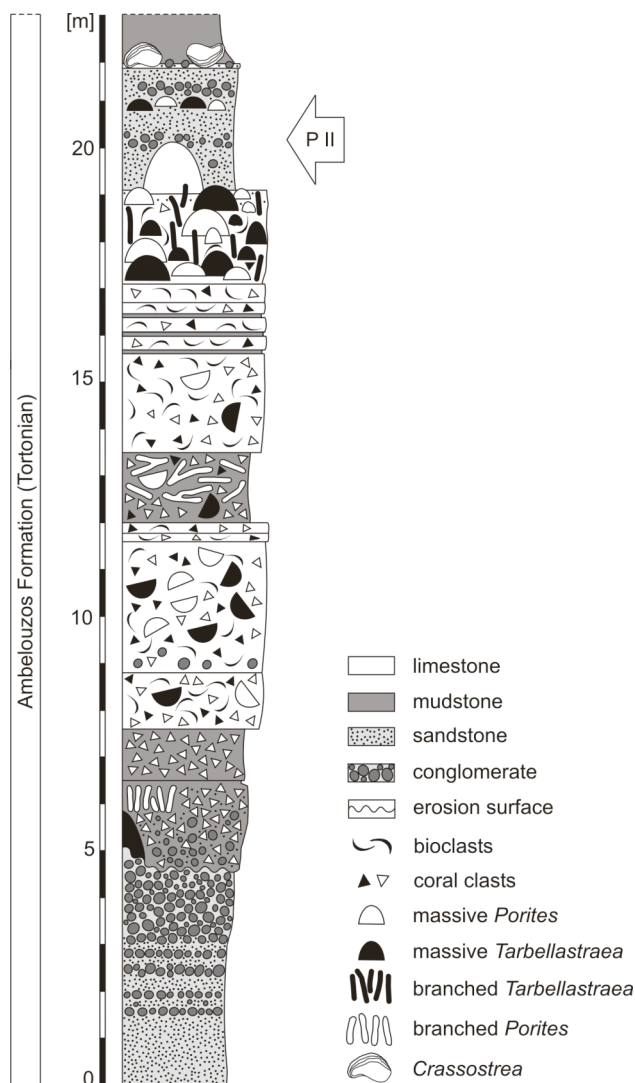


Fig. 18: Geological section at Psalidha with sampling site P II (Tortonian, Late Miocene) located in the upper part of the section. P II represents a unit composed of sandstones and conglomerates on top of a coral reef structure.

The sampling site is located in the northwestern Messara Basin in central Crete near the small village of Psalidha to the north of the town of Ambelouzos (Fig. 17). Together with the northern adjacent Iraklion Basin, the Messara Basin forms the largest Neogene basin of Crete. As a whole, this basin is bordered by the Ida Mountains to the northwest, the Dicti Mountains to the northeast and the Asteroussia Mountains to the southeast. The corals presented in this study derived from the lower Tortonian Ambelouzos Formation

(Meulenkamp et al., 1979) consisting of clastic sediments attributed to brackish-lagoonal, marginally marine and open marine depositional environments reflecting a humid climate (ten Veen and Postma, 1999; Brachert et al., 2006b; Reuter et al., 2006). The corals were sampled at Psalidha locality from a coral build-up that is formed by a stack of coral biostromes intercalated in siliciclastic sediments reflecting variable freshwater input and sediment discharge. A detailed sedimentological and paleoecological analysis of the Psalidha sampling site is given by Reuter and Brachert (2007). At Psalidha locality, corals crop out at three different sites P I to P III (Mertz-Kraus et al., in press). For this study, coral material was selected from site P II (E 24.96488°/N 35.08682°). P II is part of the unit of coarse siliciclastics on top of the build-up (Fig. 18). Combined lithostratigraphic and

biostratigraphic data (Faranda et al., 2007; Frydas et al., 2008) as well as $^{87}\text{Sr}/^{86}\text{Sr}$ chronostratigraphy (Mertz-Kraus et al., in press) indicate an age of 9 Ma for site P II.

4.4. Material and methods

4.4.1. Sample description

Porites specimen P4 was selected for high-resolution LA-ICP-MS analysis. A detailed $\delta^{18}\text{O}$ record of this specimen reflecting sea surface temperature (SST) variations is available (Brachert et al., 2006b). $\delta^{18}\text{O}$ variations indicate a seasonal chronology during coral growth and provide an age model with subannual resolution (see Appendix A, Table A5).

In transmitted-light, thin-sections of P4, as well as other coral specimen from sampling site Psalidha P II, show discrete, alternating slightly darker and lighter layers (Fig. 19a). These layers are about ≤ 2 mm wide and occur rhythmically and perpendicular to the growth direction of the coral. The darker layers result from submicroscopic particles occurring as coatings on skeletal surfaces. Brachert et al. (2006b) excluded diagenetic alteration of specimen P4 on the basis of X-ray diffraction, stereomicroscopy in reflected light, contact radiographs, as well as on homogeneous cyclic patterns in $\delta^{18}\text{O}$ and $\delta^{13}\text{C}$.

4.4.2. Scanning electron microscope (SEM), X-ray diffraction (XRD), and X-ray fluorescence (XRF) analyses

In order to identify the nature of the dark layers, we analyzed specimen P4 by SEM (Fig. 19b). In addition, a slab of the coral skeleton of 117 g weight was dissolved in 5% suprapure acetic acid yielding 2.5 g residue, which represents the insoluble bulk material of the dark layers. For identification of the mineralogical composition, this residue was analyzed by XRD using a Seifert XRD 3000 diffractometer (2θ ranging from 5° to 70°) and afterwards split for further analyses. A 1.7 g aliquot was processed for a major element XRF analysis (Philips PW1404). Budd et al. (1993) also found insoluble material after an 1N HCl dissolution procedure of corals from the Caribbean. They used the term “insoluble residue” and we will adopt this nomenclature in the following.

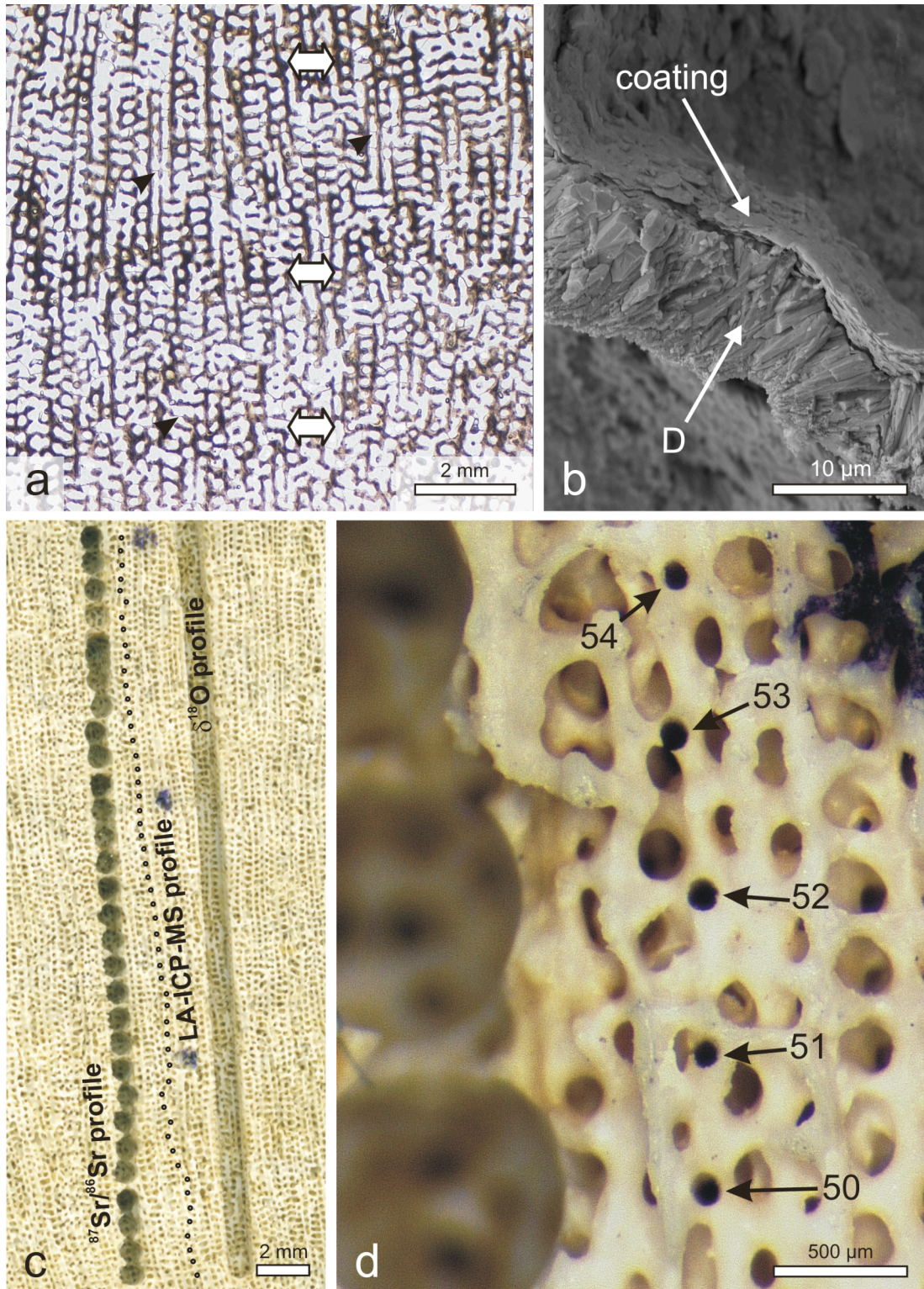


Fig. 19: (a) Thin-section photomicrograph of coral skeleton parallel to the growth direction (plane-polarized light). Alternating darker (white arrows) and lighter layers perpendicular to the growth direction are related to high-density bands and low-density bands formed during winters and summers, respectively. The intraskeletal pore spaces are completely open and delicate skeletal structures such as dissepiments (black arrowheads) are preserved. (b) SEM image of the skeleton formed during winter months. Dissepiment (D) consisting of aragonite fibers is covered by a flaked coating (thickness $\sim 1 \mu\text{m}$) of detrital particles. Aragonite fibers do not show secondary overgrowth indicating very good preservation. (c) Photograph of the laser ablation transect of 54 laser spots parallel to the $\delta^{18}\text{O}$ profile of Brachert et al. (2006b) and a $^{87}\text{Sr}/^{86}\text{Sr}$ profile (Mertz-Kraus et al., in press). (d) Photograph of laser spots 50 to 54 with a spatial resolution of approximately $500 \mu\text{m}$ parallel to the growth direction of the coral and corresponding to the internal chronology of year 6 to 7 (see Fig. 22 and 24).

4.4.3. Laser ablation ICP mass spectrometry

4.4.3.1. Insoluble residue

A homogeneous fused glass was prepared from 40 mg of the insoluble residue (see section 4.4.2.) by 14 seconds of fusion at 1550 °C using an automated iridium-strip heater (Stoll et al., 2008).

Laser ablation analyses were done using a 213 nm Nd:YAG laser (New Wave UP 213 Laser Ablation System) coupled to a ThermoFisher Element2 ICP-MS. Blanks were measured prior to each single-spot analysis and used for correcting the measured sample ion intensities. The isotopes measured were ^{25}Mg , ^{26}Mg , ^{43}Ca , ^{55}Mn , ^{66}Zn , ^{67}Zn , ^{88}Sr , ^{85}Rb , ^{89}Y , ^{90}Zr , ^{93}Nb , ^{111}Cd , ^{112}Cd , ^{133}Cs , ^{137}Ba , ^{139}La , ^{140}Ce , ^{141}Pr , ^{146}Nd , ^{147}Sm , ^{151}Eu , ^{157}Gd , ^{159}Tb , ^{163}Dy , ^{165}Ho , ^{167}Er , ^{169}Tm , ^{173}Yb , ^{175}Lu , ^{178}Hf , ^{181}Ta , ^{208}Pb , ^{232}Th and ^{238}U . Laser spots with a diameter of 120 μm were produced at an energy density of $\sim 8 \text{ J cm}^{-2}$ using a repetition rate of 10 Hz. ^{43}Ca was used for internal standardization. For data evaluation we applied a constant Ca value of 1.42 wt.% based on the XRF analysis. Element concentrations were averaged from a total of 18 laser spots randomly distributed over the glass prepared from the insoluble residue.

4.4.3.2. Coral skeleton

For LA-ICP-MS analyses, a 6 mm thick coral slab previously sampled for $\delta^{18}\text{O}$ analyses (Brachert et al., 2006b) was formatted to a thin section sized (23 mm \times 39 mm) 2 mm thick chip fitting into the sample chamber of the laser ablation system. The original thickness of the coral slab was reduced using a micro miller equipped with cylindrical milling bit ($\text{\O} 5 \text{ mm}$). The $\delta^{18}\text{O}$ sampling track was preserved. Ultrasonication for 20 minutes removed the milling dust. Laser ablation analyses along the axis of maximum growth were done parallel to the $\delta^{18}\text{O}$ profile (Fig. 19c) of Brachert et al. (2006b). Procedure of the measurement was the same as for the insoluble residue glass (section 3.3.1.) and the same isotopes were measured as for the coral skeleton, but additionally ^{27}Al and ^{84}Sr instead of ^{88}Sr . A spatial resolution of 500 μm (Fig. 19d) corresponds to eight to eleven samples per year at an average annual growth rate of $\sim 4 \text{ mm}$ (Brachert et al., 2006a). The total length of the laser ablation profile represents 54 laser spots (Fig 19c). Since the laser ablation and $\delta^{18}\text{O}$ profiles are orientated parallel $< 2 \text{ mm}$ apart, the time series of Brachert et al. (2006b) on the basis of $\delta^{18}\text{O}$ data together with annual density banding was used to derive an internally consistent time series for the laser ablation element transect.

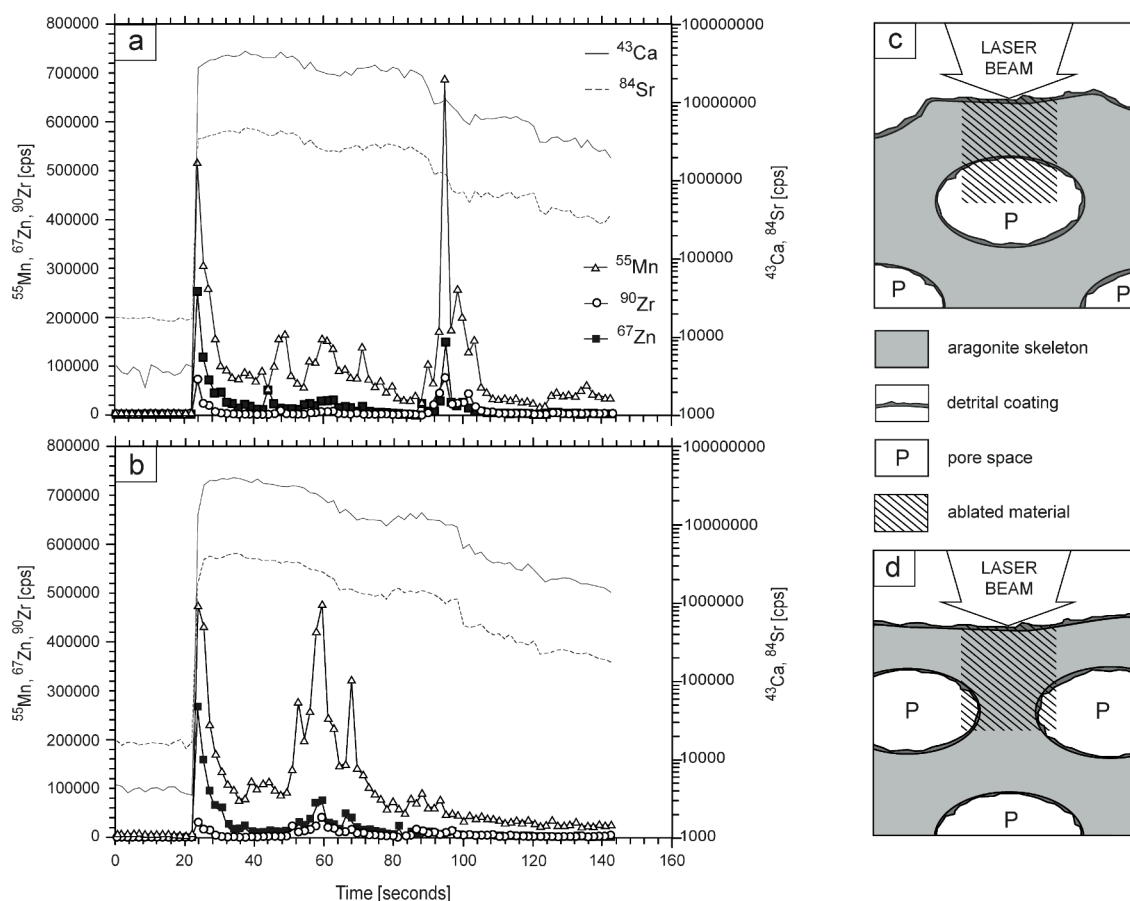


Fig. 20: (a and b) Laser ablation ICP-MS spectra showing intensity (counts per second) versus time for ^{43}Ca , ^{84}Sr , ^{55}Mn , ^{67}Zn , and ^{90}Zr of two single spot measurements on coral specimen P4. (c and d) Schematic drawings illustrating possible spatial relations between coral skeleton and detrital coating. (a) Typical time-resolved signal for a spatial situation as shown in (c) where the laser ablates first the coating identified in (a) by the steep rise in the intensities of ^{55}Mn , ^{67}Zn , and ^{90}Zr . The penetration of the coating and starting ablation of aragonite is recognizable by a transient signal where intensity of the coating related isotopes decreases stepwise. This causes an asymmetric peak shape. The second step rise in the intensity of these isotopes indicates the ablation of coating after penetration of the aragonite. The time-resolved signal in (b) is caused by a more complex spatial relation of aragonitic skeleton and detrital coating (d). Coating, aragonite and a mixture of aragonite and coating are ablated subsequently. The first peak of the isotopes related to the coating is comparable to those shown in (a), however, the ablated mixture of aragonite and coating causes a less steep rise in the intensities and a wider shape of the second peak. Comparing (a) and (b), the patterns of ^{43}Ca and ^{84}Sr are nearly identical and unaffected by the varying intensities of the contaminating elements associated with the detrital coatings.

As for the insoluble residue, we used ^{43}Ca as internal standard. For each spot measurement a time-resolved signal (Fig. 20a and b) was obtained with time corresponding to ablation crater depth. Since the insoluble residue with a low Ca content (1.42%, compare section 4.4.3.1.) forms a coating on the skeleton with high Ca contents (Fig. 20c and d) this coating was ablated first during the spot analyses. Signals recorded are therefore mixtures of residue and coral skeleton material. Fig 4a and b show changing intensities of elements related to the coating (e.g., ^{55}Mn) during the measurement. Each symbol on the diagram (Fig. 20a and b) corresponds to <1 second scan time during the ablation process. In

consequence, with the laser operating at 10 Hz and $\sim 0.1 \mu\text{m}$ ablated sample material per pulse (Jochum et al., 2007) a peak consisting of two symbols (e.g., ^{55}Mn in Fig. 20a) corresponds to $< 2 \mu\text{m}$ ablated material. This is in agreement with the dimension of the coatings visible in the SEM images (Fig. 19b). Comparing Fig. 20a and b, the pattern of ^{43}Ca and ^{84}Sr is nearly unaffected by the varying intensities of the contaminating elements associated with the coatings during one single spot measurement. There is a complex spatial relation between coral skeleton and coating. Fig. 20c illustrates an ideal possible architectural situation. The laser penetrates first the coating, then the skeletal aragonite and again the coating. Fig. 20a can be regarded as the related intensity versus time diagram with well-defined peaks identifying the coating. However, quantification of accurate element concentrations in the coating and aragonite via integration of the time-resolved laser signal of such heterogeneous samples is “somewhat complicated” (Sanborn and Telmer, 2003) for the following reasons: (1) Signals are most often mixtures of coating and coral material caused by the simultaneous ablation of both materials at the same time (Fig. 20c and d); (2) Particle washout-times and instrument response time for transition from ablation of high to low concentrations are typically in the order of several seconds (Sanborn and Telmer, 2003; Gurevich and Hergenröder, 2007). This causes mixing of particles from different layers and generates mixed signals even in cases when the laser ablates coating or aragonite alone. Therefore, LA-ICP-MS was applied to depth profile studies of multi-layered samples mainly to get qualitative results on the spatial distribution of different materials (e.g., Bleiner et al., 2000; Barnes et al., 2004; Kanický et al., 2004). However, to give an estimate of the concentrations of the non-lattice bound elements in the skeleton we evaluated the concentrations on the basis of the following assumption: (1) The spot measurement with the highest average count rate of ^{43}Ca of all 54 single spot measurements was assigned to represent a Ca concentration of 39% in the ablated material, considering $\sim 0.8\%$ Sr and $\sim 0.1\%$ Mg within the coral aragonite (Thompson and Livingston, 1970; Livingston and Thompson, 1971; Weber, 1973; Sinclair et al., 1998; Munksgaard et al., 2004); (2) On the basis of this maximum average count rate we assigned an individual Ca concentration to each spot measurement based on the corresponding average count rate of ^{43}Ca of this spot analyses assuming a linear relation between average count rate and concentration. This is justified because the intensities of ^{43}Ca measured on the reference materials prior, during and after the measurement of the 54 laser spots on the coral (see section 4.4.3.3.) can be regarded as constant during the entire measurement sequence with a relative standard deviation (RSD) of $< 4\%$. The resulting maximum value of 1.17% Al of spot 23 on the coral

corresponds to a portion of ~12% coating at maximum during one single spot measurement (consistent with a <2.5 μm thick coating on a cylindric ablation volume of 120 μm diameter) and an Al concentration of approximately 10% in the insoluble residue according to XRF results (see section 4.5.2). The results of the LA-ICP-MS analyses are taken as semi-quantitative and are given as count rates relative to the internal standard ^{43}Ca (Appendix C, Table C1) and concentrations (Appendix C, Table C2). Element/Ca ratios (e.g., Sr/Ca and U/Ca) of the aragonite are not affected by the strongly different Ca concentrations.

4.4.3.3. Reference materials

Reference materials, coral, and insoluble residue were measured under identical analytical conditions. As in other coral LA-ICP-MS studies (Fallon et al., 2002; Munksgaard et al., 2004) we used multi-element glasses NIST SRM 610 and 612 for calibration of the element concentrations. We used the NIST SRM 610 and 612 GeoReM preferred values reported in the GeoReM database (<http://georem.mpch-mainz.gwdg.de/>) (Jochum et al., 2006a) as the "true" concentrations in these reference glasses.

Integrated results on both reference materials are based on nine spot analyses in each case. Additionally, in order to test the analytical significance of the results on the coral and to overcome the difficulty of non-matrix matching reference materials, we measured USGS MACS-1 ($n = 75$) and NIST SRM 614 ($n = 54$) as QCM (quality control material). The synthetic MACS-1 carbonate was chosen, because it matches the coral matrix very well. NIST SRM 614 is a low concentration reference material allowing evaluation of concentrations at sub-ppm levels that may be expected for distinct elements in the coral skeleton.

For calibration of the insoluble residue concentrations, the certified MPI-DING KL2-G reference glass (Jochum et al., 2000; Jochum et al., 2006b) with preferred values from GeoReM database was used as third reference material in addition to NIST SRM 610 and 612. Three laser spots on each of the three reference materials were measured prior to and after 18 laser spots on the glass prepared from the insoluble residue and were averaged in each case.

Table 4: LA-ICP-MS concentrations (ppm) on MACS-1 and NIST 614 compared to recommended or preferred values. Uncertainties are 1 SD.

Element	MACS-1			NIST 614		
	recommended (1)	LA-ICPMS (2)	LA-ICPMS (3)	LA-ICPMS (4)	preferred values (5)	LA-ICPMS (6)
Al	110±16	312±49		31±4	10500±160	11200±160
Ba	114±8	130±1	117±11	115±6	3.2±0.2	3.31±0.05
Cd				82±6	0.58±0.02	0.64±0.03
Ce			116±12	123±10	0.81±0.07	0.832±0.006
Dy			124±14	135±12	0.74±0.04	0.75±0.01
Er			120±14	128±11	0.74±0.04	0.73±0.01
Eu			0.005±0.001	0.0049±0.0009	0.76±0.03	0.79±0.01
Gd			115±12	128±11	0.75±0.04	0.75±0.01
Hf			0.010±0.001	0.008±0.001	0.7±0.05	0.74±0.01
Ho			0.010±0.001	0.0052±0.0005	0.74±0.04	0.75±0.02
La	126±12	126±1	125±12	139±11	0.72±0.03	0.73±0.02
Lu			0.0030±0.0002	0.0026±0.0003	0.73±0.04	0.72±0.01
Mg	10	28.0±1.1		11.8±0.6	35±3	32.8±0.4
Mn	118±12	126±2		122±9	1.4±0.5	1.47±0.04
Nb			0.002±0.001	0.0018±0.0009	0.81±0.06	0.79±0.02
Nd			125±12	135±12	0.74±0.03	0.77±0.01
Pb	121±11	115±1	125±12	115±5	2.32±0.04*	2.73±0.07
Pr			0.006±0.001	0.0063±0.0008	0.76±0.03	0.76±0.01
Rb		0.098±0.039	0.075±0.01	0.065±0.030	0.855±0.005*	0.95±0.03
Sm			120±12	134±12	0.75±0.04	0.78±0.01
Sr	219±20	249±1	211±10	215±7	45.8±0.1*	42.4±1.8
Ta				0.0011±0.0002	0.79±0.05	0.79±0.01
Tb			0.020±0.002	0.021±0.002	0.73±0.04	0.74±0.01
Th				0.011±0.001	0.748±0.006*	0.76±0.01
Tm				0.0039±0.0006	0.73±0.04	0.72±0.01
U		0.006±0.001	0.004±0.001	0.004±0.001	0.823±0.002*	0.91±0.03
Y			0.052±0.010	0.054±0.004	0.8±0.07	0.75±0.01
Yb			123±15	132±10	0.77±0.05	0.75±0.01
Zn	123±16	118±2		98±5	2.5±0.7	3.06±0.12
Zr			0.020±0.001	0.016±0.003	0.84±0.06	0.82±0.01

(1) Personal communication S. Wilson in Munksgaard et al. 2004

(2) Munksgaard et al. 2004

(3) Jochum and Stoll 2008

(4) This work

(5) GeoReM preferred analytical values (<http://georem.mpch-mainz.gwdg.de/>)

(6) This work

* Uncertainties are 95% confidence level

4.4.3.4. Analytical quality

Precision of the LA-ICP-MS measurement depends on several factors, such as repeatability of the measurement and the homogeneity of the sample. The NIST SRM 610, 612 and 614 reference glasses are, overall, homogeneous on a scale of 60 μm (Gao et al., 2002). Internal precision (relative standard error = RSE) of an individual spot-analysis on the reference glasses NIST SRM 610 and 612 was <1.5% for the trace elements measured. For NIST SRM 614 RSE was <5% for all elements. The synthetic MACS-1 carbonate can also be considered to be homogenous and RSE of an individual spot-analysis on this QCM was at maximum 10%.

For the QCM, RSD for the averaged LA-ICP-MS measurements was <15% (MACS-1, $n = 75$) and <4% (NIST 614, $n = 54$) for most of the elements (Table 4). Regarding MACS-1, recommended values exist only for some elements (Steve Wilson, USGS, unpublished data in Munksgaard et al. (2004)). These values and additionally published element concentrations (Munksgaard et al., 2004; Jochum and Stoll, 2008) are listed in Table 4. Our results on MACS-1 agree with recommended and published values considering analytical uncertainties. An exception is Al in MACS-1, which is consistently lower by 70% than the recommended value during our measurements within a 1SD value of ± 4 ppm. In contrast, published data (Munksgaard et al., 2004) show Al concentrations higher by a factor of ca. 3 compared to the recommended value. We assume that this discrepancy is caused by heterogeneous distribution of Al in MACS-1, because corundum (Al_2O_3) grinding media had been used in the final preparation step of MACS-1 in order to reduce the particle size (Steve Wilson, USGS, personal communication). Results on NIST SRM 614 agree with preferred values (<http://georem.mpch-mainz.gwdg.de/>).

The coral aragonite can be regarded as inhomogeneous compared to the reference materials and QCM. Therefore, measured values are expected to be less precise. However, RSE of an individual spot-analysis on the coral was at maximum 1.7% and 3.0% for Sr and U, respectively, and 10% for the other trace elements (see Appendix C, Table C1).

Since reference material, QCM, coral and insoluble residue were analyzed under identical conditions and there is agreement between our QCM concentration measurements and published as well as referenced values, we consider the analytical results to be geologically and paleoclimatologically significant. The fact that most of the LA-ICP-MS data of MACS-1 agree within 1 to 10% with those of the recommended values demonstrate that possible matrix effects of LA-ICP-MS caused by differences of the calibration material

(synthetic glass) and sample (carbonate) are small. This means that the coral data are reliable.

4.5. Results

4.5.1. Coral preservation

As outlined by Brachert et al. (2006b), X-ray images of the P4 coral slab show distinct light and dark bands known as annual density bands. Each year consists of a couplet of a band of high and low density. Based on the results of Brachert et al. (2006b), the high density bands correspond with cool SSTs and the low density bands with warm SSTs, thus reflecting winter and summer, respectively. Stereomicroscopic screening of slab surfaces as well as of thin sections in reflected and transmitted light, respectively, revealed perfectly open intraskeletal pore spaces, with no secondary carbonate cements or micritic sediment fillings (Fig. 19a). Also, a dark-and-light pattern perpendicular to the growth direction is visible in thin sections under transmitted light. This pattern mimics the density-banding pattern of the X-ray images. On fresh fracture surfaces, radial arrangements of trabecular fans with minor dissolution of the centers of calcification are visible in SEM images showing no signs of recrystallization. However, there are delicate coatings (Fig. 19b) covering skeletal surfaces. These coatings consist of parallel orientated flakes, each with a diameter of $\leq 3 \mu\text{m}$ and a thickness of $<10 \text{ nm}$. The coatings are restricted to the high-density bands and are responsible for the darker layers visible in thin-sections (compare 4.4.1. and Fig. 19a). These coatings are the source of the insoluble residue. The coatings formed in the living coral and do not represent secondary fillings (see section 4.6.2).

4.5.2. Mineralogical and chemical compositions of the insoluble residue

XRD analyses on the insoluble residue document a mineralogical composition of quartz together with a mixture of the clay minerals kaolinite, montmorillonite and mixed layer kaolinite-montmorillonite as well as subordinate illite. These minerals represent the flaked components of the coating shown in Fig. 19b.

Major element composition of the insoluble residue in wt.% is 46.26 SiO₂, 0.78 TiO₂, 16.13 Al₂O₃, 9.00 Fe₂O₃, 0.06 MnO, 6.15 MgO, 1.99 CaO, 0.34 Na₂O, 2.80 K₂O, 0.12 P₂O₅, 0.06 Cr₂O₃, 0.04 NiO, and 13.72 loss on ignition (LOI). The relatively high LOI content indicates a high H₂O concentration, which is consistent with the XRD results demonstrating a substantial percentage of sheet silicate minerals with high concentrations of hydroxyl groups and lattice-bound H₂O. The averaged LA-ICP-MS trace element concentrations are listed in Table 5 and are compared in Fig. 21a to average upper continental crust (AUCC) in a North American shale composite (NASC)-normalized multi-element diagram. The largest differences are positive Cr (Cr/Cr* = 3.52) and Ni (Ni/Ni* = 4.43) anomalies as well as a negative Na anomaly in the insoluble residue compared to negative Cr and Ni as well as positive Na anomalies in AUCC. For Alkaline Earth Metals, Ba shows a negative anomaly in the insoluble residue and there is no relative Sr enrichment as found in AUCC. Additionally, the Heavy Rare Earth Elements (HREE) are enriched relative to the Middle Rare Earth Elements (MREE), whereas there is subordinate, e.g., (Tb/Lu)_{normalized} = 0.73, discrimination between MREE and HREE in average upper continental crust, e.g., with (Tb/Lu)_{normalized} = 1.08. Summarizing, distinct differences between our coral measurements and the AUCC in Alkali Metals (Na), Alkaline Earth Metals (Sr, Ba), Rare Earth Elements (MREE/HREE ratio) and Transition Elements (Cr, Ni) indicate that the insoluble coral residue does not represent a simple chemical aliquot of average upper continental crust. In particular, Cr and Ni may represent source-indicative elements, because high concentrations of these metals are commonly not related to conventional upper continental crustal rocks.

Table 5: LA-ICP-MS element concentrations on insoluble residue of coral P4

Element	ppm ± 1 SD
Rb	135 ± 6
Sr	143 ± 4
Y	16.0 ± 0.7
Zr	120 ± 4
Nb	14.4 ± 0.4
Cs	10.4 ± 2.7
Ba	262 ± 14
La	22.2 ± 1.4
Ce	42.6 ± 2.9
Pr	4.59 ± 0.33
Nd	17.2 ± 1.3
Sm	3.15 ± 0.19
Eu	0.67 ± 0.03
Gd	2.61 ± 0.13
Tb	0.42 ± 0.02
Dy	2.79 ± 0.12
Ho	0.61 ± 0.03
Er	1.85 ± 0.09
Tm	0.29 ± 0.01
Yb	2.06 ± 0.08
Lu	0.31 ± 0.01
Hf	3.09 ± 0.15
Ta	1.00 ± 0.04
Pb	13.3 ± 2.4
Th	9.58 ± 0.36
U	2.54 ± 0.19
Mg	9770 ± 340
Mn	112 ± 4
Zn	343 ± 52
Cd	0.61 ± 0.15

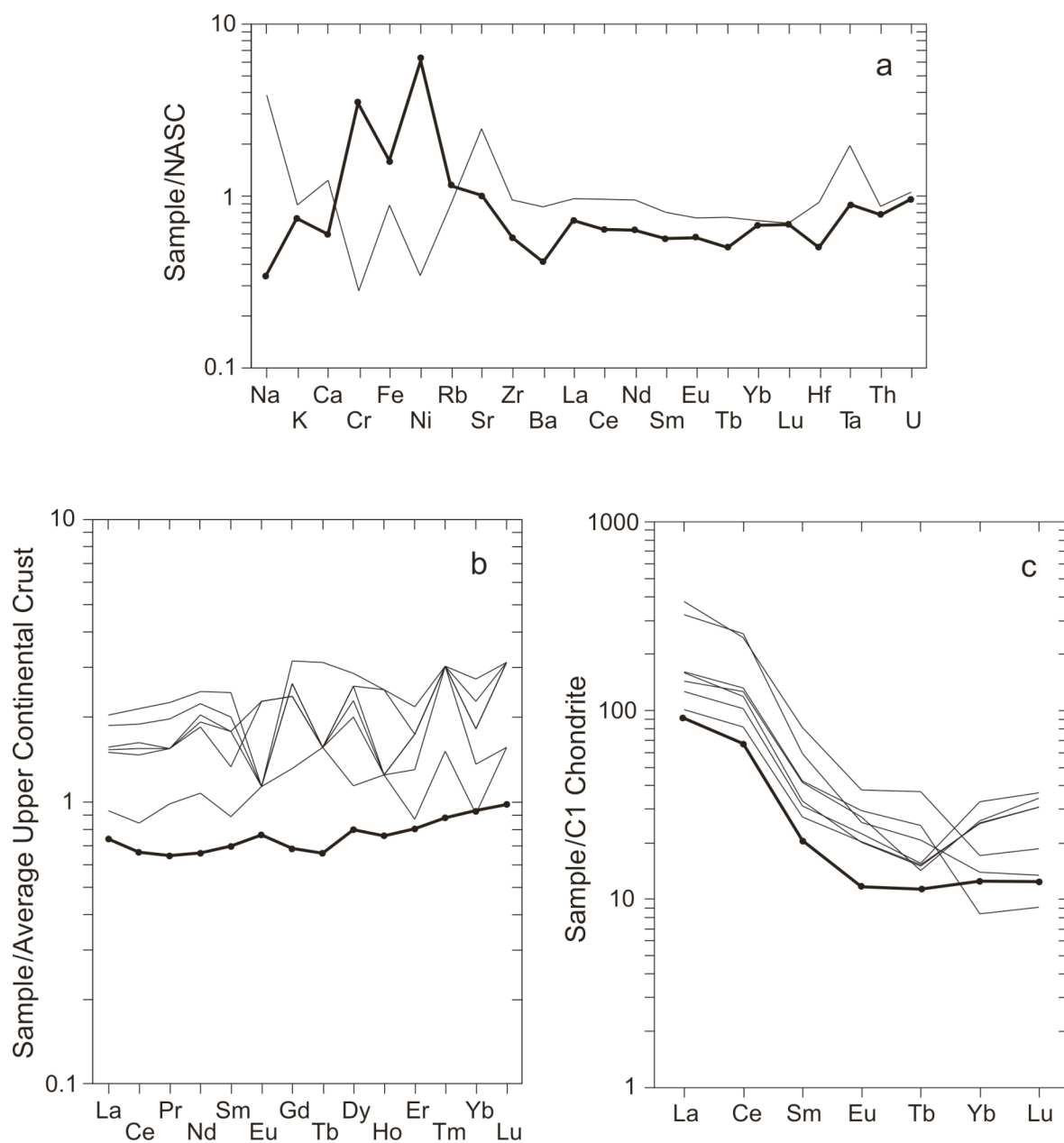


Fig. 21: (a) North American shale composite-normalized (Gromet et al., 1984) multi-element diagram of coral specimen P4 insoluble residue (bold line) compared to average upper continental crust (Taylor and McLennan, 1985) (light line). (b) Average upper continental crust-normalized Rare Earth Element diagram of coral specimen P4 insoluble residue (bold line) compared to Saharan dust (Moreno et al., 2006) (light lines). (c) C1 chondrite-normalized (Evensen et al., 1978) Rare Earth Element diagram of coral specimen P4 insoluble residue (bold line) compared to Mid-Miocene Aegean shoshonitic and high-K calc-alkaline volcanic rocks (Pe-Piper, 1980) (light lines). See text for discussion.

4.5.3. Coral trace element concentrations

The coral skeleton trace element count rates and concentrations, respectively, of a transect of 54 laser spots as well as the stable isotope data ($\delta^{18}\text{O}$, $\delta^{13}\text{C}$) of Brachert et al. (2006b) are given as supplementary online material (see Appendix A, Table A5 and Appendix C, Table C1 and C2). In the following, the results are discussed in detail.

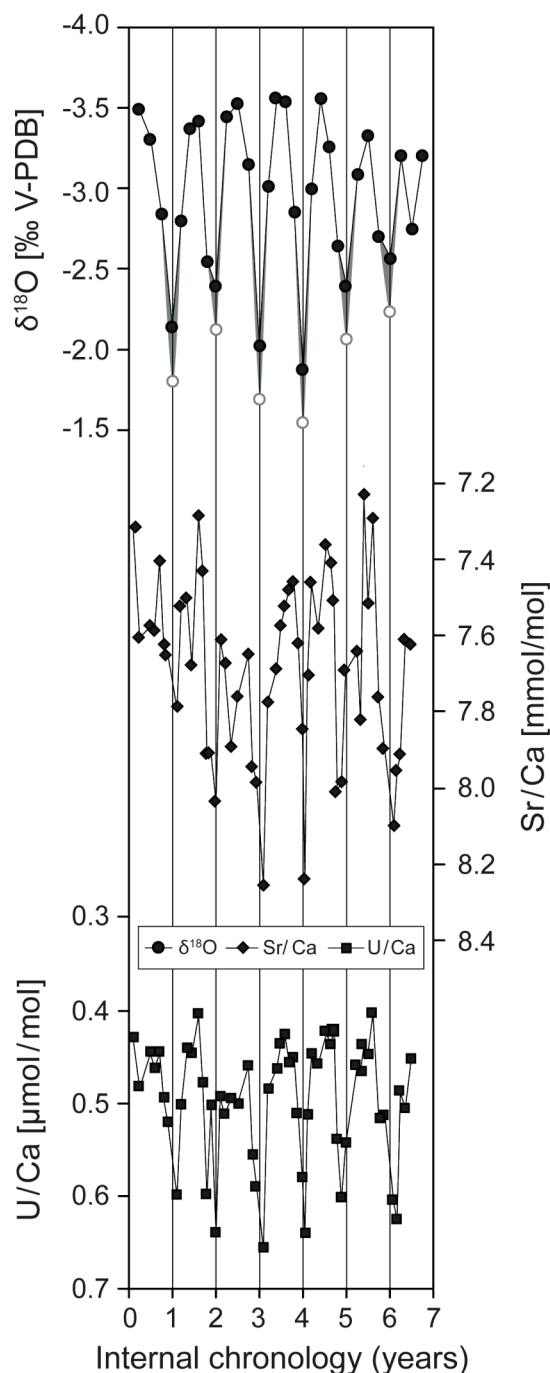


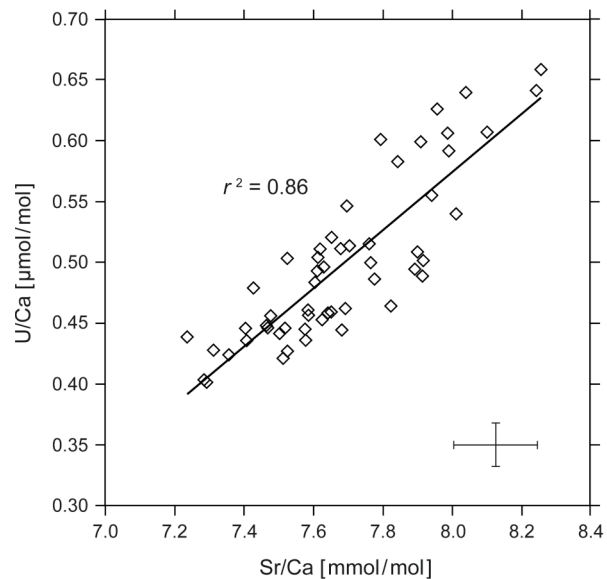
Fig. 22: $\delta^{18}\text{O}$ (Brachert et al., 2006b), Sr/Ca, and U/Ca variations along a transect representing seven years of growth of coral specimen P4. For $\delta^{18}\text{O}$, the black filled circles indicate the measured values of Brachert et al. (2006b), the grey open circles and shading the estimate of the reduction of the annual $\delta^{18}\text{O}$ cycle by seasonal SSS changes (see section 5.6.1. for discussion). For each year, high Sr/Ca and U/Ca peaks correlate with $\delta^{18}\text{O}$ -derived winters. X-axis numbering and corresponding vertical lines in the diagram represent winters 1 to 7. Error bars for Sr/Ca and U/Ca correspond to the maximum analytical error RSE of 1.7% for Sr and 3.0% for U.

4.5.3.1. Lattice-bound elements

Sr and U are known to be incorporated within the coral carbonate lattice replacing Ca^{2+} or complete CaCO_3 groups (see section 4.2.). Therefore, these elements are reported in relation to Ca, i.e., as Sr/Ca and U/Ca ratios, respectively. The records of Sr/Ca and U/Ca co-vary with $\delta^{18}\text{O}$ (Fig. 22) showing an “arched” shape of the profiles as described by Barnes et al. (1995) for summer extension increasing relative to winter extension. High and low Sr/Ca as well as U/Ca ratios are related to high-density bands formed during winter and low-density bands formed during summer, respectively. The Sr/Ca values range from 7.236 to 8.257 mmol/mol and U/Ca from 0.402 to 0.659 $\mu\text{mol/mol}$. Sr/Ca and U/Ca ratios exhibit a highly significant correlation ($r^2 = 0.86$, $n = 54$) (Fig. 23). The amplitudes of Sr/Ca between different years are highly variable. Additionally, several smaller negative and positive peaks cause a more irregular run of the arch-type curvature (Fig. 22), while the patterns of $\delta^{18}\text{O}$ and U/Ca are far more regular. Therefore, a bimonthly mean chronology for Sr/Ca and U/Ca (Appendix C, Table C3) was constructed in order to reduce the error of the annual cycle according to Kuhnert et al. (1999) and Felis et al. (2000) using the AnalySeries 2.0 software package (Paillard et al., 1996). On the basis of these

Fig. 23: Linear correlation of Sr/Ca versus U/Ca from 54 laser spots on the P4 coral with error bars corresponding to the maximum analytical error RSE of 1.7% for Sr and 3.0%

bimonthly chronologies, the average seasonal variation for Sr/Ca and U/Ca is 0.579 mmol/mol and 0.173 $\mu\text{mol/mol}$, respectively.



4.5.3.2. Non-lattice bound elements

The non-lattice bound elements (Al, Mg, Ba, Mn, Y, Zr, Zn, Pb, Th, Cd, Rb, Cs) show distinct concentration maxima (Fig. 24) that correspond to the high-density bands. These peaks also correspond to a quartz and clay mineral assemblage (compare 4.5.2.) forming the insoluble residue of the dark layers (Fig. 19a and 19b), where, according to thin-section and SEM observations, coatings cover the skeletal segments formed during the cold season. From seven winter cycles, derived from the $\delta^{18}\text{O}$ chronology, with the exception of the first year, the well-defined element peaks occur closely before, during, or shortly after the winter (Fig. 24), defined as the maximum $\delta^{18}\text{O}$ in each annual cycle. During the entire first year the non-lattice bound elements stay constantly low at background level, whereas the element-to-Ca ratios of the lattice-bound elements Sr and U show annual cyclicity during this period.

4.6. Discussion

4.6.1. Sr/Ca and U/Ca

Sr/Ca as well as U/Ca are inversely correlated with SST and for modern corals several SST calibrations have been suggested for Sr/Ca (Smith et al., 1979; Beck et al., 1992) and U/Ca (Min et al., 1995; Shen and Dunbar, 1995). However, application of these modern systems to geological samples has shown to provide SST estimations, which are not straightforward to interpret most probably due to so-called vital effects (Felis et al., 2004; Goodkin et al., 2007).

Nevertheless, since the slopes defined by Sr/Ca or U/Ca vs. SST of most modern systems are consistent within a range of 0.0504 to 0.0815 (compilation in Corrège, 2006) and 0.0286 to 0.0543 (Min et al., 1995; Shen and Dunbar, 1995; Sinclair et al., 1998; Fallon et al., 1999; Fallon et al., 2003), respectively, we consider these slope ranges significant for relative temperature estimates, i.e. for SST seasonality. Applying these slope ranges to the Late Miocene coral data, reconstructed seasonality is 7.1 to 11.5°C (9.3°C on average) for Sr/Ca and 3.2 to 6.1°C (4.6°C on average) for U/Ca, calculated from the average seasonal cycle of the bimonthly resolved chronology of both proxies.

The discrepancy in SST estimates between both proxies can be caused by modified Sr, U and Ca concentrations of Late Miocene Mediterranean seawater (Lear et al., 2003), biological effects, as well as influences of growth and calcification rates, respectively (Goodkin et al., 2007). Also, U/Ca seasonality may be biased by U depletion in the skeleton from sorption on organic matter or humic acids (Bednar et al., 2007). Alternatively, the original U/Ca and Sr/Ca ratios could be differently affected by diagenesis (Swart and

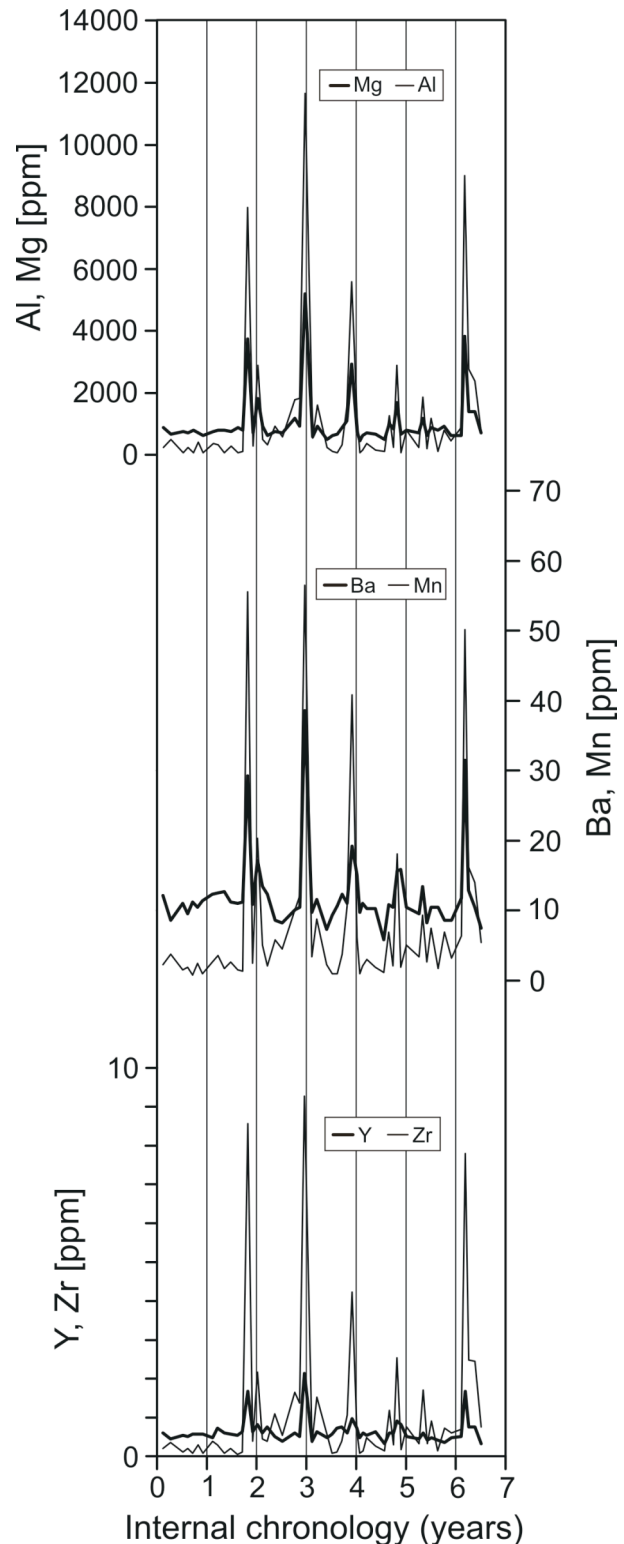


Fig. 24: Variation of non-lattice bound element concentrations along a transect representing seven years of growth of coral P4. High concentration peaks of Al, Mg, Ba, Mn, Y and Zr (as well as Zn, Pb, Th, Cd, Rb, and Cs, not shown in diagram) correlate with $\delta^{18}\text{O}$ -derived winters. X-axis numbering and corresponding vertical lines in the diagram represent winters 1 to 7.

Hubbard, 1982; Mitsuguchi et al., 1996; Enmar et al., 2000; Müller et al., 2001; McGregor and Gagan, 2003; Lazar et al., 2004; Allison et al., 2007). Data on Neogene corals from the Dominican Republic suggest Sr/Ca to be more sensitive to diagenesis than U/Ca (Lommler et al., 2006) consistent with the results of Lazar et al. (2004) indicating the U/Ca thermometer is more robust than Sr/Ca. Hendy et al. (2007) described, how skeletal dissolution causes low SST artifacts due to incongruent leaching of Sr and U. They showed that SST estimates based on Sr/Ca are less affected by dissolution than those based on U/Ca, even though Sr is preferentially leached from the aragonite compared to U. Some authors (Eisenhauer et al., 1999; Wischow, 1999) questioned the suitability of U/Ca as paleo-SST proxy. They found significant different U/Ca–SST relationships for different localities in the Indian Ocean probably caused by pH or alkalinity variability. This corresponds to the wide range of U/Ca–SST relationships compiled by Fallon et al. (2003) and their conclusion that Sr/Ca is the more reliable proxy.

The Late Miocene coral data presented here demonstrate a significant correlation of $r^2 = 0.86$ between Sr/Ca and U/Ca (Fig. 23). Comparable correlations are known from modern diagenetically unaltered corals (Min et al., 1995; Fallon et al., 1999). Based on this analogy, we conclude that the trace element concentrations of the Late Miocene coral have remained unaffected. Even if alteration occurred which cannot be defined by our analytical approach, a potential effect is so minor that the correlation between Sr/Ca and U/Ca is not influenced significantly. In this case, the discrepancy in SST seasonality estimates using Sr/Ca and U/Ca ratios, respectively, cannot be explained by diagenetic alteration. A SST seasonality of about 9°C is known for the modern Aegean Sea (Poulos et al., 1997) which is within the range of 7.1 to 11.5°C for the Late Miocene derived from the bimonthly Sr/Ca chronology, while a SST seasonality for the Late Miocene Mediterranean of only 3.2 to 6.1°C as derived from the bimonthly U/Ca chronology differs from the modern values. The inconsistency between Sr/Ca and U/Ca results may be explained by a more complex environmental control on the U seasonality (Sinclair et al., 1998) with pH, carbonate concentration of seawater, and salinity influencing the portion of U incorporated into the coral carbonate skeleton (Shen and Dunbar, 1995), as well as an U/Ca–SST relationship of the Late Miocene Eastern Mediterranean different from those of the modern oceans. Therefore the SST seasonality estimated from the Sr/Ca values is considered to be more reliable.

The annual $\delta^{18}\text{O}$ amplitudes of corals from the same sampling level as specimen P4 indicate SST seasonality of 7.2°C on average (Brachert et al., 2006b; Mertz-Kraus et al., in

press). Since seasonality in $\delta^{18}\text{O}$ is affected by both SST and seasonal changes in ambient seawater composition, the lower SST seasonality estimate from $\delta^{18}\text{O}$ compared to that derived from Sr/Ca ratios can be explained by attenuated annual $\delta^{18}\text{O}$ amplitudes caused by evaporation in summer or precipitation in winter, respectively. Applying the relationship between SST and $\delta^{18}\text{O}$ of Felis et al. (2004), the difference between the SST seasonality estimates from $\delta^{18}\text{O}$ and Sr/Ca of 2.1°C on average implies that the $\delta^{18}\text{O}$ seasonality is too low by $\sim 0.3\text{‰}$ to reflect annual SST variations alone. This component in the annual $\delta^{18}\text{O}$ cycle presumably influenced by salinity is illustrated in Fig. 22. The Late Miocene seasonal salinity change at the sampling site calculated according to Pierre (1999) with this value is 1.1‰ . Such Late Miocene SSS seasonality is comparable to the seasonal salinity changes of surface waters of the modern Aegean Sea (Eastern Mediterranean) where the inflow of low salinity waters of different sources occurs seasonally with the lowest SSS values ($<25\text{‰}$) measured adjacent to river mouths (Poulos et al., 1997). The seasonal SSS changes vary spatially from $<0.5\text{‰}$ to $>3\text{‰}$ (Poulos et al., 1997; Zervakis and Georopoulos, 2002).

4.6.2. Non-lattice bound elements and insoluble residue

Post-mortem genesis of the coatings composed of the insoluble residue is ruled out: Reuter et al. (2005) showed that marginal post-mortem infiltration of sediment grains into the coral colony leaves behind thicker deposits at the colony flank and thinner deposits towards the center. In contrast, for specimen P4 the distribution of the insoluble residue is almost uniform over the entire growth band formed during the cold season (Fig. 19a and b). The texture of the coatings visible in SEM shows no evidence of diagenetically-formed clay minerals, such as “booklets” of platy kaolinite clusters (Lanson et al., 2002).

Therefore, we suggest that the rhythmic layers of insoluble residue represent seasonal in-vivo incorporation of detrital particles. In tank experiments, living *Porites* corals exposed to large amounts of fine-grained suspended particles were shown to incorporate these particles into the aragonite skeleton at the calcification site below the coral tissue within several hours (Erez and Braun, 2007). Incorporation of silicate particles into coral skeletons has been described in several studies of modern corals and are assumed to be incorporated into the skeleton of the living coral (e.g., Howard and Brown, 1984; Budd et al., 1993; Fallon et al., 2002; Pingitore Jr et al., 2002; Wyndham et al., 2004). Barnard et al. (1974) and Neil et al. (1994) suggested that variations in composition and amount of sediment particles trapped in coral skeletons provide information about provenance and temporal differences in sediment availability and, therefore, variations in environmental

conditions. This is in agreement with observations of Naqvi (1994) on *Porites* showing detrital particles in the high density bands formed during the monsoonal period and reflecting run-off of rain water.

4.6.3. Sources of the insoluble residue

Major sediment input to the present-day and Quaternary Eastern Mediterranean Sea is related to eolian dust transported from North Africa and suspended particles of the Nile and local circum-Aegean rivers (Weldeab et al., 2002a). These sources are likely to have been of similar importance during the Late Miocene. An additional source delivering material could be Neogene volcanism of the Aegean region (Fytikas et al., 1984). Thus, the following possible Late Miocene sources of the material forming the insoluble residue in coral specimen P4 are discussed: (1) airborne Saharan dust, (2) Nile-derived suspension freight, (3) volcanic ash fall, and (4) local riverine sediment.

4.6.3.1. Airborne Saharan dust particles

Dust from the deserts of Northern Africa is the main source of sediment to the recent Eastern Mediterranean (Mattsson and Nihlén, 1996; Weldeab et al., 2002a; Larrasoana et al., 2003), and the rhythmic layers of insoluble residue within the Late Miocene coral skeleton have potential to reflect seasonality in Saharan dust plume supply. Since atmospheric pressure field systems in the Late Miocene are considered to be similar to those of the northern hemisphere today (Brachert et al., 2006b; Mertz-Kraus et al., in press), the origin and temporal distribution of Late Miocene dust events may have been comparable to present-day. In the present-day, dust reaching the Eastern Mediterranean region originates largely from the Central and Eastern Sahara (Moulin et al., 1998; Krom et al., 1999b) and is mainly composed of quartz, kaolinite, palygorskite, illite and Fe and Al oxides (Goudie and Middleton, 2001; Weldeab et al., 2002a; Ehrmann et al., 2007). However, mineralogical compositions as well as mineral abundances of Saharan dust and insoluble residue from the Miocene coral are clearly different, except for quartz and kaolinite.

This discrepancy is also indicated by differences in major and trace element compositions. Krom et al. (1999b; 1999a) chemically characterized Saharan dust by, e.g., the major element ratios Mg/Al or Ti/Al. Fig. 25a shows that Central and Eastern Saharan dust (Moreno et al., 2006) has relatively low and similar Mg/Al ratios ranging from ca. 0.05 to 0.15 and relatively high Ti/Al ratios varying between 0.08 and 0.14. In contrast, the

insoluble residue of the P4 coral has high Mg/Al and low Ti/Al ratios of ca. 0.43 and 0.055, respectively.

In an average upper continental crust-normalized Rare Earth Element (REE) diagram the dust (Moreno et al., 2006) is enriched relative to average upper continental crust up to a factor of 2, whereas the insoluble residue is slightly depleted relative to average upper continental crust (Fig. 21b). The Light REE (LREE) of dust and insoluble residue are subparallel with differences in concentration up to a factor of 3. However, there are significant differences in the MREE and HREE patterns with negative Eu and positive Tm anomalies, respectively, related to the dust in contrast to a homogeneous smooth pattern without anomalies of the insoluble residue of P4.

In addition to geochemical evidence, assuming modern seasonality in dust transport to be established already during the Miocene, the temporal pattern of the modern dust events indicates that the rhythmic layers of insoluble residue of the Late Miocene P4 coral appear not to originate mainly from Saharan dust: Dust events affecting the present-day Eastern Mediterranean generally occur from spring to early fall with a summertime maximum (Moulin et al., 1998; Balis et al., 2006; Fotiadi et al., 2006). In

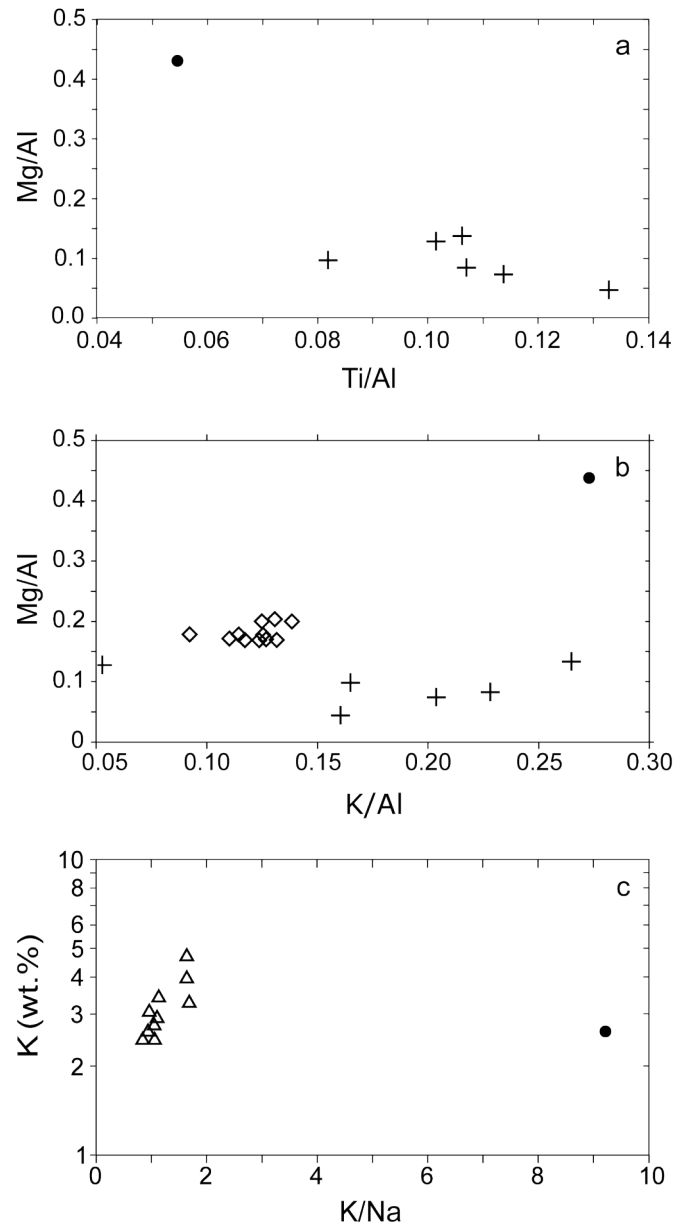


Fig. 25: (a) Ti/Al versus Mg/Al of coral specimen P4 insoluble residue (●) compared to Saharan dust (Moreno et al., 2006) (+). (b) K/Al versus Mg/Al of coral specimen P4 insoluble residue (●) compared to Saharan dust (Moreno et al., 2006) (+) and Nile derived sediments (Krom et al., 1999b) (◇). (c) K/Na versus K of coral specimen P4 insoluble residue (●) compared to Mid-Miocene Aegean shoshonitic and high-K calc-alkaline volcanic rocks (Pe-Piper, 1980) (△).

contrast, the layers of insoluble residue of the Late Miocene P4 occur around the month with the coolest SST, which is December or January for the present-day Mediterranean.

4.6.3.2. Nile-derived sediment

Before the Aswan Dam was built, Nile river sediment discharge into the Mediterranean was strongly pulsed by monsoonal rain over the Ethiopian plateau. For the Quaternary, Nile-derived sediments are documented in the Eastern Mediterranean (Krom et al., 1999a; Weldeab et al., 2002b; Ehrmann et al., 2007), however, only negligible amounts of these sediments are found to the north of the Mediterranean Ridge (Krom et al., 1999b; Weldeab et al., 2002a), which forms a barrier southeast of Crete. Moreover, low Mg/Al and K/Al ratios characterize present-day Nile sediments (Krom et al., 1999b; Wehausen and Brumsack, 2000) in contrast to relatively high values of these element ratios observed in the insoluble residue of P4 (Fig. 25b). Assuming a similar basin configuration for the Late Miocene Eastern Mediterranean and a similar composition of the Nile-derived sediments, the non-carbonate sediment particles trapped in the coral skeleton of P4 are unlikely to represent suspension load from the Nile.

4.6.3.3. Volcanic ash fall and related deposits

Particles trapped in corals representing pyroclastic products related to active volcanism are known from Indonesia, and Heikoop et al. (1996b; 1996a) suggested corals to be useful media for recording episodic volcanic phenomena like ash fall. There was volcanic activity in the Eastern Mediterranean region occurring from ca. 10 to 7 Ma (Fytikas et al., 1984). Although no Neogene volcano is known from Crete, occurrences of ash layers indicate that Crete was affected by tephra deposition during the Late Miocene. For instance, $^{40}\text{Ar}/^{39}\text{Ar}$ dating on single sanidine grains from a tuff located close to the sampling site within a section of Tortonian and Messinian sediments gave a plateau age of 6.97 ± 0.03 Ma (Hilgen et al., 1997; Kuiper et al., 2004). Therefore, primary deposition of volcanic ashes or reworked volcanic material is assumed to be a potential source for the P4 coral insoluble residue. Late Miocene volcanism in the Aegean region is characterized by a subduction-related geodynamic setting producing shoshonitic and high-K calc-alkaline volcanic products (Fytikas et al., 1984). Since there are no suitable geochemical data on the composition of the 10 to 7 Ma volcanism, we use selected major element and REE data from shoshonitic and high-K calc-alkaline volcanic rocks of Mid-Miocene age (18 to 16 Ma) from the Eastern Mediterranean island of Lesbos (Pe-Piper, 1980) for comparison with

the insoluble residue. Since volcanic activities at 18 to 16 Ma and 10 to 7 Ma have similar major element composition and geodynamic setting (relevant for the trace element composition), we consider the use of these data to be justified for comparison purposes.

In the marine realm, alteration of volcanic glass shards in ashes to clay minerals like montmorillonite is not unusual (e.g., Hein and Scholl, 1978). Correspondingly, montmorillonite as a component of the insoluble residue can be considered diagnostic if the insoluble residue represents altered tephra. In this case, quartz as a further mineral demonstrates the insoluble residue to reflect a rhyolitic composition of such a tephra originating from a shoshonitic or high-K calc-alkaline source. Zielinski (1982) showed that during alteration of a Miocene rhyolitic ash into clay minerals such as montmorillonite, alkali elements like Na and K are highly mobile. They are similarly depleted by an order of magnitude of 0.15 and 0.10, respectively. Whereas REE are largely unaffected by alteration and are therefore considered to be immobile.

In Fig. 25c major elements of hypothetical shoshonitic to high-K calc alkaline source rocks and insoluble residue are compared in a diagram wt.% K vs. K/Na. In case the insoluble residue represents an altered tephra product, depletion of K by a factor of ca. 0.1 and a more or less similar effect on Na should be expected as outlined by Zielinski (1982). However, the K concentration of the insoluble residue of ca. 3 wt.% is not depleted relative to potential source rocks but lies in the middle of their K concentration range (Fig. 25c). Also, in contrast to the expected coherent behavior of K and Na in case of alteration, Na is selectively depleted resulting in a high K/Na ratio of 9 of the insoluble residue compared to ca. 1 to 2 of hypothetical source rocks.

Also, the C1 chondrite-normalized REE patterns indicate significant differences between insoluble residue and hypothetical source rocks (Fig. 21c). Whereas the insoluble residue shows only minor discrimination between MREE and HREE with $(\text{Tb/Lu})_{\text{normalized}} = 0.91$, the potential source rocks have MREE to HREE ratios either substantially higher with $(\text{Tb/Lu})_{\text{normalized}}$ up to 2.71 or substantially lower with $(\text{Tb/Lu})_{\text{normalized}}$ down to 0.41. Since the REE are regarded as sufficiently immobile during alteration, the differences in REE patterns between potential volcanic source rocks and insoluble residue (Fig. 21c) together with major element evidence illustrated in Fig. 25b exclude interpretation of the mineral components of the insoluble residue of P4 as alteration products of primary or reworked tephra.

4.6.3.4. Local riverine suspended load

Since airborne Saharan dust, Nile-derived suspension plumes as well as particles related to reworked volcanic ash fall can be excluded as major potential sources for the insoluble residue material in coral P4 on the basis of geochemical and geological arguments, local riverine suspended load remains as plausible source. This interpretation is supported by the geological setting indicating a near-shore environment of the coral sampling site in the Late Miocene (Reuter and Brachert, 2007) forming a preferred area of sedimentation for siliciclastic particles. Also, the reef structure of the sampling site is associated with delta sediments derived from the hinterland of Crete. The Late Miocene hinterland of Crete consists of carbonates, dolomites, phyllites, quartzites, quartz-rich siliciclastic sediments, granitoid and ophiolitic rocks (ten Veen and Postma, 1999; Rahl, 2004). Montmorillonite, kaolinite and illite as mineral components of the insoluble residue are common weathering products of such rocks.

The most significant evidence for a local source comes from the major and trace element compositions of the insoluble residue. Wehausen and Brumsack (2000) have noted that Quaternary sediments in the Eastern Mediterranean with high Mg/Al and Ti/Al ratios comparable to that of the insoluble residue (Fig. 25a) have ultramafic rock sources. Regarding the geological setting of the sampling site Psalidha, ultramafic rocks associated with ophiolites crop out at the southern margin of the Ida Mountains and on top of the Asterousia Mountains (Bonneau et al., 1977; Fassoulas, 1998) forming islands (Welter-Schultes, 2000) to the north and the south of the sampling site (Fig. 17) and representing areas exposed to erosion in the Late Miocene.

Additionally, Ni and Cr are preferentially concentrated in olivine (Ni) and spinel (Ni, Cr) occurring in ophiolitic rocks. In peridotite relics within serpentinite from the Cretan ophiolite occurrences, microprobe analyses yield Ni concentrations up to 0.43 wt.% in olivine and spinel as well as Cr concentrations up to ca. 18 wt.% in spinel (Koepke et al., 2002). High positive Ni and Cr anomalies of the insoluble residue (Fig. 21a) are consistent with contributions from these Cretan ophiolites. XRD analyses did not demonstrate spinel or olivine to occur above the analytical detection limit. However, because of the high Ni and Cr concentrations in these minerals, mineralogical traces below the detection limit of XRD are already sufficient to cause the corresponding anomalies in the normalized multi-element pattern. Also, spinel and olivine are sensitive to alteration, which implies that high Cr and Ni concentrations may be related to their alteration products, and none of these primary

peridotitic minerals may be preserved to a significant amount in the sedimentary material deposited in the coral environment.

Transport of alteration products from weathering-affected hinterland rocks to the delta environment can be achieved by heavy rainfall with highest erosive power after dry seasons (Fleitmann et al., 2007). Thus, regional geology, Late Miocene topographical and environmental conditions together with the major and trace element evidence link to distinct local ophiolitic rocks indicating that the hinterland represents the essential source for the mineralogical or chemical components forming the insoluble residue of coral P4. This is in agreement with previous studies (e.g., ten Veen and Postma, 1999) regarding Neogene Cretan paleogeography and sediment supply.

4.6.4. Relation between geochemical pattern and climate

Although several studies indicate that the climate in the Mediterranean was subtropical, warm and humid during the Tortonian (Sachse and Mohr, 1996; Zidianakis et al., 2004; Ioakim et al., 2005), little is known on real seasonal variability. The present-day Mediterranean climate with a pronounced seasonality in precipitation is postulated not to be existent until the Pliocene at 3.6 Ma (Suc, 1984; Suc and Popescu, 2005). However, the regular temporal distribution of the peaks observed in the LA-ICP-MS-derived non-lattice bound element patterns of the Miocene coral skeleton indicates a strong seasonal mechanism controlling the input of suspended inorganic sediment grains into the reef environment. Since the non-lattice bound element peaks correspond with low SST values derived from Sr/Ca, U/Ca as well as $\delta^{18}\text{O}$ (Brachert et al., 2006b), the input of detrital material forming the layers of insoluble residue appears to have occurred during the cold months. Major and trace element evidence link the insoluble residue to local rock sources. The most likely process to cause seasonal input is an abrupt increase of suspension load in the reef environment by enhanced river discharge during winter. Most plausible, intense rainfall in this season produced sediment-laden fresh water input. Additional evidence for winter rainfall is given by a comparison of Sr/Ca and $\delta^{18}\text{O}$ records. The discrepancy in SST estimations based on $\delta^{18}\text{O}$ and Sr/Ca seasonality, respectively, suggests that the annual $\delta^{18}\text{O}$ amplitude is reduced either by fresh water input during winters or evaporation during summers (see section 4.6.1.). Since the element input peaks in the winter month, winter rain and associated river discharge as the fresh water source appears to be the reason for to reduced $\delta^{18}\text{O}$ amplitudes. In the present-day Mediterranean, precipitation tends to be concentrated in a few events mostly occurring during winter (Casas et al., 2006). Such

intense rainfall events in the Eastern Mediterranean are known to be related to eastward moving winter atmospheric low-pressure systems generated in the western and central Mediterranean Sea (Osetinsky and Alpert, 2006). These rainfalls can cause short-lived sediment-laden floods forming large plumes when entering the coastal waters. Since the atmospheric pressure fields during the Late Miocene are considered to be similar to today (Brachert et al., 2006b) we suggest comparable heavy winter rain events for the Tortonian causing sediment discharge by catching weathering products of outcropping rocks and transportation of suspension clouds into the reef environment. A Mediterranean-type climate with seasonality in precipitation and episodic heavy rain events during the winter month is, therefore, already documented for the early Late Miocene at 9 Ma. There is additional evidence for the development of a Mediterranean-type climate in the Late Miocene from $\delta^{18}\text{O}$ data on Tortonian and Messinian corals, indicating increasing summer aridity in the Eastern Mediterranean in the course of the Late Miocene (Mertz-Kraus et al., in press). Summarizing, it appears that the Mediterranean-type climate in the Eastern Mediterranean, today characterized by a strong precipitation seasonality, most probably is an older phenomenon developed pre-Pliocene.

4.7. Conclusions

LA-ICP-MS measurements of lattice and non-lattice bound element concentrations were made on ~9 Ma-old coral material which has fully retained its original aragonite skeleton and stable isotope ($\delta^{18}\text{O}$, $\delta^{13}\text{C}$) composition. Over a seven-year period of Late Miocene coral growth LA-ICP-MS measurements document systematic, subannual variability in major and trace elements concentrations caused by seasonal environmental variations. Clay coatings were preferentially incorporated by the living coral into the skeleton during winter rain storm events. The elemental and mineralogical composition indicates that the clay is derived from the chemical weathering of rocks in the hinterland and was fluviially transported. Significant terrigenous input from alternative sources, namely airborne Saharan dust, Nile-derived sediment suspension and volcanic ash-fall can be excluded. Salinity at the sampling site as calculated from combined skeletal Sr/Ca and $\delta^{18}\text{O}$ was by approximately 1‰ lower in winter than in summer, a magnitude known from the present-day Aegean Sea (Eastern Mediterranean) caused by seasonally controlled fresh-water input. Together with the increased sediment input in winter this suggests higher rainfall in winter rather than extreme evaporation in summer. Our results imply that the Mediterranean-type wet winter/dry summer climate existed, at least intermittently, since the

Late Miocene at 9 Ma in the Aegean region. This conclusion is in contrast to previous assumptions based on palynological data that the Mediterranean-type climate was not initiated before the Late Pliocene but indicate that the Mediterranean-type climate is an earlier and probably repetitive phenomenon.

4.8. References

- Akgün, F., Kayseri, M.S. and Akkiraz, M.S., 2007. Palaeoclimatic evolution and vegetational changes during the Late Oligocene-Miocene period in Western and Central Anatolia (Turkey). *Palaeogeography, Palaeoclimatology, Palaeoecology*, 253(1-2): 56-90.
- Alibert, C. and McCulloch, M.T., 1997. Strontium/calcium ratios in modern *Porites* corals from the Great Barrier Reef as a proxy for sea surface temperature: Calibration of the thermometer and monitoring of ENSO. *Paleoceanography*, 12(3): 345-363.
- Allison, N., Finch, A.A., Newville, M. and Sutton, S.R., 2005. Strontium in coral aragonite: 3. Sr coordination and geochemistry in relation to skeletal architecture. *Geochimica et Cosmochimica Acta*, 69(15): 3801-3811.
- Allison, N., Finch, A.A., Webster, J.M. and Clague, D.A., 2007. Palaeoenvironmental records from fossil corals: The effects of submarine diagenesis on temperature and climate estimates. *Geochimica et Cosmochimica Acta*, 71(19): 4693-4703.
- Amiel, A.J., Miller, D.S. and Friedman, G.M., 1973a. Incorporation of uranium in modern corals. *Sedimentology*, 20(4): 523-528.
- Amiel, A.J., Friedman, G.M. and Miller, D.S., 1973b. Distribution and nature of incorporation of trace elements in modern aragonitic corals. *Sedimentology*, 20(1): 47-64.
- Balis, D., Amiridis, V., Kazadzis, S., Papayannis, A., Tsaknakis, G., Tzortzakis, S., Kalivitis, N., Vrekoussis, M., Kanakidou, M., Mihalopoulos, N., Chourdakis, G., Nickovic, S., Pérez, C., Baldasano, J. and Drakakis, M., 2006. Optical characteristics of desert dust over the East Mediterranean during summer: a case study. *Annales Geophysicae*, 24(3): 807-821.
- Barnard, L.A., Macintyre, I.G. and Pierce, J.W., 1974. Possible environmental index in tropical reef corals. *Nature*, 252(5480): 219-220.
- Barnes, D.J., Taylor, R.B. and Lough, J.M., 1995. On the inclusion of trace materials into massive coral skeletons. Part II: distortions in skeletal records of annual climate cycles due to growth processes. *Journal of Experimental Marine Biology and Ecology*, 194(2): 251-275.
- Barnes, J.H., Schilling, G.D., Hieftje, G.M., Sperline, R.P., Denton, M.B., Barinaga, C.J. and Koppenaal, D.W., 2004. Use of a novel array detector for the direct analysis of solid samples by laser ablation inductively coupled plasma sector-field mass spectrometry. *Journal of the American Society for Mass Spectrometry*, 15(6): 769-776.
- Beck, J.W., Edwards, R.L., Ito, E., Taylor, F.W., Récy, J., Rougerie, F., Joannot, P. and Henin, C., 1992. Sea-surface temperature from coral skeletal strontium/calcium ratios. *Science*, 257: 644-647.
- Bednar, A.J., Medina, V.F., Ulmer-Scholle, D.S., Frey, B.A., Johnson, B.L., Brostoff, W.N. and Larson, S.L., 2007. Effects of organic matter on the distribution of uranium in soil and plant matrices. *Chemosphere*, 70(2): 237-247.

- Bleiner, D., Plotnikov, A., Vogt, C., Wetzig, K. and Günther, D., 2000. Depth profile analysis of various titanium based coatings on steel and tungsten carbide using laser ablation inductively coupled plasma - "time of flight" mass spectrometry. *Fresenius' Journal of Analytical Chemistry*, 368(2): 221-226.
- Böhme, M., Ilg, A. and Winklhofer, M., 2008. Late Miocene "washhouse" climate in Europe. *Earth and Planetary Science Letters*, 275, 393-401.
- Bonneau, M., Angelier, J. and Epting, M., 1977. Réunion extraordinaire de la Société Géologique de France en Crète. *Bulletin de la Societe Geologique de France*, 19(1): 87-102.
- Brachert, T.C., Reuter, M., Kroeger, K.F. and Lough, J., 2006a. Coral growth bands: A new and easy to use paleothermometer in paleoenvironment analysis and paleoceanography (late Miocene, Greece). *Paleoceanography* 21, PA4217.
- Brachert, T.C., Reuter, M., Felis, T., Kroeger, K.F., Lohmann, G., Micheels, A. and Fassoulas, C., 2006b. *Porites* corals from Crete (Greece) open a window into Late Miocene (10 Ma) seasonal and interannual climate variability. *Earth and Planetary Science Letters*, 245: 81-94.
- Bruch, A.A., Utescher, T., Mosbrugger, V., Gabrielyan, I. and Ivanov, D.A., 2006. Late Miocene climate in the circum-Alpine realm - a quantitative analysis of terrestrial palaeofloras. *Palaeogeography, Palaeoclimatology, Palaeoecology*, 238: 270-280.
- Budd, A.F., Mann, K.O. and Guzmán, H.M., 1993. Environmental interpretation using insoluble residues within reef coral skeletons: problems, pitfalls, and preliminary results. *Coral Reefs*, 12(1): 31-42.
- Casas, J.J., Gessner, M.O., Langton, P.H., Calle, D., Descals, E. and Salinas, M.J., 2006. Diversity of patterns and processes in rivers of eastern Andalusia. *Limnetica*, 25(1-2): 155-170.
- Corrège, T., 2006. Sea surface temperature and salinity reconstruction from coral geochemical tracers. *Palaeogeography, Palaeoclimatology, Palaeoecology*, 232(2-4): 408-428.
- David, C.P., 2003. Heavy metal concentrations in growth bands of corals: a record of mine tailings input through time (Marinduque Island, Philippines). *Marine Pollution Bulletin*, 46(2): 187-196.
- de Villiers, S., Shen, G.T. and Nelson, B.K., 1994. The Sr/Ca-temperature relationship in coralline aragonite: Influence of variability in $(\text{Sr}/\text{Ca})_{\text{seawater}}$ and skeletal growth parameters. *Geochimica et Cosmochimica Acta*, 58(1): 197-208.
- Djogic, R., Sipos, L. and Branica, M., 1986. Characterization of uranium(VI) in seawater. *Limnology and Oceanography*, 31(5): 1122-1131.
- Ehrmann, W., Schmiedl, G., Hamann, Y., Kuhnt, T., Hemleben, C. and Siebel, W., 2007. Clay minerals in late glacial and Holocene sediments of the northern and southern Aegean Sea. *Palaeogeography, Palaeoclimatology, Palaeoecology*, 249(1-2): 36-57.
- Eisenhauer, A., Wischow, D., Wyrwoll, K., Collins, L., Zhu, Z., Heiss, G., Dullo, C. and Hansen, B., 1999. Sr/Ca- and U/Ca-Thermometry of Modern and Fossil Corals from the Abrolhos Islands and the Ningaloo Reef, Western Australia, AGU Fall Meeting, San Francisco, OS52A-18.
- Enmar, R., Stein, M., Bar-Matthews, M., Sass, E., Katz, A. and Lazar, B., 2000. Diagenesis in live corals from the Gulf of Aqaba. I. The effect on paleo-oceanography tracers. *Geochimica et Cosmochimica Acta*, 64(18): 3123-3132.
- Erez, J. and Braun, A., 2007. Calcification in hermatypic corals is based on direct seawater supply to the biomineralization site. *Geochimica Cosmochimica Acta*, 71(15, Supplement 1), A260.
- Evensen, N.M., Hamilton, P.J. and O'Nions, R.K., 1978. Rare-earth abundances in chondritic meteorites. *Geochimica et Cosmochimica Acta*, 42: 1199-1212.

- Fallon, S.J., White, J.C. and McCulloch, M.T., 2002. *Porites* corals as a recorder of mining and environmental impacts: Misima Island, Papua New Guinea. *Geochimica et Cosmochimica Acta*, 66(1): 45-62.
- Fallon, S.J., McCulloch, M.T. and Alibert, C., 2003. Examining water temperature proxies in *Porites* corals from the Great Barrier Reef: a cross-shelf comparison. *Coral Reefs*, 22: 389-404.
- Fallon, S.J., McCulloch, M.T., van Woesik, R. and Sinclair, D.J., 1999. Corals at their latitudinal limits: laser ablation trace element systematics in *Porites* from Shirigai Bay, Japan. *Earth and Planetary Science Letters*, 172: 221-238.
- Faranda, C., Cipollari, P., Cosentino, D., Gliozzi, E. and Pipponzi, G., 2007. Late Miocene ostracod assemblages from eastern Mediterranean coral-reef complexes (central Crete, Greece). *Revue de Micropaléontologie*: 1-22.
- Fassoulas, C., 1998. The structural evolution of central Crete: insight into the tectonic evolution of the south Aegean (Greece). *Journal of Geodynamics*, 27(1): 23-43.
- Fassoulas, C., 2001. The tectonic development of a Neogene basin at the leading edge of the active European margin: the Heraklion basin, Crete, Greece. *Journal of Geodynamics*, 31: 49-70.
- Felis, T., Pätzold, J., Loya, Y., Fine, M., Nawar, A.H. and Wefer, G., 2000. A coral oxygen isotope record from the northern Red Sea documenting NAO, ENSO, and North Pacific teleconnections on Middle East climate variability since the year 1750. *Paleoceanography*, 15: 679-694.
- Felis, T., Lohmann, G., Kuhnert, H., Lorenz, S.J., Scholz, D., Pätzold, J., Al-Rousan, S.A. and Al-Moghrabi, S.M., 2004. Increased seasonality in Middle East temperatures during the last interglacial period. *Nature*, 429: 164-168.
- Fleitmann, D., Dunbar, R.B., McCulloch, M., Mudelsee, M., Vuille, M., McClanahan, T.R., Cole, J.E. and Eggins, S., 2007. East African soil erosion recorded in a 300 year old coral colony from Kenya. *Geophysical Research Letters*, 34: L04401.
- Fotiadi, A., Hatzianastassiou, N., Drakakis, E., Matsoukas, C., Pavlakis, K.G., Hatzidimitriou, D., Gerasopoulos, E., Mihalopoulos, N. and Vardavas, I., 2006. Aerosol physical and optical properties in the Eastern Mediterranean Basin, Crete, from Aerosol Robotic Network data. *Atmospheric Chemistry and Physics*, 6(12): 5399-5413.
- Frydas, D., Keupp, H. and Bellas, S., 2008. Stratigraphical investigations based on calcareous and siliceous phytoplankton assemblages from the upper Cenozoic deposits of Messara Basin, Crete, Greece. *Zeitschrift der Deutschen Gesellschaft für Geowissenschaften*, 159(3): 415-437.
- Fytikas, M., Innocenti, F., Manetti, P., Mazzuoli, R., Peccerillo, A. and Villari, L., 1984. Tertiary to Quaternary evolution of volcanism in the Aegean region. In: Dixon, J.E. and Robertson, A.H.F. (Editors), *The Geological Evolution of the Eastern Mediterranean*, Geological Society of London, Special Publication, 17 pp. 687-699.
- Gao, S., Liu, X., Yuan, H., Hattendorf, B., Günther, D., Chen, L. and Hu, S., 2002. Determination of forty two major and trace elements in USGS and NIST SRM glasses by laser ablation-inductively coupled plasma-mass spectrometry. *Geostandards Newsletter*, 26: 181-196.
- Goodkin, N.F., Hughen, K.A. and Cohen, A.L., 2007. A multicoral calibration method to approximate a universal equation relating Sr/Ca and growth rate to sea surface temperature. *Paleoceanography*, 22: PA1214.
- Goudie, A.S. and Middleton, N.J., 2001. Saharan dust storms: nature and consequences. *Earth-Science Reviews*, 56(1-4): 179-204.
- Gregor, R.B., Pingitore, N.E., Jr. and Lytle, F.W., 1997. Strontianite in Coral Skeletal Aragonite. *Science*, 275(5305): 1452-1454.

- Gromet, L.P., Haskin, L.A., Korotev, R.L. and Dymek, R.F., 1984. The "North American shale composite": Its compilation, major and trace element characteristics. *Geochimica et Cosmochimica Acta*, 48(12): 2469-2482.
- Gurevich, E.L. and Hergenröder, R., 2007. A simple laser ICP-MS ablation cell with wash-out time less than 100 ms. *Journal of Analytical Atomic Spectrometry*, 22: 1043-1050.
- Hanna, R.G. and Muir, G.L., 1990. Red sea corals as biomonitors of trace metal pollution. *Environmental Monitoring and Assessment*, 14(2): 211-222.
- Heikoop, J.M., Tsujita, C.J., Risk, M.J. and Tomascik, T., 1996a. Corals as proxy recorders of volcanic activity; evidence from Banda Api, Indonesia. *Palaios*, 11(3): 286-292.
- Heikoop, J.M., Tsujita, C.J., Heikoop, C.E., Risk, M.J. and Dickin, A.P., 1996b. Effects of volcanic ashfall recorded in ancient marine benthic communities: comparison of a nearshore and an offshore environment. *Lethaia*, 29(2): 125-139.
- Hein, J.R. and Scholl, D.W., 1978. Diagenesis and distribution of late Cenozoic volcanic sediment in the southern Bering Sea. *Geological Society of America Bulletin*, 89: 197-210.
- Hendy, E.J., Gagan, M.K., Lough, J.M., McCulloch, M.T. and deMenocal, P.B., 2007. Impact of skeletal dissolution and secondary aragonite on trace element and isotopic climate proxies in *Porites* corals. *Paleoceanography*, 22: PA4101.
- Hilgen, F.J., Krijgsman, W. and Wijbrans, J.R., 1997. Direct comparison of astronomical and $^{40}\text{Ar}/^{39}\text{Ar}$ ages of ash beds: Potential implications for the age of mineral dating standards. *Geophysical Research Letters* 24(16): 2043-2046.
- Howard, L.S. and Brown, B.E., 1984. Heavy metals and reef corals. *Oceanography Marine Biology Annual Review*, 22: 195-210.
- Ioakim, C., Rondoyanni, T. and Mettos, A., 2005. The Miocene Basins of Greece (Eastern Mediterranean) from a palaeoclimatic perspective. *Revue de Paléobiologie*, 24(2): 735-748.
- Jochum, K.P. and Stoll, B., 2008. Reference materials for elemental and isotopic analyses by LA-(MC)-ICPMS: Successes and outstanding needs. In: Sylvester, P. (Editor), Short Course Series, 40. Mineralogical Association of Canada, Ottawa, Canada, pp. 147-168.
- Jochum, K.P., Stoll, B., Herwig, K. and Willbold, M., 2007. Validation of LA-ICP-MS trace element analysis of geological glasses using a new solid-state 193 nm Nd:YAG laser and matrix-matched calibration. *Journal of Analytical Atomic Spectrometry*, 22: 112-121.
- Jochum, K.P., Nohl, U., Herwig, K., Lammel, E., Stoll, B. and Hofmann, A.W., 2006a. GeoReM: A new geochemical database for reference materials and standards. *Geostandards and Geoanalytical Research*, 29(3): 333-338.
- Jochum, K.P., Dingwell, D.B., Rocholl, A., Stoll, B., Hofmann, A.W., Becker, S., Besmehn, A., Bessette, D., Dietze, H.-J., Dulski, P., Erzinger, J., Hellebrand, E., Hoppe, P., Horn, I., Janssens, K., Jenner, G.A., Klein, M., McDonough, W.F., Maetz, M., Mezger, K., Münker, C., Nikogosian, I.K., Pickhardt, C., Raczek, I., Rhede, D., Seufert, H.M., Simakin, S.G., Sobolev, A.V., Spettel, B., Straub, S., Vincze, L., Wallianos, A., Weckwerth, G., Weyer, S., Wolf, D. and Zimmer, M., 2000. The preparation and preliminary characterisation of eight geological MPI-DING reference glasses for in-situ microanalysis. *Geostandards Newsletter*, 24: 87-133.
- Jochum, K.P., Stoll, B., Herwig, K., Willbold, M., Hofmann, A.W., Amini, M., Aarburg, S., Abouchami, W., Hellebrand, E., Mocek, B., Raczek, I., Stracke, A., Alard, O., Bouman, C., Becker, S., Dücking, M., Brätz, H., Klemd, R., de Bruin, D., Canil, D., Cornell, D., de Hoog, C.-J., Dalpé, C., Danyushevsky, L., Eisenhauer, A., Gao, Y., Snow, J.E., Groschopf, N., Günther, D., Latkoczy, C., Guillong, M., Hauri, E.H.,

- Höfer, H.E., Lahaye, Y., Horz, K., Jacob, D.E., Kasemann, S.A., Kent, A.J.R., Ludwig, T., Zack, T., Mason, P.R.D., Meixner, A., Rosner, M., Misawa, K., Nash, B.P., Pfänder, J., Premo, W.R., Sun, W.D., Tiepolo, M., Vannucci, R., Vennemann, T., Wayne, D. and Woodhead, J.D., 2006b. MPI-DING reference glasses for in situ microanalysis: New reference values for element concentrations and isotope ratios. *Geochemistry, Geophysics, Geosystems (G3)*, 7(2): Q02008.
- Kanický, V., Kuhn, H.-R. and Guenther, D., 2004. Depth profile studies of ZrTiN coatings by laser ablation inductively coupled plasma mass spectrometry. *Analytical and Bioanalytical Chemistry*, 380(2): 218-226.
- Koepke, J., Seidel, E. and Kreuzer, H., 2002. Ophiolites on the Southern Aegean islands Crete, Karpathos and Rhodes: composition, geochronology and position within the ophiolite belts of the Eastern Mediterranean. *Lithos*, 65(1-2): 183-203.
- Krom, M.D., Michard, A., Cliff, R.A. and Strohle, K., 1999a. Sources of sediment to the Ionian Sea and western Levantine basin of the Eastern Mediterranean during S-1 sapropel times. *Marine Geology*, 160(1-2): 45-61.
- Krom, M.D., Cliff, R.A., Eijsink, L.M., Herut, B. and Chester, R., 1999b. The characterisation of Saharan dusts and Nile particulate matter in surface sediments from the Levantine basin using Sr isotopes. *Marine Geology*, 155: 319-330.
- Kuhnert, H., Pätzold, J., Hatcher, B., Wyrwoll, K.-H., Eisenhauer, A., Collins, L.B., Zhu, Z.R. and Wefer, G., 1999. A 200-year coral stable isotope record from a high-latitude reef off Western Australia. *Coral Reefs*, 18: 1-12.
- Kuiper, K.F., Hilgen, F.J., Steenbrink, J.R. and Wijbrans, J.R., 2004. $^{40}\text{Ar}/^{39}\text{Ar}$ ages of tephras intercalated in astronomically tuned Neogene sedimentary sequences in the eastern Mediterranean. *Earth and Planetary Science Letters*, 222: 583-597.
- Lanson, B., Beaufort, D., Berger, G., Bauer, A., Cassagnabere, A. and Meunier, A., 2002. Authigenic kaolin and illitic minerals during burial diagenesis of sandstones: a review. *Clay Minerals*, 37(1): 1-22.
- Larrasoana, J.C., Roberts, A.P., Rohling, E.J., Winklhofer, M. and Wehausen, R., 2003. Three million years of monsoon variability over the northern Sahara. *Climate Dynamics*, 21: 689-698.
- LaVigne, M. and Sherrell, R.M., 2006. Sub-Annual Variations of Trace Elements in a *Montastrea* Coral (Martinique, Caribbean) Using a Novel ICP-MS Method: Potential for an Atmospheric Dust Proxy, 13th Ocean Sciences Meeting, Hawaii, Honolulu, Hawaii.
- Lazar, B., Enmar, R., Schossberger, M., Bar-Matthews, M., Halicz, L. and Stein, M., 2004. Diagenetic effects on the distribution of uranium in live and Holocene corals from the Gulf of Aqaba. *Geochimica et Cosmochimica Acta*, 68(22): 4583-4593.
- Lear, C.H., Elderfield, H. and Wilson, P.A., 2003. A Cenozoic seawater Sr/Ca record from benthic foraminiferal calcite and its application in determining global weathering fluxes. *Earth and Planetary Science Letters*, 208: 69-84.
- Lewis, S.E., Shields, G.A., Kamber, B.S. and Lough, J.M., 2007. A multi-trace element coral record of land-use changes in the Burdekin River catchment, NE Australia. *Palaeogeography, Palaeoclimatology, Palaeoecology*, 246(2-4): 471-487.
- Livingston, H.D. and Thompson, G., 1971. Trace element concentrations in some modern corals. *Limnology and Oceanography*, 16: 786-796.
- Lommler, M., Denniston, R.F. and Budd, A.F., 2006. Comparison of U/Ca and Sr/Ca ratios in Neogene corals from the Dominican Republic, Geological Society of America, North-Central Section-40th Annual Meeting, Akron, Ohio, 37-11.
- Mai, D.H., 1989. Development and regional differentiation of the European vegetation during the Tertiary. *Plant Systematics and Evolution*, 162(1): 79-91.

- Mattsson, J.O. and Nihlén, T., 1996. The transport of Saharan dust to southern Europe: a scenario. *Journal of Arid Environments*, 32(2): 111-119.
- McCulloch, M., Fallon, S., Wyndham, T., Hendy, E., Lough, J. and Barnes, D., 2003. Coral record of increased sediment flux to the inner Great Barrier Reef since European settlement. *Nature*, 421(6924): 727-730.
- McCulloch, M.T., Gagan, M.K., Mortimer, G.E., Chivas, A.R. and Isdale, P.J., 1994. A high resolution Sr/Ca and $\delta^{18}\text{O}$ coral record from the Great Barrier Reef, Australia, and the 1982-1983 El Nino. *Geochimica et Cosmochimica Acta*, 58: 2747-2754.
- McGregor, H.V. and Gagan, M.K., 2003. Diagenesis and geochemistry of *Porites* corals from Papua New Guinea: Implications for paleoclimate reconstruction. *Geochimica et Cosmochimica Acta*, 67(12): 2147-2156.
- Mertz-Kraus, R., Brachert, T.C., Reuter, M., Galer, S.J.G., Fassoulas, C. and Illiopoulos, G., in press. Late Miocene sea surface salinity variability and paleoclimate conditions in the Eastern Mediterranean inferred from coral aragonite $\delta^{18}\text{O}$. *Chemical Geology*.
- Meulenkamp, J.E., Dermitzakis, M., Georgiadou-Dikeoulia, E., Jonkers, H.A. and Böger, H., 1979. Field guide to the Neogene of Crete, University of Athens.
- Meulenkamp, J.E. and Sissingh, W., 2003. Tertiary palaeogeography and tectonostratigraphic evolution of the Northern and Southern Peri-Tethys platforms and the intermediate domains of the African-Eurasian convergent plate boundary zone. *Palaeogeography, Palaeoclimatology, Palaeoecology*, 196(1-2): 209-228.
- Min, G.R., Edwards, R.L., Taylor, F.W., Recy, J., Gallup, C.D. and Beck, W., 1995. Annual cycles of U/Ca in coral skeletons and U/Ca thermometry. *Geochimica et Cosmochimica Acta*, 59: 2025-2042.
- Mitsuguchi, T., Matsumoto, E., Abe, O., Uchida, T. and Isdale, P.J., 1996. Mg/Ca thermometry in coral skeletons. *Science*, 274(5289): 961-963.
- Moreno, T., Querol, X., Castillo, S., Alastuey, A., Cuevas, E., Herrmann, L., Mounkaila, M., Elvira, J. and Gibbons, W., 2006. Geochemical variations in aeolian mineral particles from the Sahara-Sahel Dust Corridor. *Chemosphere*, 65(2): 261-270.
- Moulin, C., Lambert, C.E., Dayan, U., Masson, V., Ramonet, M., Bousquet, P., Legrand, M., Balkanski, Y.J., Guelle, W., Marticorena, B., Bergametti, G. and Dulac, F., 1998. Satellite climatology of African dust transport in the Mediterranean atmosphere. *Journal of Geophysical Research*, 103(D11): 13137-13144.
- Müller, A., Gagan, M.K. and McCulloch, M.T., 2001. Early marine diagenesis in corals and geochemical consequences for paleoceanographic reconstructions. *Geophysical Research Letters*, 28(23): 4471-4474.
- Munksgaard, N.C., Antwertinger, Y. and Parry, D.L., 2004. Laser Ablation ICP-MS Analysis of Faviidae Corals for Environmental Monitoring of a Tropical Estuary. *Environmental Chemistry*, 1(3): 188-196.
- Naqvi, S.A.S., 1994. Seasonal variation in an annually-banded coral *Porites*: A scanning electron microscopy investigation. *Marine Geology*, 118(3-4): 187-194.
- Neil, D., Newman, S. and Isdale, P., 1994. Long-term records of sediment yield from coral skeletons: results from ion beam analyses. In: Olive, L.J., Loughran, R.J. and Kesby, J.A. (Editors), *Variability in Stream Erosion and Sediment Transport (Proceedings of the Canberra Symposium 1994)*. IAHS Publications 224, pp. 465-472.
- Osetinsky, I. and Alpert, P., 2006. Calendaricities and multimodality in the Eastern Mediterranean cyclonic activity. *Natural Hazards and Earth System Sciences*, 6(4): 587-596.
- Paillard, D., Labeyrie, L. and Yiou, P., 1996. Macintosh program performs time-series analysis. *EOS Transactions of the American Geophysical Union*, 77(39): 379.

- Palamarev, E., 1989. Paleobotanical evidences of the Tertiary history and origin of the Mediterranean sclerophyll dendroflora. *Plant Systematics and Evolution*, 162(1): 93-107.
- Pe-Piper, G., 1980. Geochemistry of Miocene Shoshonites, Lesbos, Greece. *Contributions to Mineralogy and Petrology*, 72: 387-396.
- Pierre, C., 1999. The oxygen and carbon isotope distribution in the Mediterranean water masses. *Marine Geology*, 153: 41-55.
- Pingitore Jr, N.E., Iglesias, A., Bruce, A., Lytle, F. and Wellington, G.M., 2002. Valences of iron and copper in coral skeleton: X-ray absorption spectroscopy analysis. *Microchemical Journal*, 71(2-3): 205-210.
- Poulos, S.E., Drakopoulos, P.G. and Collins, M.B., 1997. Seasonal variability in sea surface oceanographic conditions in the Aegean Sea (Eastern Mediterranean): an overview. *Journal of Marine Systems*, 13(1-4): 225-244.
- Prell, W.L. and Kutzbach, J.E., 1992. Sensitivity of the Indian monsoon to forcing parameters and implications for its evolution. *Nature*, 360(6405): 647-652.
- Quade, J., Solounias, N. and Cerling, T.E., 1994. Stable isotopic evidence from paleosol carbonates and fossil teeth in Greece for forest or woodlands over the past 11 Ma. *Palaeogeography, Palaeoclimatology, Palaeoecology*, 108(1-2): 41-53.
- Rahl, J.M., 2004. Exhumation of high-pressure metamorphic rocks within an active convergent margin, Crete, Greece. *Field-trip guide book*, 32nd International Geological Congress, Florence, Italy, pp. 36.
- Ramos, A.A., Inoue, Y. and Ohde, S., 2004. Metal contents in *Porites* corals: Anthropogenic input of river run-off into a coral reef from an urbanized area, Okinawa. *Marine Pollution Bulletin*, 48(3-4): 281-294.
- Reeder, R.J., Nugent, M., Lamble, G.M., Tait, C.D. and Morris, D.E., 2000. Uranyl Incorporation into Calcite and Aragonite: XAFS and Luminescence Studies. *Environmental Science & Technology*, 34(4): 638-644.
- Reuter, M. and Brachert, T.C., 2007. Freshwater discharge and sediment dispersal - Control on growth, ecological structure and geometry of Late Miocene shallow-water coral ecosystems (early Tortonian, Crete/Greece). *Palaeogeography, Palaeoclimatology, Palaeoecology*, 255: 308-328.
- Reuter, M., Brachert, T.C. and Kroeger, K.F., 2005. Diagenesis of growth bands in fossil scleractinian corals: Identification and modes of preservation. *Facies*, 51: 155-168.
- Reuter, M., Brachert, T.C. and Kroeger, K.F., 2006. Shallow-marine carbonates of the tropical - temperate transition zone: effects of hinterland climate and basin physiography (Late Miocene, Crete/Greece). In: Pedley, H.M. and Carannante, S. (Editors), *Cool-Water Carbonates*. Geological Society of London, Special Publication, 255, pp. 157-178.
- Sachse, M. and Mohr, B.A.R., 1996. Eine obermiozäne Makro- und Mikroflora aus Südkreta (Griechenland), und deren paläoklimatische Interpretation.- Vorläufige Betrachtungen. *Neues Jahrbuch für Geologie und Paläontologie - Abhandlungen*, 200(1/2): 149-182.
- Sanborn, M. and Telmer, K., 2003. The spatial resolution of LA-ICP-MS line scans across heterogeneous materials such as fish otoliths and zoned minerals. *Journal of Analytical Atomic Spectrometry*, 18: 1231-1237.
- Shen, G.T. and Dunbar, R.B., 1995. Environmental controls on uranium in reef corals. *Geochimica et Cosmochimica Acta*, 59(10): 2009-2024.
- Sinclair, D.J., 2005. Non-river flood barium signals in the skeletons of corals from coastal Queensland, Australia. *Earth and Planetary Science Letters*, 237(3-4): 354-369.

- Sinclair, D.J., Kinsley, L.P.J. and McCulloch, M.T., 1998. High resolution analysis of trace elements in corals by laser ablation ICP-MS. *Geochimica et Cosmochimica Acta*, 62(11): 1889-1901.
- Smith, S.V., Buddemeier, R.W., Redalje, R.C. and Houck, J.E., 1979. Strontium-calcium thermometry in coral skeletons. *Science*, 204: 404-407.
- Stoll, B., Jochum, K.P., Herwig, K., Amini, M., Flanz, M., Kreuzburg, B., Kuzmin, D., Willbold, M. andENZWEILER, J., 2008. An Automated Iridium-Strip Heater for LA-ICP-MS Bulk Analysis of Geological Samples. *Geostandards and Geoanalytical Research*, 32: 5-26.
- Suc, J.-P., 1984. Origin and evolution of the Mediterranean vegetation and climate in Europe. *Nature*, 307: 429-432.
- Suc, J.-P. and Popescu, S.-M., 2005. Pollen records and climatic cycles in the North Mediterranean region since 2.7 Ma. Geological Society, London, Special Publications, 247(1): 147-158.
- Swart, P.K. and Hubbard, J.A.E.B., 1982. Uranium in Scleractinian Coral Skeletons. *Coral Reefs*, 1: 13-19.
- Taylor, S.R. and McLennan, S.M., 1985. The continental crust: its composition and evolution. Blackwell Scientific Publications, Oxford, England, 312 pp.
- ten Veen, J.H. and Postma, G., 1999. Neogene tectonics and basin fill patterns in the Hellenic outer-arc (Crete, Greece). *Basin Research*, 11(3): 223-242.
- Thompson, G. and Livingston, H.D., 1970. Strontium and uranium concentrations in aragonite precipitated by some modern corals. *Earth and Planetary Science Letters*, 8: 439-442.
- Tzedakis, P.C., 2007. Seven ambiguities in the Mediterranean palaeoenvironmental narrative. *Quaternary Science Reviews*, 26(17-18): 2042-2066.
- Weber, J.N., 1973. Incorporation of strontium into reef coral skeletal carbonate. *Geochimica et Cosmochimica Acta*, 37: 2173-2190.
- Wehausen, R. and Brumsack, H.-J., 2000. Chemical cycles in Pliocene sapropel-bearing and sapropel-barren eastern Mediterranean sediments. *Palaeogeography, Palaeoclimatology, Palaeoecology*, 158(3-4): 325-352.
- Weldeab, S., Emeis, K.C., Hemming, N.G. and Siebel, W., 2002a. Provenance of lithogenic surface sediments and pathways of riverine suspended matter in the Eastern Mediterranean Sea: evidence from $^{143}\text{Nd}/^{144}\text{Nd}$ and $^{87}\text{Sr}/^{86}\text{Sr}$ ratios. *Chemical Geology*, 186: 139-149.
- Weldeab, S., Emeis, K.-C., Hemleben, C., Vennemann, T.W. and Schulz, H., 2002b. Sr and Nd isotope composition of Late Pleistocene sapropels and nonsapropelic sediments from the Eastern Mediterranean Sea: implications for detrital influx and climatic conditions in the source areas. *Geochimica et Cosmochimica Acta*, 66(20): 3585-3598.
- Welter-Schultes, F.W., 2000. The paleogeography of late Neogene central Crete inferred from the sedimentary record combined with *Albinaria* land snail biogeography. *Palaeogeography, Palaeoclimatology, Palaeoecology*, 157(1-2): 27-44.
- Wischow, D., 1999. Sr-Ca- und U-Ca-Thermometrie an Korallen (*Porites lutea*) aus dem Indischen Ozean. PhD Thesis, Universität Göttingen, 78 pp.
- Wyndham, T., McCulloch, M., Fallon, S. and Alibert, C., 2004. High-resolution coral records of rare earth elements in coastal seawater: biogeochemical cycling and a new environmental proxy. *Geochimica et Cosmochimica Acta*, 68(9): 2067-2080.
- Zervakis, V. and Georopoulos, D., 2002. Hydrology and circulation in the North Aegean (eastern Mediterranean) throughout 1997 and 1998. *Mediterranean Marine Science*, 3(1): 5-19.

- Zhisheng, A., Kutzbach, J.E., Prell, W.L. and Porter, S.C., 2001. Evolution of Asian monsoons and phased uplift of the Himalaya-Tibetan plateau since Late Miocene times. *Nature*, 411(6833): 62-66.
- Zidianakis, G., Mohr, B. and Fassoulas, C., 2004. The Late-Miocene flora of Vrysses, Western Crete - A contribution to the climate and vegetation history, 5th International Symposium on Eastern Mediterranean Geology, Thessaloniki, Greece, pp. 515-518.
- Zidianakis, G., Mohr, B.A.R. and Fassoulas, C., 2007. A late Miocene leaf assemblage from Vrysses, western Crete, Greece, and its paleoenvironmental and paleoclimatic interpretation. *Geodiversitas*, 29(3): 351-377.
- Zielinski, R.A., 1982. The mobility of Uranium and other elements during alteration of rhyolite ash to montmorillonite: a case study in the Troublesome Formation, Colorado, U.S.A. *Chemical Geology*, 35: 185-204.

Acknowledgements

I thank the following persons for their support during the development of this thesis:

For reasons of data protection the content of the acknowledgements is not displayed in the online version of this thesis.

Appendix

Appendix A: Stable oxygen and carbon isotope data

The supplementary material is available on the enclosed data CD.

Sampling site P I

Table A1: Specimen P2

Table A2: Specimen P16

Sampling site P II

Table A3: Specimen P1

Table A4: Specimen P3

Table A5: Specimen P4

Table A6: Specimen P7

Table A7: Specimen P8

Table A8: Specimen P8B

Table A9: Specimen P9

Sampling site P III

Table A10: Specimen P12

Table A11: Specimen P14

Sampling site G I

Table A12: Specimen SF1

Table A13: Specimen SF2

Table A14: Specimens SF3, SF4 and SF5

Sampling site G II

Table A15: Specimens MG9/2, MG9/4 and MG9/6

Sampling site G III

Table A16: Specimens MG10-11/1, MG10-11/2, MG10-11/3, MG10-11/4 and MG10-11/5

Sampling site G IV

Table A17: Specimens MG16/1 and MG16/2

Sampling site G V

Table A18: Specimens MG24/2 and MG24/3

Appendix B: Radiogenic strontium isotope data

The supplementary material is available on the enclosed data CD

Table B1: Measurements of the NIST SRM 987 Sr standard

Table B2: $^{87}\text{Sr}/^{86}\text{Sr}$ values of coral and evaporite samples

Appendix C: LA-ICP-MS data

The supplementary material is available on the enclosed data CD

Table C1: Count rates

Table C2: Element concentrations

Table C3: Bimonthly mean chronology of Sr/Ca and U/Ca

Appendix D: Conference and workshop contributions

- Mertz-Kraus R.**, Brachert T.C. (2008): Mediterranean-type climate in the South Aegean region during the Late Miocene: Evidence from isotope and element proxies. 26th Regional Meeting of the International Association of Sedimentologists (IAS) / SEPM-CES Sediment 2008 Meeting, Bochum. Schriftenreihe der Deutschen Geologischen Gesellschaft, 58, 187.
- Brachert T.C., Vescogni A., Bosellini F.R., Reuter M., **Mertz-Kraus R.** (2008): High salinity variability during the early Messinian revealed by stable isotope signatures from vermetid and *Halimeda* reefs of the Mediterranean region. 26th Regional Meeting of the International Association of Sedimentologists (IAS) / SEPM-CES Sediment 2008 Meeting, Bochum. Schriftenreihe der Deutschen Geologischen Gesellschaft, 58, 62.
- Brachert T.C., **Mertz-Kraus R.**, Reuter M., Fassoulas C., Iliopoulos G. (2008): Coral Proxies in Miocene Palaeoclimatology. EGU General Assembly 2008, Vienna. Geophysical Research Abstracts, Vol. 10, EGU2008-A-03891.
- Mertz-Kraus R.**, Brachert T.C., Galer S.J.G., Stoll B. and Jochum K.P., Reuter M. (2007): Late Miocene freshwater runoff seasonality inferred by LA-ICP-MS and TIMS analyses on Eastern Mediterranean corals. AGU Fall Meeting 2007, San Francisco. PP31D-0657.
- Mertz-Kraus R.**, Brachert T.C., Reuter M. (2007): Increase in evaporation in the Mediterranean during the Late Miocene indicated by $\delta^{18}\text{O}$ records of the reef corals *Porites* and *Tarbellastraea*. GV International Conference 2007, Bremen.
- Brachert T.C., **Mertz-Kraus R.**, Reuter M., Kroeger K.F. (2007): Mediterranean sea-level changes and climate: Inferences from Late Miocene reef corals. "Drilling to Decipher Long-term Sea-level Changes and Effects", JOI-ICDP-IODP-DOSECC-Chevron Workshop 2008, Salt Lake City.
- Brachert T.C., Bosellini F.R., Reuter M., Vescogni A., **Mertz-Kraus R.** (2007): Stable isotope data from Early Messinian aragonite cements reveal high salinity variability prior to the "Messinian Salinity Crisis" (Late Miocene) in the Mediterranean region. GV International Conference 2007, Bremen.
- Mertz-Kraus R.**, Brachert T.C., Galer S.J.G., Stoll B. and Jochum K.P. (2007): Seasonal element and Sr isotope ratio variations in Late Miocene corals from Crete, Eastern

- Mediterranean. 17th Goldschmidt Conference 2007, Cologne. *Geochimica et Cosmochimica Acta*, 71(15, Suppl. 1), A656.
- Brachert T.C., Bosellini F.R., Reuter M., Vescogni A., **Mertz-Kraus R.** (2007): Early Messinian aragonite event reveals high salinity variability prior to the “Messinian Salinity Crisis” (Late Miocene) in the Mediterranean region. EGU General Assembly 2007, Vienna. *Geophysical Research Abstracts*, Vol. 9, 04036.
- Mertz-Kraus R.**, Brachert T.C., Reuter M. (2007): *Tarbellastraea*: a new archive for paleoenvironmental studies. EGU General Assembly 2007, Vienna. *Geophysical Research Abstracts*, Vol. 9, 03390.
- Brachert T.C., Reuter M., Felis T., Kroeger K.F., **Mertz-Kraus R.**, Lohmann G., Micheels A. (2006): Seasonal and interannual climate variability during the Late Miocene: First stable isotope records from *Porites* corals (Crete, Greece). GV International Conference 2006, Potsdam.
- Mertz-Kraus R.**, Brachert T.C., Reuter M., Felis T., Fassoulas C., Iliopoulos G. (2006): Seasonal $\delta^{18}\text{O}$ records from *Porites* document decreasing seasonality and increasing salinity during the Late Miocene in the Eastern Mediterranean. GV International Conference 2006, Potsdam.
- Mertz-Kraus R.**, Brachert T.C., Reuter M., Felis T., Fassoulas C., Iliopoulos G. (2006): Seasonal $\delta^{18}\text{O}$ records from *Porites* document decreasing seasonality and increasing salinity during the Late Miocene in the Eastern Mediterranean. International Society for Reef Studies, 6th European Meeting, Bremen.
- Brachert T.C., Reuter M., Kroeger K.F., **Mertz-Kraus R.**, Lough J.M. (2006): Coral growth bands: A new and easy to use palaeothermometer in palaeoenvironment analysis and palaeoceanography (late Miocene, Greece). *Sediment 2006*, Göttingen.
- Brachert T.C., Reuter M., Felis T., Kroeger K.F., **Mertz-Kraus R.**, Lohmann G., Micheels A. (2006): *Porites* corals from Crete (Greece) open a window into Late Miocene (10 Ma) seasonal and interannual climate variability. *Sediment 2006*, Göttingen.
- Mertz-Kraus R.**, Brachert T.C., Reuter M., Felis T., Fassoulas C., Iliopoulos G. (2006): Seasonal $\delta^{18}\text{O}$ and $\delta^{13}\text{C}$ records from *Porites*: Decreasing seasonality and increasing salinity during the Late Miocene in the Eastern Mediterranean. RCOM Workshop 2006, Bremen.